# THEORETICAL AND NUMERICAL ASPECTS OF EULERIAN POLYDISPERSITY TREATMENTS IN GAS-SOLID SYSTEMS

by

John C. Parra-Álvarez

A dissertation submitted to the faculty of
The University of Utah
in partial fulfillment of the requirements for the degree of

Doctor of Philosophy

Department of Chemical Engineering

The University of Utah

August 2017

**The University of Utah Graduate School**

**STATEMENT OF DISSERTATION APPROVAL**

The dissertation of **John C. Parra-Álvarez**
has been approved by the following supervisory committee members:

| | | |
|---|---|---|
| **Philip J. Smith** , | Chair(s) | **January 6th 2017** Date Approved |
| **Sean T. Smith** , | Member | **January 6th 2017** Date Approved |
| **Alejandro Molina** , | Member | **January 6th 2017** Date Approved |
| **Jeremy Thornock** , | Member | **January 6th 2017** Date Approved |
| **Terry Ring** , | Member | **January 6th 2017** Date Approved |

by **Milind Deo** , Chair/Dean of
the Department/College/School of **Chemical Engineering**
and by **David B. Kieda** , Dean of The Graduate School.

# ABSTRACT

The purpose of this research is the development of mathematical formalisms for the numerical modeling and simulation of multiphase systems with emphasis in *polydisperse* flows. The framework for these advancements starts with the William-Boltzmann equation which describes the evolution of joint distributions of particle properties: size, velocity, mass, enthalpy, and other scalars. The amount of statistical information that can be obtained from the direct evolution of particle distribution functions is extensive and detailed, but at a computational cost not yet suitable in usable computational fluid dynamics (CFD) codes. Alternatives to the direct evolution of particle distribution functions have been proposed and we are interested in the family of solutions involving the evolution of the statistical moments from the joint distributions. Rather than tracking every single particle characteristic from the joint distribution, transport equations for their joint moments are formulated; these equations share many of the properties of the regular transport equations formulated in the finite volume framework, making them very attractive for their implementation in current Eulerian CFD codes. The information they produce is general enough to provide the characteristic behavior of many multiphase systems to the point of improvement over the current Eulerian methodologies implemented on standard CFD modeling and simulation approaches.

Based on the advantages and limitations of the solutions of the ongoing methodologies and the degree of the information provided by them, we propose formalisms to extend their modeling capabilities focusing on the influence of the size distribution in many of the related multiphase phenomena. The first methodology evolves joint moments based on the evolution of primitive variables (size among them) and conditional moments that are approximants of the joint moments at every time step. The second methodology reconstructs completely the marginal size distribution using the concept of parcel and approximate characteristic behavior of the rest of the conditional moments in each parcel. In both approaches, the representation of size distribution plays a fundamental role and

accounts for the polydisperse nature of the system. Also, the numerics of the moment transport equations are to be consistent with the theory of general hyperbolic transport equations but the formulation of the discretization schemes are based on the properties of the underlying distribution.

A final contribution is presented in the form of an appendix and it analyzes the role of maximum entropy-based methodologies on the formulation of Eulerian moment-based methods. Attempts to derive new transport equations on the framework of maximum entropy methodologies will be considered and reconstruction of distribution strategies will be presented as preliminary results that might impact future research on Eulerian moment-based methods.

*To my mom, Lucía Álvarez, whose wisdom came not from knowledge, but from grit and guts. From her, I learned how to rise when life let me down and how to set the path I am walking right now. To this day, I still carry her toughness, perseverance and will-power. To her, I am eternally thankful.*

# CONTENTS

# LIST OF FIGURES

# LIST OF TABLES

# NOTATION AND SYMBOLS

| Abbreviations | |
|---|---|
| CFD | Computational Fluid Dynamics |
| CFL | Courant, Friedrichs, Lewy condition |
| CQMOM | Conditional Quadrature Method of Moments |
| DNMC | Direct Numerical Montecarlo Simulation |
| DNS | Direct Numerical Simulation |
| DVM | Discrete Velocity Methods |
| DQMOM | Direct Quadrature Method of Moments |
| EQMOM | Extended Quadrature Method of Moments |
| LES | Large Eddy Simulation |
| LHS | Left Hand Side |
| ME | Maximum Entropy |
| MEP | Maximum Entropy Principle |
| NDF | Number Density Function |
| PDE | Partial Differential Equation |
| pdf | Probability Density Function |
| PSD | Particle Size Distribution |
| PTC | Particle Trajectory Crossing |
| QBMM | Quadrature-Based Method of Moments |
| RHS | Right Hand Side |
| SM | Sectional Methods |
| **Uppercase Roman** | |
| $A_p$ | Particle surface area |
| $\mathbb{C}[\mathfrak{F},\mathfrak{F}]$ | Rate of collisions |
| $C_p$ | Specific heat of particles |
| $C_D$ | Drag coefficient |
| $\mathbb{D}$a | Damköler number |
| $\mathfrak{F}$ | Number Density Function |
| $\mathbf{F}$ | Rate of advection in velocity space |
| $\mathbf{G}$ | Rate of advection in size space |
| $G_F$ | Magnitude of velocity gradient in shear flow |
| $\mathbb{E}$ | Expected value of a distribution |
| $\mathbf{H}$ | Rate of advection in scalar space |
| $H_p$ | Particle enthalpy |
| $\mathbf{J}(\zeta)$ | General phase-advection rate |
| $\mathbb{K}$n | Knudsen Number |
| $K_A$ | Added-mass force constant |
| $K_B$ | Basset history force constant |
| $K_L$ | Lift force constant |
| $M$ | Scalar moment index |

| | |
|---|---|
| $\mathfrak{M}^{l,M,N}$ | Joint size-velocity-scalar moments |
| $M_w$ | Molecular weight of the particle |
| $N$ | Velocity moment index |
| $\mathbb{St}$ | Stokes number |
| $\mathbb{St}_c$ | Critical Stokes number |
| $\mathfrak{S}$ | Rates of advection and collision in the kinetic equation |
| $\overline{\mathfrak{S}}$ | Integrated rates of advection and collision in the kinetic equation |
| $\mathbf{U}_f$ | Fluid velocity |
| $\bar{U}_{p,char}$ | Characteristic velocity of the system |
| $\overline{\mathbf{U}}_p$ | Particle velocity in physical space |
| $V_p$ | Particle volume |
| **Lowercase Roman** | |
| $\mathfrak{f}(\boldsymbol{\theta})$ | Conditional scalar distribution |
| $f'$ | Fine-grained number density function |
| $\mathfrak{g}(\xi)$ | Marginal size distribution |
| $\mathbf{g}$ | Gravity |
| $g_0$ | Radial distribution function |
| $l$ | Size moment index |
| $l_s$ | Order of the polynomial approximation |
| $m_k$ | Particle mass |
| $\langle \mathfrak{m} \rangle$ | Conditional velocity moments |
| $\mathbf{q}$ | Heat transfer to and from the particles |
| $t$ | time |
| $\Delta t$ | Size of time step |
| $\mathbf{v}$ | Particle velocity in velocity space |
| $w_\alpha$ | Weights of the NDF approximation |
| $\mathbf{x}$ | Position in physical space |
| $\Delta x$ | Smallest size of Eulerian grid |
| $\mathbf{z}$ | General property in phase space |
| **Uppercase Greek** | |
| $\Delta^{(N)}$ | Moments of the Maxwell equilibrium distribution |
| $\boldsymbol{\Xi}$ | Particular realization of in size coordinate |
| $\boldsymbol{\Theta}$ | Particular realization of in scalar coordinate |
| $\mathbf{X}$ | Particular realization of in physical coordinate |
| **Lowercase Greek** | |
| $\alpha_p$ | Volume fraction |
| $\alpha_p^c$ | Packing-limit volume fraction |
| $\delta_\sigma$ | Common probability distribution |
| $\varepsilon$ | Emissivity |
| $\boldsymbol{\theta}$ | Array of scalar properties of particles in phase space |
| $\boldsymbol{\theta}_\alpha$ | Scalar abscissas at a quadrature node in physical space |
| $\overline{\boldsymbol{\theta}}_k$ | Averaged scalar abscissa over parcel $k$ |

| | |
|---|---|
| $\mu_j$ | jth canonical moment |
| $\mu_f$ | Fluid viscosity |
| $\lambda$ | Lagrangian multiplier in ME functions |
| $\xi$ | Particle size distribution in phase space |
| $\xi_\alpha$ | Particle size at a quadrature node in physical space |
| $\rho_f$ | Fluid density |
| $\rho_p$ | Particle density |
| $\rho_{\beta_1}$ | Velocity weight in direction 1 |
| $\rho_{\beta_1,\beta_2}$ | Velocity weight in direction 2 conditioned on direction 1 |
| $\rho_{\beta_1,\beta_2,\beta_3}$ | Velocity weight in direction 3 conditioned on direction 1 and 2 |
| $\sigma$ | Variance |
| $\sigma_h$ | Stefan-Boltzmann constant |
| $\tau_p$ | Particle time scale |
| $\tau_f$ | Fluid time scale |
| $\tau_c$ | Characteristic time scale |
| $\boldsymbol{\zeta}$ | General phase-advection property |

# ACKNOWLEDGEMENTS

I would like to thank my advisor Professor *Phil Smith*; his way of supervising forced creativity and independence in my work, traits that I, judiciously, extended to many other aspects of my life. Needless to say, without his endless support, none of this would have been possible.

I wish also to express my sincere appreciation to all the people who, in one way or another, inspired me to be a better version of myself at every step of this long road that began many, many years ago. Among the many: my fifth grade teacher, *Teresita Gutierrez*; my tenth grade chemistry teacher, *Ramón Oquendo*; my thermodynamic professors, *Carlos Sánchez* and *Farid Chejne*; and my master's degree advisor, *Alejandro Molina*.

Support and encouragement come in many ways, but the kind that I received from *Rosalía Villegas* made me feel that I could do anything and everything; she was that mental boost the athlete needs to reach that finish line.

Finally, I would like to thank the many people in this group whom I have shared many moments with during this program and from whom I learned many useful skills that I now appreciate: *Ben Isaac*, *Michal Hradisky*, *Tony Saad*, *Sean Smith*, *Jeremy Thornock*, *Oscar Diaz-Ibarra*, and *Charles Reid*.

# CHAPTER 1

# INTRODUCTION

Modeling in multiphase particulate flow is an area of active research,[1–13] and the current trend presents a clear shift from phenomenological models to fundamental physics-based models. In theory, particle direct numerical simulation (particle DNS) should be the correct approach to capture the physics occurring at a particle *microscale* level, but it comes at a very high computational expense, inaccessible to industrial processes.

On the other hand, *macroscopic*, phenomenological modelling, based on proper averaging of the DNS equations, has been used mainly in Computational Fluid Dynamics (CFD) at the industrial level for modelling large scale engineering processes.[14–26] This approach gives rise to different approximations with unclosed terms (hydrodynamics models) whose accuracy depends on the accuracy of the closure models used. When phenomenological parameters for the macroscopic approach are well defined, the methodology is useful for design and optimization at an engineering level but it cannot be used as a predictive tool for multiphase flow regime transitions or as a starting point to develop accurate multiphase modelling approaches.

The continuous growth of computational power,[27,28] has slowly allowed research to move from hydrodynamic approaches to high fidelity models based on the underlying physics of the dispersed phase and the fluid flow.[6,11,29,30] For those modelling approaches, the behaviour of the distributed properties of the dispersed phase are described in terms of kinetic-type[a] transport equations for the one-point particle number density function (NDF). This kinetic formulation accounts for changes in particle property distributions (velocity, volume, enthalpy), the effects of the fluid on the particle state (body forces), and the interaction between particles (collisions). The same way DNS is categorized as a

[a] Kinetic as in the *kinetic theory of rarefied gases*; the mathematical description of the approach presented here and the one from the kinetic theory present similarities in many aspects.

microscale approach and hydrodynamic modelling as a macroscale approach, kinetic type modeling for particulate phases has been categorized as *mesoscale* approach. Closure terms at this mesoscale level require some a priori knowledge of the underlying physics present at the microscale level so appropriate closures can be developed based on mesoscale variables.[5,13]

Although the mesoscale approach represents a step forward for a reliable representation of real multiphase systems, its numerical treatment still presents us with open challenges. Consider a particle[b] distribution function for the particle velocity in space and time; there are three phase space variables $(v_x, v_y, v_z)$ representing the particle velocity, three physical space variables $(x, y, z)$, and time $(t)$. In addition to these 7 independent variables, more might be required if other scalar particle properties are taken into account: polydisperse character of the system (different particle sizes), particle mass, and particle enthalpy. It is clear that due to the high dimensionality of this problem, specialized methodologies must be developed to tackle this problem in the CFD sense.

There are several methodologies that allow representative solutions for the evolution of the particle distribution function from kinetic-type transport equations, among them: direct discretization methods, Lagrangian methods, and moment methods. Direct discretization methods numerically approximate the particle distribution function in phase space.[c] Among them, Discrete velocity methods[d] (DVM), have been developed for particle velocity distributions that take into account the effects of the collisional process on the particle behaviour;[31–34] while for passive scalars (size, mass, enthalpy), sectional methods (SM) discretize the scalar phase space describing growth, aggregation, and breakage of particles, accounting for changes in mass, size, and any other scalar property involved in the process.[35–38] Lagrangian methods describe the motion and interactions of single particles or clusters of them in the system, requiring evolution equations for each particle or cluster in the system.[39,40] In general, the application of direct discretization methods or

---

[b] Particle is a general term that refers to a member of the dispersed phase: solid particles, liquid droplets, suspensions, and so on.

[c] The term denotes the description of the dynamic state of the particles. The coordinates of the phase space correspond to all the independent variables of the NDF but the physical space variables $x, y, z$.

[d] Lattice Boltzmann and Lattice Gas Automata methods are among DVM.

Lagrangian methods is computationally expensive, marginally developed for CFD applications, and in many processes it is more valuable to focus in some important statistics instead of the evolution of the entire distribution.

Grad[41] proposed a mathematical approximation to reduce the dimensionality of the kinetic equations to describe the macroscopic dynamic behavior of rarefied gases in an Eulerian framework, based on a particular set of moments of the velocity distribution. Hulburt and Katz[42] introduced a similar approximation for population balance equations. McGraw and Fox,[30,43,44] and Frenklach,[45] among others, have extended the method to handle more complex physics at the macroscale level and have developed closure relations based on quadrature approximations[e] for the transport equations.[f] These equations are obtained from a transformation over the original kinetic-type transport equation and the quantities originated from this transformation are called *moments*. The term quadrature-based moment methods (QBMM) have been coined[46] to group the many different techniques,[29,30,43,46,47] related to the closure of kinetic equations and population balances based on quadrature approximations and moments of the distribution.

One attractive factor for the use of QBMM, is the possibility to increase their accuracy based on the accuracy of the proposed closure quadratures. Nevertheless, some challenges remain unsolved in developing efficient and cheap algorithms to relate variables of the quadrature approximation (velocity, volume, enthalpy) with the approximated moments of the distribution. Ideally, such procedures, should be well-posed in order to guarantee realizability of the moment space obtained from the population balances or the kinetic-based equations.[8] The core idea behind QBMM is to obtain transport equations in terms of the moments of the joint distribution, the evolution of these moments would describe the principal characteristics of the particle behavior in terms of raw statistics. Due to the nature of the moment transformation, some of the transport equations would need especial closures for high order moments; in this regard, several QBMM methodologies have been developed with varying degrees of complexity and ability to handle common systems in

---

[e] In the sense of quadrature approximation of integrals.

[f] For instance, integro-differential terms appearing as source terms in population balances for some scalar properties, are unclosed; same as the flux in physical space for the moment transport equations for the velocity distribution.

multiphase flows.

Marchisio and Fox[43], proposed the direct quadrature method of moments (DQMOM), in which the evolution of the moment equations are expressed in terms of the variables of a quadrature approximation (weights and abscissas). The technique has been proven to properly represent particle changes in scalar phase space.[48–56] However, the method has been reported to fail in conserving the computed moments from the weights and abscissas, for active variables.[57–59] Given that the transport equations are stated in terms of weights and abscissas, any error induced by the numerical scheme used to discretize the equations will extend to the calculation of the moment set from the evolved weights and abscissas; in general, any moment method that relies on the numerical transport of weights and/or abscissas can be affected by the numerical error and is susceptible to degenerate into a nonrealizable space. This issue is especially problematic when particle velocity is included as an independent variable of the distribution function, because phenomena like particle trajectory crossing (PTC) in dilute and moderately dilute gas-particle flows, might not be properly represented by DQMOM. This DQMOM limitation has motivated researchers to develop better approximations that include the effects of particle velocity in physical space.

Fox and co-workers,[29,30,46,47] among others, have proposed quadrature-based moment methods (QBMM) that are specialized in the kinetic behavior of the dispersed phase (particle velocities). Desjardins and Fox[47] and Desjardins et al.[29] have found that transporting moments instead of weights and abscissas allows for better control of numerical errors by using specialized discretization techniques, which in turn aid in capturing complex particle physics like PTC in dilute and moderately dilute particulate flows. In these methods, moment transport equations are evolved directly and weights and abscissas are used to approximate high order moments that might appear in the calculations. The methods require two types of specialized algorithms: *inversion* algorithms, from which weights and abscissas can be calculated from the moments, and *projection* algorithms from which moments are defined in the Eulerian grid in terms of the weights and abscissas.[29,47] The inversion algorithms that relate the quadratures of the approximation with the moments of the system are closely related to the *truncated* $\mathbb{K}$*-moment problem* for which realizability of the moment space depends entirely on the properties of special arrangements of moment

matrices. In general, formulation of inversion algorithms is complex from both the mathematical and the computational point of view and there are still open questions in the field. For instance, some of the existing moment inversion algorithms[29,30,46,47] define an infinite number of quadratures for each rotation of the diagonalization of the velocity covariance matrix, producing quadrature errors that depend on the angle of rotation. Additionally, the number of moments transported is greater than the moments controlled by the inversion algorithm, producing numerical errors for higher order transported moments. In order to formulate the closures for the equations, an approximation to the NDF is required; the functional form of the distribution used in all QBMM is a weighted Dirac-delta, which corresponds to a minimal, unique, representation at the boundary of the moment space, as shown in Dette and Studden.[60]

Yuan and Fox,[61] proposed a well-posed inversion algorithm for the conditional quadrature method of moments (CQMOM), which accurately relates moments with weights and abscissas. It also improves the quadrature approximation, when each quadrature reproduces exactly an N-point quadrature and reduces the error when a continuous distribution is represented as an N-point distribution. The proposed method also reduces the number of transported moments because it transports the optimal moment set used in the direct quadrature method of moments (DQMOM).[62] However, the technique is originally formulated for kinetic monodisperse flows (particles with the same scalar state: mass, volume, and enthalpy but distributed in velocity space) leaving an open questions about its extension to polydisperse flows distributed also in scalar space.

Other classes of methods use some of the ideas of SM and discretize one or more coordinates of the phase space and, within each section, related quantities of the NDF are evolved. These Eulerian-multifluid models[63] would guarantee the conservation of few moments, leaving out extra information about the correlation of different variables of the phase space.[g] Improvements on the numerical aspects, representation of larger moment sets, and the ability to capture complex physics have been proposed since then.[51,64–70] On the other hand, some researchers have realized the importance of the issues that the Dirac-delta approximation of the NDF might bring, regarding the conservation of the moment

[g] For instance, size and velocity.

space. Some[71–77] have proposed different approximations for the NDF to solve for the closure issue, by using canonical distribution functions: Gaussian, Gamma, Log-normal. More advanced techniques are also able to reconstruct the distribution of properties based on information about the evolved moments. Techniques based on maximum entropy methods are promising and valuable information about the the polydisperse character of multiphase systems can be obtained if used in conjunction with moment-based methods.[76,78]

It is then desirable to formulate moment-based methods to model and simulate polydisperse multiphase systems that take advantage and overcome some of the difficulties associated with the current methodologies. The main aim of this research is to develop mathematical formalisms that:

- Use a moment-based method to represent multiphase phenomena,
- take advantage of the inversion process presented for CQMOM to capture PTC,
- take advantage of DQMOM to extend the formalism to arbitrary dimensions in scalar space to account for the polydisperse character of the flow (size) and changes in other scalar properties (mass, enthalpy), and
- are able to describe the polydispersity behavior of a multiphase system by reconstructing the distribution of particle sizes based on the evolved moments.

The remainder of this dissertation is divided as follow: **Chapter 2** presents an introduction to the characterization of the fluid dynamic behavior of gas-particle systems and the models to represent them. **Chapter 3** describes a moment-based technique that takes into account the polydisperse character gas-particle multiphase systems by evolving transport equations for representative particle sizes and other scalars, as well as particle velocity moments conditioned on size, that are able to capture PTC. **Chapter 4** describes a moment-based technique that explains the polydisperse character of a multiphase system by reconstructing the size distribution based on the evolved joint moments. This reconstruction-based technique provides more detailed information about the polydispersity of the system than other moment-based techniques. **Chapter 5** provides numerical applications of the techniques described in previous chapters. **Appendix A** presents new

perspectives on maximum entropy methods (ME) as a framework to develop Eulerian multiphase models

# CHAPTER 2

# MOMENT METHODS IN MULTIPHASE FLOW

Gas-particle flows are commonly found in many industrial and environmental applications like fluidization, drying, separation, and pneumatic transport, among other chemical engineering unit operations. The presence of additional particulate phases in gas-particle systems makes computational approaches challenging and far more difficult than the descriptions for single-phase flows. For instance, very complex phenomena affect the interaction between time and length scales among the different phases: turbulence, particle collisions, wall collisions, particle aggregation, particle breakage, and particle reaction, among others. Before reviewing and explaining current and new computational approaches for multiphase flows, it is necessary to explain the existing regimes of the complex multiphase phenomena in order to understand the approximations for many of the systems usually modeled and simulated in multiphase flows

## 2.1 Kinematic Characterization of Multiphase Flows

Along with the length and time scales for the fluid flow, it is necessary to account for the length and time scales of the particulate phase, which in general are not independent from the ones in the fluid phase.[79] van der Hoef et al.,[1] and references wherein, summarized this interphase coupling in terms of the mass and the volume occupied by the particulate phase immersed in the fluid phase as: one-way, two-way, and four-way coupled. The phases are one-way coupled when the turbulence of the fluid phase is dominant and the inertia, and volume occupied by the particulate phase is small (low volume fraction). When the inertia of the particulate phase cannot be ignored and the turbulence of the fluid phase is affected by the motion of the particulate phase, it is said that both phases are two-way coupled. If the inertia and volume occupied by the particulate phase is such that there are interactions among particles, the phases are four-way coupled. In a four-way coupled regime effects such as agglomeration and break-up due to collision become important and

add up to the nonlinear character of multiphase modelling approaches. **Figure 2.1** depicts this interphase coupling in terms of the volume fraction.

A more general and inclusive classification is given by Marchisio and Fox.[8] In their account, they distinguish the inertia of the particles characterized by the Stokes number as one of the key factors in multiphase modelling approaches. To summarize their point of view, they identify two main cases in multiphase flows: when the inertia of small particles is negligible respect to that of the fluid and when the particles are big enough that their inertia cannot be neglected. In the first case, particles will advect, diffuse, aggregate, and break throughout the domain in a shear-dominated flow regime; changes in the joint NDF will be governed by the aggregation and breakage events. In the second case, particles will move at their own velocity; multivalued velocity solutions will be possible (PTC phenomena) and the particle velocity distribution will affect the behavior of the joint NDF.

In the first case, regimes for particulate behavior can be classified by identifying the time scales for advection, diffusion, aggregation, and breakage and define the corresponding nondimensional quantities that relate those time scales: Peclet number ($\mathbb{P}e$), aggregation Damköler number ($\mathbb{D}a_a$), and breakage Damköler number ($\mathbb{D}a_b$). In most common cases, diffusion has smaller time scales than aggregation and breakage which are responsible for the gradients in the transported distribution. Essentially, three regimes can be

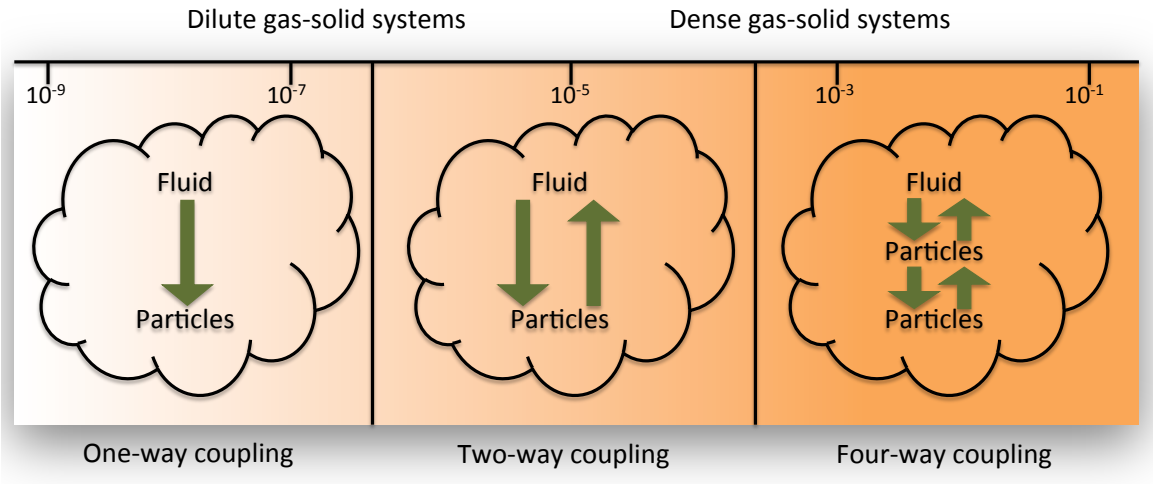


**Figure 2.1**: Representation of interphase coupling as a function of solid volume fraction. Adapted from van der Hoef et al.[1]

established, as shown in **Table 2.1**.

In the second case the velocity of the particles affect the velocity of the fluid and vice versa, allowing momentum exchange between the phases to happen. Different length and time scales are simultaneously involved and different nondimensional parameters can be identified that are correlated to a large number of flow regimes. Two of the most important are the Stokes number (St) and the Knudsen number (Kn). The first one characterizes the particle inertia relative to the fluid[13] and it is defined as the ratio of the particle time scale to that of the fluid.

$$\mathrm{St} = \frac{\tau_p}{\tau_f} \tag{2.1}$$

The second one indicates the relative importance of particle interactions[8] (collisions) and is defined as the ratio of the collision length scale to the characteristic length scale of the system:

$$\mathrm{Kn} = \frac{\bar{U}_{p,char}\tau_c}{L_{char}}, \tag{2.2}$$

where $\bar{U}_{p,char}$ is the characteristic particle velocity and $L_{char}$ is the characteristic particle length scale. The Kn number depends on the volume fraction based on the definition of the length scales. Increasing or decreasing the volume fraction will decrease or increase the Kn number. According to Marchisio and Fox,[8] the volume fraction *alone* is not a reliable indicator of the rate of collisions and interphase coupling as in the descriptions of Balachandar and Eaton[79] and van der Hoef,[1] because it can be affected by the granular temperature and even for high values of volume fraction it is possible to have a collisionless regime (very high Kn) due to energy dissipation by inelastic collisions. Four major

**Table 2.1**: Regimes for noninertial particles

| Regime | Limit | Characteristic |
|---|---|---|
| *Dilute* | $\mathrm{Da}_a < 0.01, \mathrm{Da}_b < 0.01$ | Controlling phenomena are the aggregation and breakage events. The system is spatially homogeneous. |
| *Moderately dense* | $0.01 < \mathrm{Da}_a, \mathrm{Da}_b < 100$ | Mixing, aggregation and breakage are competing effects. |
| *Dense* | $\mathrm{Da}_a, \mathrm{Da}_b > 100$ | Aggregation and breakage are very fast. Particles reach a local equilibrium when these two effects counterbalance each other. |

regimes can be identified in terms of volume fraction $\alpha_p$, St for particles with no negligible inertia, as shown in **Table 2.2**.

Such variety of regimes for multiphase flows make modeling descriptions and computational approaches very challenging, but can provide valuable insight of the behavior of the phases for the formulation of physics-based multiphase models. In this research, we are interested in *very dilute* and *dilute* systems; particularly, we are interested in developing numerical tools to characterize the polydispersity behavior of disperse reactive particles in the event of particle trajectory crossing. As pointed out before, different numerical tools have been developed to such end[29,30,43,44,46,47,61,76,78] and many of them are specialized to particular regimes; this research will benefit from improvement upon some of them in terms of trajectory crossing prediction and polydispersity behavior. Among some of the engineering applications of these techniques, Pedel et al.[80] used DQMOM[43] to describe the combustion characteristics of polydisperse coal particles in a turbulent jet; they established for a fixed particle relaxation time $\tau_p$, particle regimes as a function of the wave number in a homogeneous turbulence system. Their analysis places the particles in the very dilute regime described in **Section 2.1** with the possibility of multivalued velocity values and PTC. Unfortunately, the way DQMOM is formulated makes it difficult to capture any phenomena related to trajectory crossing. The research in this dissertation is motivated to capture PTC in velocity space as well as other scalar characteristics (polydispersity), applicable to multiscale and multiphysics modelling approaches.

## 2.2 Kinetic Description of Multiphase Flows

Several authors have described the status of the modelling techniques on multiphase flows based on kinetic[a] approaches[1,13,79,83–85] covering the multiscale (microscale, mesoscale, macroscale) nature of these kind of systems. In particular, Tenneti and Subramaniam[13] discuss the ability of statistical modelling approaches to provide information at the macroscopic and mesoscopic levels from the microscopic descriptions. They categorize the modelling approaches according to three criteria: (a) each field is represented by a random field or a stochastic point process, (b) each phase is represented using an Eulerian or Lagrangian

[a] Kinetic as in *kinetic theory of gases*. Most of the QBMM techniques are based on similar statistical mechanic principles used to explain the behavior of gases at the molecular level.

**Table 2.2**: Regimes for inertial particles

| Regime | Limit | Characteristics |
|---|---|---|
| *Very dilute* | $\alpha_p \ll 1$ with phase-mass ratio is very small | Collisions and coupling with the continuous phase are not important. |
| | $\mathbb{St} \ll \mathbb{St}_c$ | This is also referred as the *dusty gas* regime,[79] and references wherein. Particles share the same velocity as the flow field. |
| | $\mathbb{St} \leq \mathbb{St}_c$ | It falls into the regime of the *equilibrium eulerian* approach.[79] The particle velocity is allowed to be different than the fluid velocity, but it is not multivalued. |
| | $\mathbb{St} > \mathbb{St}_c$ | The particle velocity distribution is multivalued and trajectory crossing is possible (PTC), producing nonzero granular temperatures. |
| | $\mathbb{St} \gg 1$ | Collisionless granular gas. |
| *Dilute* | $\alpha_p \ll 1$ with phase-mass ratio of the order of one | Collisions and interphase coupling are not negligible. According to the Knudsen number $\mathbb{Kn}$, this regime can be subdivided as: |
| | two-way coupling, $\mathbb{Kn} \gg 1$ | collisions can be neglected but there is significant interphase coupling. |
| | four-way coupling, $\mathbb{Kn} \leq 1$ | collisions are significant as well as interphase coupling. |
| | hydrodynamic, $\mathbb{Kn} \ll 1$ | collision-dominated flow. |
| | | The dilute regime can be also subdivided based on the Stokes number St producing the same subclasses as in the very dilute regime; with the difference that because mass-phase ratio is of the order of one, there will be flow instabilities for which the flow would become turbulent even if the continuous phase laminar. |
| *Moderately dense* | $\alpha_p < \alpha_p^c$, $g_0 > 1$ | The volume fraction is lesser than the packing limit $\alpha_p^c$ and the radial distribution function $g_0$ is greater than unity. Fluidized beds fall into this regime, the collisional-flux term (granular pressure) cannot be neglected and binary particle-particle interactions are too simple to represent long-range hydrodynamic interactions.[81] |
| *Dense* | $\alpha_p \approx \alpha_p^c$ | Particles move in a frictional regime close to the packing limit. Contact between particles is constant and long range interactions must be taken into account.[82] |

reference frame, and (c) according to the level of closure in the statistical theory. In most of the current modelling approaches multiphase systems are represented as:

- a random field in an Eulerian framework, or
- the continuous phase is represented as a random field in an Eulerian framework and the dispersed phases as a point process in a Lagrangian framework.

Fox[5] has discussed the mathematical formulation of Eulerian models with a mesoscopic approach at a mesoscale level. Formally, the mesoscopic approach is a stochastic point process that results in a NDF equation at the one-particle description level,[13] but correspondence between the stochastic point process and the random field approach has been shown at the mesoscale and macroscale level under different conditions allowing the method to represent different scales of the particle state.[11] An Eulerian model can be obtained from the mesoscopic approach of Fox,[5] at the level of the moments of the one-particle NDF. The closures used to close the mesoscopic kinetic formulation relate only mesoscopic variables. In the following, we explore Eulerian models obtained in this way.

The mesoscopic formulation discussed by Fox[5] is based in the Klimontovich approach[86] where the ensemble of particles is characterized in a (6+m)-dimensional position-velocity-scalar space by a fine-grained density function $f'$ defined as

$$\begin{aligned} f'(\xi, \boldsymbol{\theta}, \mathbf{v}, \mathbf{x}, t) &= \sum_{i=1}^{N_s(t)} f'_i(\xi, \boldsymbol{\theta}, \mathbf{v}, \mathbf{x}, t) \\ &= \sum_{i=1}^{N_s(t)} \delta(\xi - \boldsymbol{\Xi}_i(t))\delta(\mathbf{x} - \mathbf{X}_i(t))\delta(\mathbf{v} - \mathbf{U}_i(t))\delta(\boldsymbol{\theta} - \boldsymbol{\Theta}_i(t)), \end{aligned} \tag{2.3}$$

where $f'_i(\xi, \boldsymbol{\theta}, \mathbf{v}, \mathbf{x}, t)$ is the fine-grained density function associated with each particle. The statistical description in terms of $f'_i$ contains much more information than is needed for the description of engineering systems, for which averaged behavior descriptions are usually enough. Succinct information can be obtained from ensemble-average of $f'_i$ and defines the joint size-velocity-scalar NDF $\mathfrak{F}(\xi, \boldsymbol{\theta}, \mathbf{v}, \mathbf{x}, t)$ as in Subramaniam.[86] The NDF is found by solving a kinetic-type[b] equation of the form

[b] From the kinetic theory point of view, a kinetic equation involves the evolution of particles distributed in velocity space. The modifier *type* is added to signify evolution of the NDF not only in velocity space but in any other scalar property space.

$$\frac{\partial \mathfrak{F}}{\partial t} + \underbrace{\nabla_{\mathbf{x}} \cdot (\mathbf{v}\mathfrak{F})}_{\text{(i)}} + \underbrace{\nabla_{\xi} \cdot (\mathbf{G}(\xi, \boldsymbol{\theta}, \mathbf{v})\mathfrak{F})}_{\text{(ii)}} + \underbrace{\nabla_{\theta} \cdot (\mathbf{H}(\xi, \boldsymbol{\theta}, \mathbf{v})\mathfrak{F})}_{\text{(iii)}} + \underbrace{\nabla_{\mathbf{v}} \cdot (\mathbf{F}(\xi, \mathbf{v})\mathfrak{F})}_{\text{(iv)}} = \underbrace{\mathbb{C}[\mathfrak{F}, \mathfrak{F}]}_{\text{(v)}}. \quad (2.4)$$

**Equation** (2.4) describes the evolution of all the particle properties described by $\mathfrak{F}$. The first term (i) corresponds to the advection of the NDF in physical space with velocity $\mathbf{v}$. The second term (ii) corresponds to changes in particle size with rate $\mathbf{G}(\xi, \boldsymbol{\theta}, \mathbf{v})$. The third term (iii) corresponds to changes in scalar properties (mass composition, energy content among others) with rate $\mathbf{H}(\xi, \boldsymbol{\theta}, \mathbf{v})$. The fourth (iv) term corresponds to changes in particle velocity due to body and superficial forces (gravity, drag, added mass) with rates $\mathbf{F}(\xi, \boldsymbol{\theta}, \mathbf{v})$, and the last term (v) corresponds to changes in particle velocity $\mathbf{v}$ and scalar property $\xi$ due to interactions between particles in the particulate phase (collisions, aggregation, breakage). The rates $\mathbf{G}(\xi, \boldsymbol{\theta}, \mathbf{v})$, $\mathbf{H}(\xi, \boldsymbol{\theta}, \mathbf{v})$, and $\mathbf{F}(\xi, \boldsymbol{\theta}, \mathbf{v})$ usually involve interactions between the continuous phase and the particulate phase and must be coupled with a model for the continuous phase (for instance, the Navier-Stokes equations), as well as closures for the high order terms in order to achieve a complete specification of the process. Complete details of the derivation of this equation starting from a stochastic point process can be found in Subramaniam.[86]

The rates $\mathbf{F}(\xi, \boldsymbol{\theta}, \mathbf{v})$ involve all the body and superficial forces experienced by particles interacting with a continuous phase. When the density of the dispersed phase is much greater than the density of the gas phase and the size of the dispersed phase is much smaller than the Kolmogorov length scale (see **Table 2.2**), the predominant force is the fluid drag. Tenneti and Subramaniam[13] have used DNS data to validate drag models as a function of mesoscopic variables $\mathbf{v}$ and $\xi$. At the mesoscale level, the variables can be correlated to each other (for instance, size-conditioned velocity) and capturing these correlations is critical in applications where the mesoscopic variables change in a couple manner.[5] The rate of collisions $\mathbb{C}[\mathfrak{F}, \mathfrak{F}]$ involves all possible collisions between pair of particles in the system through the pair distribution function. In general, this function is not known through the solution of the NDF **Equation** (2.4) and it is necessary to provide approximations in terms of the one-particle distribution function.[87–89] In the simplest case (very dilute systems), correlations between particles can be neglected and, for moderately dense flows, correlations are introduced through the radial distribution function. Closure models for the rate of collisions in dense flows are an area of active and current

research.[16,90,91]

**Equation** (2.4) requires solution strategies based on the properties of the kinetic type equations and several approaches have been developed across different research fields that implement those strategies. As mentioned before, some of those strategies are based on Lagrangian treatment of notional particles for which increasing the number of particle would increase the fidelity of the model to represent the physical system. Direct models like Direct Numerical Monte Carlo simulation (DNMC) and Discrete Velocity Methods (DVM)[31–34,92] provide a direct discretization of the kinetic equation in phase space. However, when coupling between phases is substantial, statistical noise can affect the continuous phase solution. For the same reasons, their implementation in CFD codes can be difficult and computational costs become expensive.

On the other hand, it is possible to obtain an Eulerian model from **Equation** (2.4) that is more suitable for implementation in finite volume CFD codes at a lower computational cost. The Eulerian model can be obtained by obtaining a subset of moments from **Equation** (2.4) and evolving them in physical space and time. The moments of the NDF are fields that don't depend on the phase space variables, but describe the low order statistics of the distribution in physical space. A moment transformation over the NDF can be written as

$$\mathfrak{M}^{(l,M,N)} = \int_{\mathbb{R}} \int_{\mathbb{R}^M} \int_{\mathbb{R}^3} \xi^l \boldsymbol{\theta}^{(M)} \mathbf{v}^{(N)} \mathfrak{F}(\xi, \boldsymbol{\theta}, \mathbf{v}) \mathrm{d}\mathbf{v}\mathrm{d}\boldsymbol{\theta}\mathrm{d}\xi, \tag{2.5}$$

and its application over the transport equation **Equation** (2.4) reads as

$$\int_{\mathbb{R}} \int_{\mathbb{R}^M} \int_{\mathbb{R}^3} \xi^l \boldsymbol{\theta}^{(M)} \mathbf{v}^{(N)} \frac{\partial \mathfrak{F}}{\partial t} \mathrm{d}\mathbf{v}\mathrm{d}\boldsymbol{\theta}\mathrm{d}\xi + \int_{\mathbb{R}} \int_{\mathbb{R}^M} \int_{\mathbb{R}^3} \xi^l \boldsymbol{\theta}^{(M)} \mathbf{v}^{(N)} \nabla_{\mathrm{x}} \cdot (\mathbf{v}\mathfrak{F}) \mathrm{d}\mathbf{v}\mathrm{d}\boldsymbol{\theta}\mathrm{d}\xi = \overline{\mathfrak{S}}. \tag{2.6}$$

Producing the set of moment transport equations:

$$\frac{\partial \mathfrak{M}^{(l,M,N)}}{\partial t} + \nabla_{\mathrm{x}} \cdot (\mathfrak{M}^{(l,M,N+1)}) = \overline{\mathfrak{S}}, \tag{2.7}$$

where

$$\begin{aligned} \overline{\mathfrak{S}} = \int_{\mathbb{R}} \int_{\mathbb{R}^M} \int_{\mathbb{R}^3} \xi^l \boldsymbol{\theta}^{(M)} \mathbf{v}^{(N)} \Big[ & - \nabla_{\xi} \cdot (\mathbf{G}(\xi, \boldsymbol{\theta}, \mathbf{v}) \mathfrak{F}) - \nabla_{\theta} \cdot (\mathbf{H}(\xi, \boldsymbol{\theta}, \mathbf{v}) \mathfrak{F}) \\ & - \nabla_{\mathbf{v}} \cdot (\mathbf{F}(\xi, \mathbf{v}) \mathfrak{F}) + \mathbb{C}[\mathfrak{F}, \mathfrak{F}] \Big] \mathrm{d}\mathbf{v}\mathrm{d}\boldsymbol{\theta}\mathrm{d}\xi. \end{aligned} \tag{2.8}$$

To put this in perspective and assign some physical meaning, assume an NDF distributed only in velocity space: $\mathfrak{F} = \mathfrak{F}((\mathbf{v}; \mathbf{x}, t)$, the rate $\mathbf{F}(\mathbf{v}; \mathbf{x}, t) = \mathbf{g}$ corresponds to the action of

body forces (gravity), and the rate of collisions, $\mathbb{C}[\mathfrak{F},\mathfrak{F}]$, is closed by the BKG (Bhatnagar-Gross-Krook) approximation:

$$\mathbb{C} = \frac{1}{\tau_c}(\mathfrak{F}^* - \mathfrak{F}). \tag{2.9}$$

Here $\tau_c$ represents the collision time scale and $\mathfrak{F}^*$ is the equilibrium distribution, given by

$$\mathfrak{F}^* = \frac{\langle m \rangle^{(0)}}{(2\pi\sigma^*)^{3/2}} \exp\left(-\frac{|\mathbf{v}-\overline{\mathbf{U}}_\mathbf{p}|^2}{2\sigma^*}\right). \tag{2.10}$$

$\langle m \rangle^{(0)}$ is the zero-order velocity moment, $\overline{\mathbf{U}}_\mathbf{p}$ is the mean particle velocity, and $\sigma^*$ is the equilibrium variance matrix. Let $\langle \mathfrak{m} \rangle^{(N)}$ be the particle velocity moments of order $N = n_1 + n_2 + n_3$ with $n_1, n_2, n_3$ the individual orders for each velocity component. The moments are defined as

$$\langle \mathfrak{m} \rangle^{(N)}(\mathbf{x},t) = \int_{\mathbb{R}^3} v_x^{n_1} v_y^{n_2} v_z^{n_3} \mathfrak{F}(\mathbf{v};\mathbf{x},t)\,\mathrm{d}\mathbf{v}. \tag{2.11}$$

Similarly, the N-order moments of the equilibrium distribution are given by

$$\Delta^{(N)}(\mathbf{x},t) = \int_{\mathbb{R}^3} v_x^{n_1} v_y^{n_2} v_z^{n_3} \mathfrak{F}^*(\mathbf{v};\mathbf{x},t)\,\mathrm{d}\mathbf{v}. \tag{2.12}$$

In this particular case, the velocity moment transport equation can be written as

$$\frac{\partial \langle \mathfrak{m} \rangle^{(N)}}{\partial t} + \nabla_\mathrm{x}(\langle \mathfrak{m} \rangle^{(N)+1}) = (N)\mathbf{g} \cdot \langle \mathfrak{m} \rangle^{(N)-1} + \frac{1}{\tau_c}(\Delta^{(N)} - \langle \mathfrak{m} \rangle^{(N)}). \tag{2.13}$$

More complex expressions for the rates $\mathbf{F}(\mathbf{v})$ and $\mathbb{C}[\mathfrak{F},\mathfrak{F}]$ can be proposed with no further complications on the formulation of the problem.[29,30,90]

**Equation** (2.7) and **Equation** (2.13) represent Eulerian models for the particulate phase obtained from the transport equations for the NDF given by **Equation** (2.4). The moments in these Eulerian models are related to physical quantities in the dispersed flow. For instance, the components of mean particle velocities are related to the first-order moments of the NDF:

$$\langle m_{1,0,0} \rangle^{(1)} \equiv \rho\overline{U}_x, \qquad \langle m_{0,1,0} \rangle^{(1)} \equiv \rho\overline{U}_y, \qquad \langle m_{0,0,1} \rangle^{(1)} \equiv \rho\overline{U}_z. \tag{2.14}$$

It is also possible to obtain the mean momentum and the granular temperature due to collisions (for collisional flows) from the second order moments.[61] It is important to realize that in order to solve for the Eulerian models presented, a priori knowledge of the NDF is necessary. In general, that information is not available and assumptions about the shape of the NDF are required in order to solve for the Eulerian model in **Equation** (2.7) and **Equation** (2.13).

## 2.3 Physics Models in the Dilute Regime

The different terms described in **Equation** (2.4), except for the first one (i), are related to phase-advection[c] physical models that describe the changes taking place in the particle property space. There are mainly three phase-advection phenomena that happen across most of the scales of the flow and describe most of the particle-related phenomena: mass transfer, heat transfer, and momentum transfer. A general representation of these rates is

$$\begin{aligned} \frac{\mathrm{d}\boldsymbol{\zeta}}{\mathrm{d}t} &= \mathbf{J}(\boldsymbol{\zeta}, t), \\ \boldsymbol{\zeta} &= [\xi, \boldsymbol{\theta}, \mathbf{v}], \\ &= [\xi, \theta_1 \cdots \theta_m, v_x, v_y, v_z], \end{aligned} \tag{2.15}$$

where $\boldsymbol{\zeta}$ represents all possible coordinates in phase space present in the system and $\mathbf{J}(\boldsymbol{\zeta})$ represents all the driving forces that advect the properties in phase space. This mathematical model accounts for the most common phenomena occurring in multiphase phenomena: crystallization and precipitation processes, stirred tanks reaction processes, reactive aerosol processes, fluidization processes, reactive particle laden processes, and many others. For instance, when $\zeta = m_p$ the particle mass, the rate of change of mass can be written as

$$\frac{\mathrm{d}m_p}{\mathrm{d}t} = M_w A_p \mathbf{J}_{m_p}, \tag{2.16}$$

where $\mathbf{J}$ is the molar flux per unit area and time of mass leaving or entering the particle surface. Most general mass transfer models for dispersed quantities have this functional form and, depending on the application, different degrees of approximations are made in order to relate the mass of the particles with the surface area.[8]

If energy is being exchanged between all the involved phases, the rate of heat transfer can be expressed as

$$\frac{\mathrm{d}H_p}{\mathrm{d}t} = A_p \mathbf{J}_Q, \tag{2.17}$$

---

[c] The term *phase-advection* refers to the advection of particle properties along a coordinate of the phase space: size, enthalpy, mass, composition, etc.

where $\mathbf{J}_Q$ is the heat flux per unit area from the surface of the particle to the fluid phase and vice versa. The enthalpy $H_p$ can be written in terms of the temperature of the particle as

$$\frac{\mathrm{d}(m_p C_p \theta_p)}{\mathrm{d}t} = A_p \mathbf{J}_Q. \tag{2.18}$$

The heat flux $\mathbf{J}_Q$ contains all the fluxes due to convection from and to the surface of the particles, radiation, and source terms that change the enthalpy of the particles, like chemical reactions. Some of these will be explored for a specific application in **Chapter 5**.

Body forces exerted over the dispersed phase result in momentum exchange between the fluid phase and the particles. The forces acting on the dispersed phase can be classified as: i) forces due to the motion of the particles; ii) forces due to the motion of the surrounding fluid; iii) forces on immersed particles independent of the motion of the particles or the motion of the fluid, and iv) forces on immersed particles independent of the motion of the particles and the motion of the fluid.[93] Among the most common forces we find: drag, added mass, Basset history, lift, gravity, and buoyancy.[8] The momentum exchange can be expressed as

$$\begin{aligned}
\frac{\mathrm{d}(m_p \overline{\mathbf{U}}_p)}{\mathrm{d}t} = & \underbrace{\frac{\pi}{8}\rho_f \xi^2 C_D (\mathbf{U}_f - \overline{\mathbf{U}}_p)|\mathbf{U}_f - \overline{\mathbf{U}}_p|}_{\text{drag}} \\
& + \underbrace{K_A \rho_f V_p \frac{\mathrm{d}(\mathbf{U}_f - \overline{\mathbf{U}}_p)}{\mathrm{d}t}}_{\text{added mass}} \\
& + \underbrace{K_B \xi^2 \sqrt{\pi \rho_f \mu_f} \int_{t_0}^{t} \frac{\mathrm{d}(\mathbf{U}_f - \overline{\mathbf{U}}_p)}{\mathrm{d}t} \frac{\mathrm{d}s}{\sqrt{t-s}}}_{\text{Basset history}} \\
& + \underbrace{K_L \mu_f \xi^2 (\mathbf{U}_f - \overline{\mathbf{U}}_p) \sqrt{\frac{\rho_f G_L}{\mu_f}}}_{\text{lift}} \\
& + \underbrace{\rho_p V_p \mathbf{g}}_{\text{Buoyancy}} \\
& - \underbrace{\rho_f V_p \mathbf{g}}_{\text{gravity}}.
\end{aligned} \tag{2.19}$$

In the applications considered in this research we are interested in the deterministic part of those forces and we are more focused on the drag force. Finally, in most processes, the

size of the particle is directly related to the mass and size changes can be accounted for, following the evolution of equations like **Equation** (2.16). If the particle density is assumed constant, an equation for the evolution of the size can be written as

$$\frac{\mathrm{d}\xi}{\mathrm{d}t} = \frac{M_w k_{A_p}}{3\rho_p k_{V_p}} \mathbf{J}_\xi, \tag{2.20}$$

where $k_{A_p}$ and $k_{V_p}$ relate the particle size with their area and volume, respectively, and account for particles not being completely spherical.[8]

Ramkrishna[94] provides explanation between the relationship of the physics models explained in **Section 2.3** and the terms in **Equation** (2.4). He characterizes the phase-space as composed by internal coordinates and external coordinates. External coordinates are composed by the variables of the physical space **x** while internal coordinates provide quantitative characterization of the distinguishing traits of the particles other than its location in physical space. Changes in internal coordinates refers to motion (advection) through the property space and they are given by

$$\begin{aligned} \mathbf{G}(\xi, \boldsymbol{\theta}, \mathbf{v}) &= \frac{\mathrm{d}\xi}{\mathrm{d}t} \\ \mathbf{H}(\xi, \boldsymbol{\theta}, \mathbf{v}) &= \frac{\mathrm{d}\boldsymbol{\theta}}{\mathrm{d}t} \\ \mathbf{F}(\xi, \boldsymbol{\theta}, \mathbf{v}) &= \frac{\mathrm{d}(m_p \overline{\mathbf{U}}_p)}{\mathrm{d}t}. \end{aligned} \tag{2.21}$$

These expressions appear in the RHS of **Equation** (2.8) and because the integration is performed over the entire phase-space, the single particle physics models presented can be used to describe the behavior of the entire particle population, therefore completing the general Eulerian model **Equation** (2.7).

## 2.4 Solution Methods for the Moment Equations

Once the feasibility of evolving the moments of the NDF instead of the distribution itself has been established, it is necessary to present solution methods for the proposed Eulerian moment model. A careful inspection of **Equation** (2.7) determines its hyperbolic characteristics, making it possible to use finite volumes for its numerical solution.[95] In reality, **Equation** (2.7) corresponds to an arbitrary system of PDE with an unspecified and arbitrary number of moments to transport. Clearly, for the Eulerian moment model to be useful, the number of moments to transport should be finite, but also should approximate

the particle behavior as accurately as possible.[d] Note that in **Equation** (2.13), that the convective flux appears in terms of higher order moments of velocity; this is true for the most general model, **Equation** (2.7), especially when particle velocity is one of the coordinates of phase space. In the following, the evolution of the techniques necessary to tackle the closure issue will be explained and will become the basis of the developments presented in this research.

### 2.4.1 The Quadrature Method of Moments

The quadrature method of moments (QMOM) is largely based on the the method of moments[42,96] in which the NDF is assumed to be locally known in order to achieve closure of the moment transport equations. Common choices for NDF in early applications were normal and log-normal distributions. For instance, in determining size distributions $r$ in dispersed flows, the NDF might be approximated as

$$\mathfrak{F}(r) = \frac{N_p}{\sigma r\sqrt{2\pi}} \exp\left[-\frac{1}{2\sigma^2}\ln\left(\frac{r}{r_0}\right)^2\right]. \tag{2.22}$$

The assumption of a presumed locally known pdfs limited the applicability of the method to the introduction of complex physics. QMOM[44] was developed to overcome this difficulty. In QMOM, low-order moments are transported and higher order moments are approximated using n-point Gaussian quadrature:

$$k\int_{\Omega_\xi} \xi^{k-1}\phi(\xi)f(\xi)\mathrm{d}\xi \approxeq k\sum_{\alpha=1}^{N} \langle\xi\rangle_\alpha^{k-1}\,\phi(\langle\xi\rangle_\alpha)w_\alpha. \tag{2.23}$$

In this case, closure for higher order moments was achieved through the variables of the quadrature approximation (weights $w_\alpha$ and abscissas $\langle\xi\rangle_\alpha$) and the assumption of presumed, analytical NDF was no longer necessary. In order to establish a relationship between the transported moments, the weights and abscissas, an inversion procedure is necessary. The technique is based on the Lanczos algorithm,[97,98] the product difference (PD) algorithm. Without the need to know the exact form of the NDF, the capabilities of the method of moments to represent more complex particulate phenomena were greatly extended. Although the range of applicability has been broadening[96,99–102] since its adoption,

[d] An infinity set of moment transport equations is equivalent to the direct solution of **Equation** (2.4).

the extension of the method to joint NDFs in more than 2 dimensions and simultaneous calculation of joint moments is still not straight forward.[43,103,104]

### 2.4.2 The Direct Quadrature Method of Moments

Fox[105] and Marchisio and Fox[43] proposed the direct quadrature method of moments (DQMOM) which overcame the limitations presented by QMOM. In this technique, the moment evolution equations from QMOM are further approximated by proposing evolution equations for the variables of the quadrature approximation, namely weights and abscissas. In doing so, a linear system of equations might arise depending on the physics considered in the problem (body forces, growth, chemical reaction, aggregation and breakage, etc.). Details of the formulation for monovariate flows and its multivariate extension can be found in the original reference.[43] Besides extending the number of internal coordinates handled by QMOM, the technique eliminated the need of an inversion algorithm at each time step. Given that the quadrature variables are directly evolved, closures are directly applied to hyperbolic or source terms.

Due to the hyperbolic nature of the evolution equations for the weights and abscissas, the numerics for the convective flux reconstruction play an important role on the validity of the technique.[106,107] Introduction of numerical errors in the evolution of weights and abscissas might yield unrealizable[e] moments,[8] which ultimately do not correspond to an accurate moment prediction. For the multivariate extension, another known issue is the choice of the multivariate moments; this choice is essentially arbitrary and some of the choices lead to unrealizable moments. Fox[62] numerically sampled a broad region of the weights and abscissas space in order to obtain a subspace of moments for which the matrix **A** is full rank. This subspace is called the *optimal moment set* and has been studied in up to 3 dimensions and 27 quadrature nodes. DQMOM has been proven successful for low Stoke particles,[50,51,53–56,108,109] however, in highly nonequilibrium flows with PTC, singularities might occur at finite Stokes numbers.[47]

---

[e] Moments outside the realizable region, where the NDF is not always positive.

### 2.4.3 The Two Point Quadrature-Based Moment Method

Inertial particles in turbulent flows tend to respond very slowly to fluid velocity fluctuations of the flow and the effect of body forces can cause the particles to cross trajectory into the paths with other particles and fluid eddies. This phenomena is called particle trajectory crossing (PTC) and it is usually a two-way interaction that affects fluid turbulence as well.[9,84,110] Hydrodynamic-based Eulerian models assume a monokinetic behaviour of the particle velocity, disregarding the possibility of multi-modal velocity distribution at the same location. At finite Stokes numbers,[f] PTC allows for multimodal velocity distributions, breaking the assumptions of the hydrodynamic models.[73] Advanced PDF and stochastic methods are required to estimate the effects of PTC.[9,110]

On the other hand, the major disadvantage of DQMOM regarding the conservation of moments and the loss of accuracy at finite Stokes numbers limits applicability of the technique, specially in dilute or moderately dilute flows, while QMOM has the advantage of evolving and close directly higher order moments, playing an important role on their numerical conservation. The development of a technique that evolved the moments directly and extendible to higher dimensions in phase space was the next logical step. Desjardins and Fox[47] formulated a two-point quadrature method for the evolution and closure of velocity moments; the closure was able to capture the effects of PTC and represent accurately moments up to second order. One of the advantages of the two-point quadratures is that the relationship between moments, weights, and abscissas is algebraic and calculating an inversion based on two quadrature nodes is numerically fast. On the contrary, the set of high-order moments for multidimensional extension is somewhat arbitrary and the choice might affecting the realizability of the moment space.

The integral nature of the moment transformation allows using kinetic schemes naturally in the numerical discretization and approximation of the moment transport equations. Desjardins et al.[29] first proposed a sufficient CFL-like[g] condition in order to preserve the moment space. This condition held up for first order numerical schemes, but not for higher order. Extension for higher order numerical schemes was given without proof.

---

[f] See **Section 2.1**.

[g] Courant -Friedrichs -Lewy condition for PDEs convergence.

Vikas et al.[111] presented a formal proposition in order to extend the technique to higher order numerical schemes. Although their results were not fully second or third order,[h] they showed improvement over first order results. Fox[30] extended the methodology to represent moments up to third order, the extension required to work with central moments and a rotation of the moment space, in order to perform the calculations. In both papers the numbers of nodes required to perform the moment transformation was of the form $\beta = 2^d$ where $d = [1, 2, 3]$ fixing (even restricting) the amount of nodes required for the calculation. In a similar way as in Fox,[30] Fox[46] extended the technique to represent velocity moments up to ninth order, showing accurate results applying the technique to Riemann solvers. One of the issues with these techniques is that the rotation matrices don't guarantee the positivity of the calculated weights or, in other words, the realizability of the moment space.

### 2.4.4 The Conditional Quadrature Method of Moments

An improvement over previous techniques was presented again in Yuan and Fox;[61] they proposed the conditional quadrature method of moments (CQMOM), which circumvented the need for regularization[i] used in the two-point quadrature technique. CQMOM guaranteed the positivity of the weights, directly related to the realizability of the moment space and the nonnegativity of the NDF. There are several fundamental concepts involved at the core of the technique; one of them is the use of conditioning in order to compute moments in different coordinated of the phase space, the other one is related to the accuracy of the inversion algorithm that improves upon the ones proposed in previous techniques; in its current form, CQMOM is capable of representing passive scalar variables[112,113] as well as kinetic variables (velocity).[61] In the original contribution, the method was proven to reproduce exactly N-point quadratures in velocity space, as well as providing reasonable good approximation to the moments of continuous distributions. A NDF can be written in terms of its conditional forms according to the Bayes rule, for instance:

$$\mathfrak{F}(\boldsymbol{\xi}, \mathbf{v}; \mathbf{x}, t) = \mathfrak{F}(\boldsymbol{\xi}; \mathbf{x}, t)\mathfrak{F}(\mathbf{v}|\boldsymbol{\xi}; \mathbf{x}, t). \tag{2.24}$$

[h] Quasi-second and quasi-third order, as they coined them.

[i] Basically using central moments and a space transformation (usually via a Cholesky decomposition) to reduce the number of moment variables.

This extension can be performed for every individual coordinate of the phase space. For each dimension a 1-dimensional algorithm is used in order to invert the conditional moments corresponding to that dimension to obtain the corresponding weights and abscissas; there is a potential reduction in computational cost compared to the use of multidimensional nonlinear solvers. On the downside, the number of computed quadrature nodes could increase the cost exponentially, limiting the applicability to very complex multiphysics systems and the natural extension to polydisperse systems is still an open question in this methodology.

### 2.4.5 The Extended Quadrature Method of Moments

Fox and co-workers developed further the Gaussian closures introduced by Chalons et al.[71] and explored new closures with other explicit NDFs forms. Yuan et al.[77] introduced the extended quadrature method of moments (EQMOM) to solve homogeneous population balances with different drift velocities (aggregation, breakage, condensation, and evaporation), although it is claimed in the paper that the technique also applies to spatially inhomogeneous population balances. The NDF is written in terms of a weighted sum of nonnegative distribution functions:

$$p_n(\xi) = \sum_{\alpha=1}^{N} w_\alpha \delta_\sigma(\xi, \xi_\alpha), \tag{2.25}$$

with the property

$$\lim_{\sigma \to 0} \delta_\sigma(\xi, \xi_\alpha) = \delta(\xi - \xi_\alpha). \tag{2.26}$$

The functions $\delta_\sigma(\xi, \xi_\alpha)$ can be the gamma distribution

$$\delta_\sigma(\xi, \xi_\alpha) = \frac{\xi^{\lambda_\sigma - 1} \exp(-\xi/\sigma)}{\Gamma(\lambda_\sigma)\sigma^{\lambda_\sigma}}, \tag{2.27}$$

or beta distribution

$$\delta_\sigma(\xi, \xi_\alpha) = \frac{\xi^{\lambda_\sigma - 1}(1-\xi)^{\mu_\sigma - 1}}{B(\lambda_\sigma, \mu_\sigma)}. \tag{2.28}$$

Details of the formulation are given in Yuan et al.[77] This technique is promising in the sense that realizability is absolutely guaranteed and size-velocity correlations are easier to deal with.

### 2.4.6 Sectional and Multifluid Methods

In the same way that Fox and colleagues were exploring the ideas of McGraw on moment closures and quadrature methods for kinetic and population balance equations that resulted in all the publications cited before, Massot, Villedieu, and colleagues were exploring the ideas of Tambour [114] on sectional methods from an Eulerian point of view. [63] Laurent et al. [115] presented an extension of the sectional method introduced by Tambour [114] in order to treat polydispersed flows in dense gas-liquid sprays. The method approximated the NDF in two different independent distributions: size and velocity.

$$\mathfrak{F}(\xi, \mathbf{v}; \mathbf{x}, t) = n(\xi; \mathbf{x}, t)\delta(\mathbf{v} - \overline{\mathbf{U}}_p(\xi; \mathbf{x}, t)) \tag{2.29}$$

$n(\xi; \mathbf{x}, t)$ is further discretized into different size sections; in each section, evolution equations for the particle concentration and the mean momentum were developed. Sections could exchange mass and momentum but only an averaged velocity was calculated to compute to momentum exchange; due to this monokinetic approximation, the technique is unable to capture PTC. This idea was developed into the so-called Eulerian multifluid models. de Chaisemartin et al. [116] coupled the methodology of Desjardins et al. [29] for velocity moments with the sectional method of Laurent et al. [115] and were able to capture PTC for a polydisperse spray flow. Research has revolved around these techniques focusing on different issues and tackling different challenges. On one hand, the exploration of the hyperbolic nature of the moment space and its consequences on PTC has been an issue in turbulence applications. [117] On the other hand, research on realizable, high order numerical schemes capable of preserving the moment space and represent high order moments, has caught the attention of many researchers due to its impact on the numerical representation of multiphase systems. [68,76,118–120] Multifluid methods have been also studied for different ranges of Knudsen and Stokes numbers using explicit Gaussian closures in order to determine higher order moments. [65,71,72,74,75,116,121] One of the most challenging tasks in this method (and in Fox's method for that matter) is the representation of the rates of change of properties in phase space in terms of the computed moments, these rates usually involve integrals or variable dependencies that make multiphase system even more difficult to simulate; for instance, some of the most common phenomena in dilute and moderately dilute sprays are related to drag, coalescence, evaporation and splashing. [67,69,70,78] When

polydispersity is taken into account, correlations between particle size and particle velocity arise and PTC can become a common phenomena difficult to simulate.[122] Schneider et al.[69] and Schneider et al.[70] have also coupled the Eulerian-Multifluid with a quadrature-based moment method for the velocity coordinate in order to capture PTC. The techniques developed in this dissertation take elements from the ideas on quadrature methods developed by Fox and colleagues and the ideas on sectional methods from Schneider and colleagues. In what follows, two new formalisms for Eulerian moment methods will be developed in **Chapter 3** and **Chapter 4** and some of their application will be presented in **Chapter 5**.

# CHAPTER 3

# A NOVEL FORMULATION OF THE METHOD OF MOMENTS: THE DIRECT QUADRATURE OF CONDITIONAL MOMENTS

As described in **Section 2.4** and Yuan and Fox,[61] CQMOM accurately describe the moment evolution of the velocity fields in a variety of physical scenarios. The most interesting physical systems usually involve the distribution of scalar properties and, among the most important, size distribution, which determines the polydispersity character of the system. Under a particular set of conditions it is possible to extend CQMOM to other scalar fields, although not in a straightforward way. Indeed, for every new coordinate in phase space included in the analysis, the number of quadrature nodes required for the additional inversion increases and the cost also increases non-linearly. On the other hand, the original DQMOM has a low computational cost as a quadrature method, but the evolution of the weights and abscissas might degrade the accuracy of higher order moments, especially when kinetic variables (velocities) are considered. It would be desirable to have a trade off between the accurate representation of the moment space by CQMOM at a lower cost in polydisperse systems where scalar rates are determinant for the evolution of the system. A new moment method formulation based on CQMOM[61] and DQMOM[43,80,123–125] is explained, in which the basic idea is to evolve the velocity fields with CQMOM and the scalar fields with a DQMOM-like method. The advantage of this formulation lies in the linear increase of the overall computational cost when scalar transport fields are added.

## 3.1 NDF Approximation and Moment Closure

Starting from the transport equation for the joint velocity-scalar particle distribution function, $\mathfrak{F} = \mathfrak{F}(\xi, \boldsymbol{\theta}, \mathbf{v}; \mathbf{x}, t)$ we have

$$\frac{\partial \mathfrak{F}}{\partial t} + \nabla_{\mathrm{x}} \cdot (\mathbf{v}\mathfrak{F}) = \mathfrak{S}, \tag{3.1}$$

where the right hand side is represented by

$$\mathfrak{S} = -\nabla_{\xi} \cdot (\mathbf{G}(\xi, \boldsymbol{\theta}, \mathbf{v})\mathfrak{F}) - \nabla_{\theta} \cdot (\mathbf{H}(\xi, \boldsymbol{\theta}, \mathbf{v})\mathfrak{F}) - \nabla_{\mathrm{v}} \cdot (\mathbf{F}(\xi, \mathbf{v})\mathfrak{F}) + \mathbb{C}[\mathfrak{F}, \mathfrak{F}]. \tag{3.2}$$

The meaning of each term was explained in **Section 2.2**. In its current form, the transport equation **Equation** (3.1) has more dimensions than those that can be represented on regular CFD codes; the root of the problem is essentially the lack of knowledge of the NDF and a common solution is to provide an approximation that allows dealing with the problem in physical space. First, we rewrite the NDF in a more convenient form according to Bayes' rule:

$$\mathfrak{F}(\xi, \boldsymbol{\theta}, \mathbf{v}) = \mathfrak{g}(\xi)\mathfrak{f}(\boldsymbol{\theta}|\xi)\mathfrak{F}(\mathbf{v}|\xi, \boldsymbol{\theta}). \tag{3.3}$$

Here, the approximations to the shape of the marginal and conditional distributions of size, velocity, and other scalars are to be considered separately as expressed mathematically in equation **Equation** (3.3).

## 3.2 Joint Moment Transport Equations

**Equation** (3.3) can be replaced directly into equation **Equation** (3.1) to obtain

$$\frac{\partial}{\partial t}(\mathfrak{g}(\xi)\mathfrak{f}(\boldsymbol{\theta}|\xi)\mathfrak{F}(\mathbf{v}|\xi, \boldsymbol{\theta})) + \nabla_{\mathrm{x}} \cdot (\mathbf{v}\mathfrak{g}(\xi)\mathfrak{f}(\boldsymbol{\theta}|\xi)\mathfrak{F}(\mathbf{v}|\xi, \boldsymbol{\theta})) = \mathfrak{S}. \tag{3.4}$$

Using the chain rule for derivatives, equation **Equation** (3.4) can be rewritten as

$$\begin{aligned} &\Big[\mathfrak{g}(\xi)\mathfrak{f}(\boldsymbol{\theta}|\xi)\frac{\partial}{\partial t}(\mathfrak{F}(\mathbf{v}|\xi, \boldsymbol{\theta})) + \mathfrak{F}(\mathbf{v}|\xi, \boldsymbol{\theta})\frac{\partial}{\partial t}(\mathfrak{g}(\xi)\mathfrak{f}(\boldsymbol{\theta}|\xi))\Big] \\ &\quad + \Big[\mathfrak{g}(\xi)\mathfrak{f}(\boldsymbol{\theta}|\xi)\nabla_{\mathrm{x}} \cdot (\mathbf{v}\mathfrak{F}(\mathbf{v}|\xi, \boldsymbol{\theta})) + \mathfrak{F}(\mathbf{v}|\xi, \boldsymbol{\theta})\nabla_{\mathrm{x}} \cdot (\mathbf{v}\mathfrak{g}(\xi)\mathfrak{f}(\boldsymbol{\theta}|\xi))\Big] = \mathfrak{S}. \end{aligned} \tag{3.5}$$

**Equation** (3.5) can be reorganized as

$$\begin{aligned} &\mathfrak{g}(\xi)\mathfrak{f}(\boldsymbol{\theta}|\xi)\Big[\frac{\partial}{\partial t}(\mathfrak{F}(\mathbf{v}|\xi, \boldsymbol{\theta})) + \nabla_{\mathrm{x}} \cdot (\mathbf{v}\mathfrak{F}(\mathbf{v}|\xi, \boldsymbol{\theta}))\Big] \\ &\quad + \mathfrak{F}(\mathbf{v}|\xi, \boldsymbol{\theta})\Big[\frac{\partial}{\partial t}(\mathfrak{g}(\xi)\mathfrak{f}(\boldsymbol{\theta}|\xi)) + \nabla_{\mathrm{x}} \cdot (\mathbf{v}\mathfrak{g}(\xi)\mathfrak{f}(\boldsymbol{\theta}|\xi))\Big] = \mathfrak{S}. \end{aligned} \tag{3.6}$$

Now, the approximation reads as

$$\begin{aligned} \mathfrak{F}(\xi, \boldsymbol{\theta}, \mathbf{v}) &\approx \sum_{\alpha=1}^{N} w_{\alpha} g(\xi, \xi_{\alpha}) f(\boldsymbol{\theta}, \boldsymbol{\theta}_{\alpha}|\xi)\mathfrak{F}(\mathbf{v}|\xi, \boldsymbol{\theta}) \\ &\approx \sum_{\alpha=1}^{N} w_{\alpha} g(\xi, \xi_{\alpha}) f(\boldsymbol{\theta}, \boldsymbol{\theta}_{\alpha})\mathfrak{F}(\mathbf{v}|\xi). \end{aligned} \tag{3.7}$$

Here, it is also assumed that the conditional velocity distribution is affected mainly by size and that the marginal distribution of the rest of the scalars are independent of the size distribution. With this approximation, **Equation** (3.5) reads as

$$\sum_{\alpha}^{N} w_\alpha \mathfrak{g}(\xi,\xi_\alpha)\mathfrak{f}(\boldsymbol{\theta},\boldsymbol{\theta}_\alpha)\Big[\frac{\partial}{\partial t}(\mathfrak{F}(\mathbf{v}|\xi))+\nabla_{\mathrm{x}}\cdot(\mathbf{v}\mathfrak{F}(\mathbf{v}|\xi))\Big] \tag{3.8}$$
$$+\sum_{\alpha}^{N}\mathfrak{F}(\mathbf{v}|\xi)\Big[\frac{\partial}{\partial t}(w_\alpha\mathfrak{g}(\xi,\xi_\alpha)\mathfrak{f}(\boldsymbol{\theta},\boldsymbol{\theta}_\alpha))+\nabla_{\mathrm{x}}\cdot(\mathbf{v}w_\alpha\mathfrak{g}(\xi,\xi_\alpha)\mathfrak{f}(\boldsymbol{\theta},\boldsymbol{\theta}_\alpha))\Big]=\mathfrak{S}.$$

Before making more assumptions to further simplify the complexity of the NDF, let us reduce the dimensionality of both **Equation** (3.8) and **Equation** (3.1) by applying the moment transformation:

$$\mathfrak{M}^{(l,M,N)}=\int_{\Omega_\xi}\int_{\Omega_\theta}\int_{\Omega_v}\xi^l\boldsymbol{\theta}^{(M)}\mathbf{v}^{(N)}\mathfrak{F}(\xi,\boldsymbol{\theta},\mathbf{v})\mathrm{d}\xi\mathrm{d}\boldsymbol{\theta}\mathrm{d}\mathbf{v}. \tag{3.9}$$

With the moment transformation, **Equation** (3.1) reads as

$$\int_{\Omega_\xi}\int_{\Omega_\theta}\int_{\Omega_v}\xi^l\boldsymbol{\theta}^{(M)}\mathbf{v}^{(N)}\frac{\partial\mathfrak{F}}{\partial t}\mathrm{d}\xi\mathrm{d}\boldsymbol{\theta}\mathrm{d}\mathbf{v}+\int_{\Omega_\xi}\int_{\Omega_\theta}\int_{\Omega_v}\xi^l\boldsymbol{\theta}^{(M)}\mathbf{v}^{(N)}\nabla_{\mathrm{x}}\cdot(\mathbf{v}\mathfrak{F})\mathrm{d}\xi\mathrm{d}\boldsymbol{\theta}\mathrm{d}\mathbf{v} \tag{3.10}$$
$$=\int_{\Omega_\xi}\int_{\Omega_\theta}\int_{\Omega_v}\xi^l\boldsymbol{\theta}^{(M)}\mathbf{v}^{(N)}\mathfrak{S}\mathrm{d}\xi\mathrm{d}\boldsymbol{\theta}\mathrm{d}\mathbf{v},$$

and according to **Equation** (3.9)

$$\frac{\partial\mathfrak{M}^{(l,M,N)}}{\partial t}+\nabla_{\mathrm{x}}\cdot\mathfrak{M}^{(l,M,N+1)}=\overline{\mathfrak{S}}, \tag{3.11}$$

where

$$\overline{\mathfrak{S}}=\int_{\Omega_\xi}\int_{\Omega_\theta}\int_{\Omega_v}\xi^l\boldsymbol{\theta}^{(M)}\mathbf{v}^{(N)}\mathfrak{S}\mathrm{d}\xi\mathrm{d}\boldsymbol{\theta}\mathrm{d}\mathbf{v}. \tag{3.12}$$

Now, applying the moment transformation to **Equation** (3.8):

$$\sum_{\alpha=1}^{N} w_\alpha\int_{\Omega_\xi}\int_{\Omega_\theta}\int_{\Omega_v}\xi^l\boldsymbol{\theta}^{(M)}\mathbf{v}^{(N)}\mathfrak{g}(\xi,\xi_\alpha)\mathfrak{f}(\boldsymbol{\theta},\boldsymbol{\theta}_\alpha)\Big[\frac{\partial}{\partial t}(\mathfrak{F}(\mathbf{v}|\xi))+\nabla_{\mathrm{x}}\cdot(\mathbf{v}\mathfrak{F}(\mathbf{v}|\xi))\Big]\mathrm{d}\xi\mathrm{d}\boldsymbol{\theta}\mathrm{d}\mathbf{v} \tag{3.13}$$
$$+\sum_{\alpha=1}^{N}\int_{\Omega_\xi}\int_{\Omega_\theta}\int_{\Omega_v}\xi^l\boldsymbol{\theta}^{(M)}\mathbf{v}^{(N)}\mathfrak{F}(\mathbf{v}|\xi)\Big[\frac{\partial}{\partial t}(w_\alpha\mathfrak{g}(\xi,\xi_\alpha)\mathfrak{f}(\boldsymbol{\theta},\boldsymbol{\theta}_\alpha))+$$
$$\nabla_{\mathrm{x}}\cdot(\mathbf{v}w_\alpha\mathfrak{g}(\xi,\xi_\alpha)\mathfrak{f}(\boldsymbol{\theta},\boldsymbol{\theta}_\alpha))\Big]\mathrm{d}\xi\mathrm{d}\boldsymbol{\theta}\mathrm{d}\mathbf{v}=\int_{\Omega_\xi}\int_{\Omega_\theta}\int_{\Omega_v}\xi^l\boldsymbol{\theta}^{(M)}\mathbf{v}^{(N)}\mathfrak{S}\mathrm{d}\xi\mathrm{d}\boldsymbol{\theta}\mathrm{d}\mathbf{v}.$$

By comparing **Equation** (3.9) and **Equation** (3.13) we write

$$\frac{\partial \mathfrak{M}^{(l,M,N)}}{\partial t} + \nabla_{\mathrm{x}} \cdot \mathfrak{M}^{(l,M,N+1)} = \tag{3.14}$$
$$\sum_{\alpha=1}^{N} w_\alpha \int_{\Omega_\xi} \int_{\Omega_\theta} \int_{\Omega_v} \xi^l \boldsymbol{\theta}^{(M)} \mathbf{v}^{(N)} \mathfrak{g}(\xi, \xi_\alpha) \mathfrak{f}(\boldsymbol{\theta}, \boldsymbol{\theta}_\alpha) \Big[ \frac{\partial}{\partial t} (\mathfrak{F}(\mathbf{v}|\xi)) + \nabla_{\mathrm{x}} \cdot (\mathbf{v} \mathfrak{F}(\mathbf{v}|\xi)) \Big] \mathrm{d}\xi \mathrm{d}\boldsymbol{\theta} \mathrm{d}\mathbf{v}$$
$$+ \sum_{\alpha=1}^{N} \int_{\Omega_\xi} \int_{\Omega_\theta} \int_{\Omega_v} \xi^l \boldsymbol{\theta}^{(M)} \mathbf{v}^{(N)} \mathfrak{F}(\mathbf{v}|\xi) \Big[ \frac{\partial}{\partial t} (w_\alpha \mathfrak{g}(\xi, \xi_\alpha) \mathfrak{f}(\boldsymbol{\theta}, \boldsymbol{\theta}_\alpha)) +$$
$$\nabla_{\mathrm{x}} \cdot (\mathbf{v} w_\alpha \mathfrak{g}(\xi, \xi_\alpha) \mathfrak{f}(\boldsymbol{\theta}, \boldsymbol{\theta}_\alpha)) \Big] \mathrm{d}\xi \mathrm{d}\boldsymbol{\theta} \mathrm{d}\mathbf{v} = \int_{\Omega_\xi} \int_{\Omega_\theta} \int_{\Omega_v} \xi^l \boldsymbol{\theta}^{(M)} \mathbf{v}^{(N)} \mathfrak{S} \mathrm{d}\xi \mathrm{d}\boldsymbol{\theta} \mathrm{d}\mathbf{v}.$$

Now reorganizing the integrals in **Equation** (3.14):

$$\frac{\partial \mathfrak{M}^{(l,M,N)}}{\partial t} + \nabla_{\mathrm{x}} \cdot \mathfrak{M}^{(l,M,N+1)} = \tag{3.15}$$
$$\sum_{\alpha=1}^{N} w_\alpha \int_{\Omega_\xi} \xi^l \mathfrak{g}(\xi, \xi_\alpha) \int_{\Omega_\theta} \boldsymbol{\theta}^{(M)} \mathfrak{f}(\boldsymbol{\theta}, \boldsymbol{\theta}_\alpha) \int_{\Omega_v} \mathbf{v}^{(N)} \Big[ \frac{\partial}{\partial t} (\mathfrak{F}(\mathbf{v}|\xi)) + \nabla_{\mathrm{x}} \cdot (\mathbf{v} \mathfrak{F}(\mathbf{v}|\xi)) \Big] \mathrm{d}\mathbf{v} \mathrm{d}\boldsymbol{\theta} \mathrm{d}\xi$$
$$+ \sum_{\alpha=1}^{N} \int_{\Omega_v} \mathbf{v}^{(N)} \mathfrak{F}(\mathbf{v}|\xi) \int_{\Omega_\xi} \int_{\Omega_\theta} \xi^l \boldsymbol{\theta}^{(M)} \Big[ \frac{\partial}{\partial t} (w_\alpha \mathfrak{g}(\xi, \xi_\alpha) \mathfrak{f}(\boldsymbol{\theta}, \boldsymbol{\theta}_\alpha)) +$$
$$\nabla_{\mathrm{x}} \cdot (\mathbf{v} w_\alpha \mathfrak{g}(\xi, \xi_\alpha) \mathfrak{f}(\boldsymbol{\theta}, \boldsymbol{\theta}_\alpha)) \Big] \mathrm{d}\xi \mathrm{d}\boldsymbol{\theta} \mathrm{d}\mathbf{v}.$$

The transport equations for the scalar marginal distributions $\mathfrak{g}$ and $\mathfrak{f}$ present terms that depend on variables of the phase space. Additional treatment is required for those equations. For instance, the right hand side of **Equation** (3.15) has the following transport equation

$$\frac{\partial}{\partial t} (w_\alpha \mathfrak{g}(\xi, \xi_\alpha) \mathfrak{f}(\boldsymbol{\theta}, \boldsymbol{\theta}_\alpha)) + \nabla_{\mathrm{x}} \cdot (\mathbf{v} w_\alpha \mathfrak{g}(\xi, \xi_\alpha) \mathfrak{f}(\boldsymbol{\theta}, \boldsymbol{\theta}_\alpha)), \tag{3.16}$$

which describes the transport characteristics of the marginal distribution of size and other scalars. By applying the chain rule for derivatives it is possible to arrive at the following expression

$$\frac{\partial}{\partial t} (w_\alpha \mathfrak{g}(\xi, \xi_\alpha) \mathfrak{f}(\boldsymbol{\theta}, \boldsymbol{\theta}_\alpha)) + \nabla_{\mathrm{x}} \cdot (\mathbf{v} w_\alpha \mathfrak{g}(\xi, \xi_\alpha) \mathfrak{f}(\boldsymbol{\theta}, \boldsymbol{\theta}_\alpha)) = \tag{3.17}$$
$$w_\alpha \mathfrak{g}(\xi, \xi_\alpha) \Big[ \frac{\partial}{\partial t} \mathfrak{f}(\boldsymbol{\theta}, \boldsymbol{\theta}_\alpha) + \mathbf{v} \cdot \nabla_{\mathrm{x}} \mathfrak{f}(\xi, \xi_\alpha) \Big] + w_\alpha \mathfrak{f}(\boldsymbol{\theta}, \boldsymbol{\theta}_\alpha) \Big[ \frac{\partial}{\partial t} \mathfrak{g}(\xi, \xi_\alpha)$$
$$+ \mathbf{v} \cdot \nabla_{\mathrm{x}} (\mathfrak{g}(\xi, \xi_\alpha)) \Big] + \mathfrak{g}(\xi, \xi_\alpha) \mathfrak{f}(\boldsymbol{\theta}, \boldsymbol{\theta}_\alpha) \Big[ \frac{\partial w_\alpha}{\partial t} + \mathbf{v} \cdot \nabla_{\mathrm{x}} (w_\alpha) \Big].$$

The functions $\mathfrak{g}(\xi, \xi_\alpha)$ and $\mathfrak{f}(\boldsymbol{\theta}, \boldsymbol{\theta}_\alpha)$ are also implicit functions of physical space and time and an additional application of the chain rule is necessary in order to obtain derivatives as functions of space and time only. For instance, for the function $\mathfrak{g}$:

$$\frac{\partial}{\partial t} \mathfrak{g}(\xi, \xi_\alpha(\mathbf{x}, t)) = \mathfrak{g}'(\xi, \xi_\alpha(\mathbf{x}, t)) \frac{\partial \xi_\alpha(\mathbf{x}, t)}{\partial t}, \tag{3.18}$$

where

$$\mathfrak{g}'(\xi,\xi_\alpha) = \pm\frac{\mathrm{d}}{\mathrm{d}\xi}\mathfrak{g}(\xi,\xi_\alpha), \tag{3.19}$$

is the Jacobian of function $\mathfrak{g}(\xi,\xi_\alpha)$. With this transformation the transport equation reads

$$\begin{aligned}\frac{\partial}{\partial t}(w_\alpha\mathfrak{g}(\xi,\xi_\alpha)\mathfrak{f}(\boldsymbol{\theta},\boldsymbol{\theta}_\alpha)) + \nabla_{\mathrm{x}}\cdot(\mathbf{v}w_\alpha\mathfrak{g}(\xi,\xi_\alpha)\mathfrak{f}(\boldsymbol{\theta},\boldsymbol{\theta}_\alpha)) = \\ \mathfrak{g}(\xi,\xi_\alpha)\mathfrak{f}'(\xi,\xi_\alpha)\Big[w_\alpha\frac{\boldsymbol{\theta}_\alpha}{\partial t} + w_\alpha\mathbf{v}\cdot\nabla_{\mathrm{x}}(\boldsymbol{\theta}_\alpha)\Big] \\ + \mathfrak{g}'(\xi,\xi_\alpha)\mathfrak{f}(\boldsymbol{\theta},\boldsymbol{\theta}_\alpha)\Big[w_\alpha\frac{\partial\xi_\alpha}{\partial t} + w_\alpha\mathbf{v}\cdot\nabla_{\mathrm{x}}(\xi_\alpha)\Big] \\ + \mathfrak{g}(\xi,\xi_\alpha)\mathfrak{f}(\boldsymbol{\theta},\boldsymbol{\theta}_\alpha)\Big[\frac{\partial w_\alpha}{\partial t} + \mathbf{v}\cdot\nabla_{\mathrm{x}}(w_\alpha)\Big].\end{aligned} \tag{3.20}$$

DQMOM-like equations can be obtained by rearranging and applying the chain rule to the scalar transport equation:

$$\begin{aligned}&\frac{\partial}{\partial t}(w_\alpha\mathfrak{g}(\xi,\xi_\alpha)\mathfrak{f}(\boldsymbol{\theta},\boldsymbol{\theta}_\alpha)) + \nabla_{\mathrm{x}}\cdot(\mathbf{v}w_\alpha\mathfrak{g}(\xi,\xi_\alpha)\mathfrak{f}(\boldsymbol{\theta},\boldsymbol{\theta}_\alpha)) \\ &= \mathfrak{g}(\xi,\xi_\alpha)\mathfrak{f}'(\xi,\xi_\alpha)\Big[\frac{\partial(w_\alpha\boldsymbol{\theta}_\alpha)}{\partial t} + \mathbf{v}\cdot\nabla_{\mathrm{x}}(w_\alpha\boldsymbol{\theta}_\alpha)\Big] \\ &+ \mathfrak{g}'(\xi,\xi_\alpha)\mathfrak{f}(\boldsymbol{\theta},\boldsymbol{\theta}_\alpha)\Big[\frac{\partial(w_\alpha\xi_\alpha)}{\partial t} + \mathbf{v}\cdot\nabla_{\mathrm{x}}(w_\alpha\xi_\alpha)\Big] \\ &+ \Big(\mathfrak{g}(\xi,\xi_\alpha)\mathfrak{f}(\boldsymbol{\theta},\boldsymbol{\theta}_\alpha) - \boldsymbol{\theta}_\alpha\mathfrak{g}(\xi,\xi_\alpha)\mathfrak{f}'(\boldsymbol{\theta},\boldsymbol{\theta}_\alpha) - \xi_\alpha\mathfrak{g}'(\xi,\xi_\alpha)\mathfrak{f}(\boldsymbol{\theta},\boldsymbol{\theta}_\alpha)\Big)\Big[\frac{\partial w_\alpha}{\partial t} + \mathbf{v}\cdot\nabla_{\mathrm{x}}(w_\alpha)\Big].\end{aligned} \tag{3.21}$$

Now replacing **Equation** (3.21) with **Equation** (3.15):

$$\begin{aligned}&\frac{\partial\mathfrak{M}^{(l,M,N)}}{\partial t} + \nabla_{\mathrm{x}}\cdot\mathfrak{M}^{(l,M,N+1)} = \\ &\sum_{\alpha=1}^{N_n} w_\alpha\int_{\Omega_\xi}\xi^l\mathfrak{g}(\xi,\xi_\alpha)\int_{\Omega_\theta}\boldsymbol{\theta}^{(M)}\mathfrak{f}(\boldsymbol{\theta},\boldsymbol{\theta}_\alpha)\int_{\Omega_v}\mathbf{v}^{(N)}\Big[\frac{\partial}{\partial t}(\mathfrak{F}(\mathbf{v}|\xi)) + \nabla_{\mathrm{x}}\cdot(\mathbf{v}\mathfrak{F}(\mathbf{v}|\xi))\Big]\mathrm{d}\mathbf{v}\mathrm{d}\boldsymbol{\theta}\mathrm{d}\xi \\ &+ \sum_{\alpha=1}^{N_n}\int_{\Omega_\xi}\xi^l\mathfrak{g}(\xi,\xi_\alpha)\int_{\Omega_\theta}\boldsymbol{\theta}^{(M)}\mathfrak{f}'(\boldsymbol{\theta},\boldsymbol{\theta}_\alpha)\int_{\Omega_v}\mathbf{v}^{(N)}\mathfrak{F}(\mathbf{v}|\xi)\Big[\frac{\partial(w_\alpha\boldsymbol{\theta}_\alpha)}{\partial t} + \mathbf{v}\cdot\nabla_{\mathrm{x}}(w_\alpha\boldsymbol{\theta}_\alpha)\Big]\mathrm{d}\mathbf{v}\mathrm{d}\boldsymbol{\theta}\mathrm{d}\xi \\ &+ \sum_{\alpha=1}^{N_n}\int_{\Omega_\xi}\xi^l\mathfrak{g}'(\xi,\xi_\alpha)\int_{\Omega_\theta}\boldsymbol{\theta}^{(M)}\mathfrak{f}(\boldsymbol{\theta},\boldsymbol{\theta}_\alpha)\int_{\Omega_v}\mathbf{v}^{(N)}\mathfrak{F}(\mathbf{v}|\xi)\Big[\frac{\partial(w_\alpha\xi_\alpha)}{\partial t} + \mathbf{v}\cdot\nabla_{\mathrm{x}}(w_\alpha\xi_\alpha)\Big]\mathrm{d}\mathbf{v}\mathrm{d}\boldsymbol{\theta}\mathrm{d}\xi \\ &+ \sum_{\alpha=1}^{N_n}\int_{\Omega_\xi}\xi^l\mathfrak{g}(\xi,\xi_\alpha)\int_{\Omega_\theta}\boldsymbol{\theta}^{(M)}\mathfrak{f}(\boldsymbol{\theta},\boldsymbol{\theta}_\alpha)\int_{\Omega_v}\mathbf{v}^{(N)}\mathfrak{F}(\mathbf{v}|\xi)\Big[\frac{\partial w_\alpha}{\partial t} + \mathbf{v}\cdot\nabla_{\mathrm{x}}(w_\alpha)\Big]\mathrm{d}\mathbf{v}\mathrm{d}\boldsymbol{\theta}\mathrm{d}\xi \\ &- \sum_{\alpha=1}^{N_n}\boldsymbol{\theta}_\alpha\int_{\Omega_\xi}\xi^l\mathfrak{g}(\xi,\xi_\alpha)\int_{\Omega_\theta}\boldsymbol{\theta}^{(M)}\mathfrak{f}'(\boldsymbol{\theta},\boldsymbol{\theta}_\alpha)\int_{\Omega_v}\mathbf{v}^{(N)}\mathfrak{F}(\mathbf{v}|\xi)\Big[\frac{\partial w_\alpha}{\partial t} + \mathbf{v}\cdot\nabla_{\mathrm{x}}(w_\alpha)\Big]\mathrm{d}\mathbf{v}\mathrm{d}\boldsymbol{\theta}\mathrm{d}\xi \\ &- \sum_{\alpha=1}^{N_n}\xi_\alpha\int_{\Omega_\xi}\xi^l\mathfrak{g}'(\xi,\xi_\alpha)\int_{\Omega_\theta}\boldsymbol{\theta}^{(M)}\mathfrak{f}(\boldsymbol{\theta},\boldsymbol{\theta}_\alpha)\int_{\Omega_v}\mathbf{v}^{(N)}\mathfrak{F}(\mathbf{v}|\xi)\Big[\frac{\partial w_\alpha}{\partial t} + \mathbf{v}\cdot\nabla_{\mathrm{x}}(w_\alpha)\Big]\mathrm{d}\mathbf{v}\mathrm{d}\boldsymbol{\theta}\mathrm{d}\xi.\end{aligned} \tag{3.22}$$

Note the dependency of the conditional velocity moment transport equation on size and the dependency of the scalar transport equation on velocity in **Equation** (3.22).

### 3.2.1 Right Hand Side Treatment

The integration of **Equation** (3.2) is represented by **Equation** (3.12) which in turn can be written as

$$\begin{aligned}\overline{\mathfrak{S}} = &-\int_{\Omega_\xi}\int_{\Omega_\theta}\int_{\Omega_v}\xi^l\boldsymbol{\theta}^{(M)}\mathbf{v}^{(N)}\nabla_\xi\cdot(\mathbf{G}\mathfrak{F}(\xi,\boldsymbol{\theta},\mathbf{v}))\mathrm{d}\mathbf{v}\mathrm{d}\boldsymbol{\theta}\mathrm{d}\xi \\ &-\int_{\Omega_\xi}\int_{\Omega_\theta}\int_{\Omega_v}\xi^l\boldsymbol{\theta}^{(M)}\mathbf{v}^{(N)}\nabla_\theta\cdot(\mathbf{H}\mathfrak{F}(\xi,\boldsymbol{\theta},\mathbf{v}))\mathrm{d}\mathbf{v}\mathrm{d}\boldsymbol{\theta}\mathrm{d}\xi \\ &-\int_{\Omega_\xi}\int_{\Omega_\theta}\int_{\Omega_v}\xi^l\boldsymbol{\theta}^{(M)}\mathbf{v}^{(N)}\nabla_{\mathrm{v}}\cdot(\mathbf{F}\mathfrak{F}(\xi,\boldsymbol{\theta},\mathbf{v}))\mathrm{d}\mathbf{v}\mathrm{d}\boldsymbol{\theta}\mathrm{d}\xi.\end{aligned} \tag{3.23}$$

Replacing the approximation to the NDF, **Equation** (3.3):

$$\begin{aligned}\overline{\mathfrak{S}} = &-\sum_{\alpha=1}^{N_n}\int_{\Omega_\xi}\int_{\Omega_\theta}\int_{\Omega_v}\xi^l\boldsymbol{\theta}^{(M)}\mathbf{v}^{(N)}\nabla_\xi\cdot(\mathbf{G}\mathfrak{g}(\xi,\xi_\alpha)\mathfrak{f}(\boldsymbol{\theta},\boldsymbol{\theta}_\alpha)\mathfrak{F}(\mathbf{v}|\xi))\mathrm{d}\mathbf{v}\mathrm{d}\boldsymbol{\theta}\mathrm{d}\xi \\ &-\sum_{\alpha=1}^{N_n}\int_{\Omega_\xi}\int_{\Omega_\theta}\int_{\Omega_v}\xi^l\boldsymbol{\theta}^{(M)}\mathbf{v}^{(N)}\nabla_\theta\cdot(\mathbf{H}\mathfrak{g}(\xi,\xi_\alpha)\mathfrak{f}(\boldsymbol{\theta},\boldsymbol{\theta}_\alpha)\mathfrak{F}(\mathbf{v}|\xi))\mathrm{d}\mathbf{v}\mathrm{d}\boldsymbol{\theta}\mathrm{d}\xi \\ &-\sum_{\alpha=1}^{N_n}\int_{\Omega_\xi}\int_{\Omega_\theta}\int_{\Omega_v}\xi^l\boldsymbol{\theta}^{(M)}\mathbf{v}^{(N)}\nabla_{\mathrm{v}}\cdot(\mathbf{F}\mathfrak{g}(\xi,\xi_\alpha)\mathfrak{f}(\boldsymbol{\theta},\boldsymbol{\theta}_\alpha)\mathfrak{F}(\mathbf{v}|\xi))\mathrm{d}\mathbf{v}\mathrm{d}\boldsymbol{\theta}\mathrm{d}\xi.\end{aligned} \tag{3.24}$$

An additional transformation can be done to **Equation** (3.24) applying the chain rule to the derivatives inside the integral signs:

$$\begin{aligned}\overline{\mathfrak{S}} = &-\sum_{\alpha=1}^{N_n}\Big[\int_{\Omega_\xi}\int_{\Omega_\theta}\int_{\Omega_v}\nabla_\xi\cdot(\xi^l\boldsymbol{\theta}^{(M)}\mathbf{v}^{(N)}\mathbf{G}\mathfrak{g}(\xi,\xi_\alpha)\mathfrak{f}(\boldsymbol{\theta},\boldsymbol{\theta}_\alpha)\mathfrak{F}(\mathbf{v}|\xi))\mathrm{d}\mathbf{v}\mathrm{d}\boldsymbol{\theta}\mathrm{d}\xi \\ &-\int_{\Omega_\xi}\int_{\Omega_\theta}\int_{\Omega_v}\mathbf{G}\mathfrak{g}(\xi,\xi_\alpha)\mathfrak{f}(\boldsymbol{\theta},\boldsymbol{\theta}_\alpha)\mathfrak{F}(\mathbf{v}|\xi)\nabla_\xi\cdot(\xi^l\boldsymbol{\theta}^{(M)}\mathbf{v}^{(N)})\mathrm{d}\mathbf{v}\mathrm{d}\boldsymbol{\theta}\mathrm{d}\xi\Big] \\ &-\sum_{\alpha=1}^{N_n}\Big[\int_{\Omega_\xi}\int_{\Omega_\theta}\int_{\Omega_v}\nabla_\theta\cdot(\xi^l\boldsymbol{\theta}^{(M)}\mathbf{v}^{(N)}\mathbf{H}\mathfrak{g}(\xi,\xi_\alpha)\mathfrak{f}(\boldsymbol{\theta},\boldsymbol{\theta}_\alpha)\mathfrak{F}(\mathbf{v}|\xi))\mathrm{d}\mathbf{v}\mathrm{d}\boldsymbol{\theta}\mathrm{d}\xi \\ &-\int_{\Omega_\xi}\int_{\Omega_\theta}\int_{\Omega_v}\mathbf{H}\mathfrak{g}(\xi,\xi_\alpha)\mathfrak{f}(\boldsymbol{\theta},\boldsymbol{\theta}_\alpha)\mathfrak{F}(\mathbf{v}|\xi)\nabla_\theta\cdot(\xi^l\boldsymbol{\theta}^{(M)}\mathbf{v}^{(N)})\mathrm{d}\mathbf{v}\mathrm{d}\boldsymbol{\theta}\mathrm{d}\xi\Big] \\ &-\sum_{\alpha=1}^{N_n}\Big[\int_{\Omega_\xi}\int_{\Omega_\theta}\int_{\Omega_v}\nabla_{\mathrm{v}}\cdot(\xi^l\boldsymbol{\theta}^{(M)}\mathbf{v}^{(N)}\mathbf{F}\mathfrak{g}(\xi,\xi_\alpha)\mathfrak{f}(\boldsymbol{\theta},\boldsymbol{\theta}_\alpha)\mathfrak{F}(\mathbf{v}|\xi))\mathrm{d}\mathbf{v}\mathrm{d}\boldsymbol{\theta}\mathrm{d}\xi \\ &-\int_{\Omega_\xi}\int_{\Omega_\theta}\int_{\Omega_v}\mathbf{F}\mathfrak{g}(\xi,\xi_\alpha)\mathfrak{f}(\boldsymbol{\theta},\boldsymbol{\theta}_\alpha)\mathfrak{F}(\mathbf{v}|\xi)\nabla_{\mathrm{v}}\cdot(\xi^l\boldsymbol{\theta}^{(M)}\mathbf{v}^{(N)})\mathrm{d}\mathbf{v}\mathrm{d}\boldsymbol{\theta}\mathrm{d}\xi\Big].\end{aligned} \tag{3.25}$$

Except in a few cases of nucleation, in general, no particle size starts at zero size or goes to infinity size. Also, no particle velocity or scalar property of the particles goes to plus or minus infinity; therefore, no flux of any property $(\xi, \boldsymbol{\theta}, \mathbf{v})$ is present at the boundaries of each coordinate space. The method described in this chapter offers the same potential for the application of nucleation and evaporation cases as in Fox et al.,[51] with the same kind

of solutions to treat flux of properties at zero size, but a study of those physical processes is out of the scope of this research. With these assumptions, the integrals at lines 1, 3, and 5 of **Equation** (3.25) vanish and the source term can be written as

$$\begin{aligned}\overline{\mathfrak{S}} = & l\sum_{\alpha=1}^{N_n} w_\alpha \int_{\Omega_\theta} \boldsymbol{\theta}^{(M)} \mathfrak{f}(\boldsymbol{\theta},\boldsymbol{\theta}_\alpha) \int_{\Omega_\xi} \xi^{l-1} \mathfrak{g}(\xi,\xi_\alpha) \int_{\Omega_v} \mathbf{v}^{(N)} \mathfrak{F}(\mathbf{v}|\xi)\mathbf{G}\,\mathrm{d}\mathbf{v}\mathrm{d}\xi\mathrm{d}\boldsymbol{\theta} \\ & + M\sum_{\alpha=1}^{N_n} w_\alpha \int_{\Omega_\theta} \boldsymbol{\theta}^{M-1} \mathfrak{f}(\boldsymbol{\theta},\boldsymbol{\theta}_\alpha) \int_{\Omega_\xi} \xi^{l} \mathfrak{g}(\xi,\xi_\alpha) \int_{\Omega_v} \mathbf{v}^{(N)} \mathfrak{F}(\mathbf{v}|\xi)\mathbf{H}\,\mathrm{d}\mathbf{v}\mathrm{d}\xi\mathrm{d}\boldsymbol{\theta} \\ & + N\sum_{\alpha=1}^{N_n} w_\alpha \int_{\Omega_\theta} \boldsymbol{\theta}^{(M)} \mathfrak{f}(\boldsymbol{\theta},\boldsymbol{\theta}_\alpha) \int_{\Omega_\xi} \xi^{l} \mathfrak{g}(\xi,\xi_\alpha) \int_{\Omega_v} \mathbf{v}^{N-1} \mathfrak{F}(\mathbf{v}|\xi)\mathbf{F}\,\mathrm{d}\mathbf{v}\mathrm{d}\xi\mathrm{d}\boldsymbol{\theta}.\end{aligned} \tag{3.26}$$

The final system of transport equations can be obtained by pairing **Equation** (3.22) and **Equation** (3.26) as

$$\begin{aligned}& \sum_{\alpha=1}^{N_n} w_\alpha \int_{\Omega_\xi} \xi^l \mathfrak{g}(\xi,\xi_\alpha) \int_{\Omega_\theta} \boldsymbol{\theta}^{(M)} \mathfrak{f}(\boldsymbol{\theta},\boldsymbol{\theta}_\alpha) \int_{\Omega_v} \mathbf{v}^{(N)} \Big[\frac{\partial}{\partial t}(\mathfrak{F}(\mathbf{v}|\xi)) + \nabla_{\mathrm{x}}\cdot(\mathbf{v}\mathfrak{F}(\mathbf{v}|\xi))\Big]\mathrm{d}\mathbf{v}\mathrm{d}\boldsymbol{\theta}\mathrm{d}\xi \\ & + \sum_{\alpha=1}^{N_n} \int_{\Omega_\xi} \xi^l \mathfrak{g}(\xi,\xi_\alpha) \int_{\Omega_\theta} \boldsymbol{\theta}^{(M)} \mathfrak{f}'(\boldsymbol{\theta},\boldsymbol{\theta}_\alpha) \int_{\Omega_v} \mathbf{v}^{(N)} \mathfrak{F}(\mathbf{v}|\xi) \Big[\frac{\partial (w_\alpha \boldsymbol{\theta}_\alpha)}{\partial t} + \mathbf{v}\cdot\nabla_{\mathrm{v}}(w_\alpha\boldsymbol{\theta}_\alpha)\Big]\mathrm{d}\mathbf{v}\mathrm{d}\boldsymbol{\theta}\mathrm{d}\xi \\ & + \sum_{\alpha=1}^{N_n} \int_{\Omega_\xi} \xi^l \mathfrak{g}'(\xi,\xi_\alpha) \int_{\Omega_\theta} \boldsymbol{\theta}^{(M)} \mathfrak{f}(\boldsymbol{\theta},\boldsymbol{\theta}_\alpha) \int_{\Omega_v} \mathbf{v}^{(N)} \mathfrak{F}(\mathbf{v}|\xi) \Big[\frac{\partial (w_\alpha \xi_\alpha)}{\partial t} + \mathbf{v}\cdot\nabla_{\mathrm{x}}(w_\alpha\xi_\alpha)\Big]\mathrm{d}\mathbf{v}\mathrm{d}\boldsymbol{\theta}\mathrm{d}\xi \\ & + \sum_{\alpha=1}^{N_n} \int_{\Omega_\xi} \xi^l \mathfrak{g}(\xi,\xi_\alpha) \int_{\Omega_\theta} \boldsymbol{\theta}^{(M)} \mathfrak{f}(\boldsymbol{\theta},\boldsymbol{\theta}_\alpha) \int_{\Omega_v} \mathbf{v}^{(N)} \mathfrak{F}(\mathbf{v}|\xi) \Big[\frac{\partial w_\alpha}{\partial t} + \mathbf{v}\cdot\nabla_{\mathrm{v}}(w_\alpha)\Big]\mathrm{d}\mathbf{v}\mathrm{d}\boldsymbol{\theta}\mathrm{d}\xi \\ & - \sum_{\alpha=1}^{N_n} \boldsymbol{\theta}_\alpha \int_{\Omega_\xi} \xi^l \mathfrak{g}(\xi,\xi_\alpha) \int_{\Omega_\theta} \boldsymbol{\theta}^{(M)} \mathfrak{f}'(\boldsymbol{\theta},\boldsymbol{\theta}_\alpha) \int_{\Omega_v} \mathbf{v}^{(N)} \mathfrak{F}(\mathbf{v}|\xi) \Big[\frac{\partial w_\alpha}{\partial t} + \mathbf{v}\cdot\nabla_{\mathrm{v}}(w_\alpha)\Big]\mathrm{d}\mathbf{v}\mathrm{d}\boldsymbol{\theta}\mathrm{d}\xi \\ & - \sum_{\alpha=1}^{N_n} \xi_\alpha \int_{\Omega_\xi} \xi^l \mathfrak{g}'(\xi,\xi_\alpha) \int_{\Omega_\theta} \boldsymbol{\theta}^{(M)} \mathfrak{f}(\boldsymbol{\theta},\boldsymbol{\theta}_\alpha) \int_{\Omega_v} \mathbf{v}^{(N)} \mathfrak{F}(\mathbf{v}|\xi) \Big[\frac{\partial w_\alpha}{\partial t} + \mathbf{v}\cdot\nabla_{\mathrm{x}}(w_\alpha)\Big]\mathrm{d}\mathbf{v}\mathrm{d}\boldsymbol{\theta}\mathrm{d}\xi \end{aligned} \tag{3.27}$$

$$\begin{aligned}= & \\ & l\sum_{\alpha=1}^{N_n} w_\alpha \int_{\Omega_\theta} \boldsymbol{\theta}^{(M)} \mathfrak{f}(\boldsymbol{\theta},\boldsymbol{\theta}_\alpha) \int_{\Omega_\xi} \xi^{l-1} \mathfrak{g}(\xi,\xi_\alpha) \int_{\Omega_v} \mathbf{v}^{(N)} \mathfrak{F}(\mathbf{v}|\xi)\mathbf{G}\mathrm{d}\mathbf{v}\mathrm{d}\xi\mathrm{d}\boldsymbol{\theta} \\ & + M\sum_{\alpha=1}^{N_n} w_\alpha \int_{\Omega_\theta} \boldsymbol{\theta}^{M-1} \mathfrak{f}(\boldsymbol{\theta},\boldsymbol{\theta}_\alpha) \int_{\Omega_\xi} \xi^{l} \mathfrak{g}(\xi,\xi_\alpha) \int_{\Omega_v} \mathbf{v}^{(N)} \mathfrak{F}(\mathbf{v}|\xi)\mathbf{H}\mathrm{d}\mathbf{v}\mathrm{d}\xi\mathrm{d}\boldsymbol{\theta} \\ & + N\sum_{\alpha=1}^{N_n} w_\alpha \int_{\Omega_\theta} \boldsymbol{\theta}^{(M)} \mathfrak{f}(\boldsymbol{\theta},\boldsymbol{\theta}_\alpha) \int_{\Omega_\xi} \xi^{l} \mathfrak{g}(\xi,\xi_\alpha) \int_{\Omega_v} \mathbf{v}^{(N)} N-1 \mathfrak{F}(\mathbf{v}|\xi)\mathbf{F}\mathrm{d}\mathbf{v}\mathrm{d}\xi\mathrm{d}\boldsymbol{\theta}.\end{aligned}$$

### 3.2.2 Scalar Functions Approximations

**Equation** (3.27) is only completely defined after the scalar functions $\mathfrak{g}$ and $\mathfrak{f}$ are completely described. They require a functional approximation in the form of marginal NDFs; the approximation would allow the integration of the expressions in the right hand side of

**Equation** (3.27). Several distribution functions have been studied in quadrature methods as NDF approximations.[43,47,74,77] In this case, the *Dirac-delta* as in Marchisio and Fox[43] and Yuan and Fox[61] have been chosen to represent the NDF in both velocity space and size space:

$$\begin{aligned} \mathfrak{g}(\xi, \xi_\alpha) &= \delta(\xi - \xi_\alpha) \\ \mathfrak{f}(\boldsymbol{\theta}, \boldsymbol{\theta}_\alpha) &= \delta(\boldsymbol{\theta} - \boldsymbol{\theta}_\alpha), \end{aligned} \tag{3.28}$$

with the Jacobian:

$$\frac{\mathrm{d}}{\mathrm{d}t}\delta(\mathbf{z} - \mathbf{z}_\alpha) = \delta'(\mathbf{z} - \mathbf{z}_\alpha)\left(-\frac{\partial \mathbf{z}_\alpha}{\partial t}\right). \tag{3.29}$$

Now, taking into account that

$$\begin{aligned} \int_{-\infty}^{\infty} z^k \delta(z - z_\alpha)\mathrm{d}z &= z_\alpha^k \\ \int_{-\infty}^{\infty} z^k \delta'(z - z_\alpha)\mathrm{d}z &= -k z_\alpha^{z-1}, \end{aligned} \tag{3.30}$$

**Equation** (3.27) can be rewritten as

$$\begin{aligned} &\sum_{\alpha=1}^{N_n} w_\alpha \xi_\alpha^l \boldsymbol{\theta}_\alpha^M \int_{\Omega_v} \mathbf{v}^{(N)} \Big[\frac{\partial}{\partial t}(\mathfrak{F}(\mathbf{v}|\xi)) + \nabla_{\mathrm{x}} \cdot (\mathbf{v}\mathfrak{F}(\mathbf{v}|\xi))\Big]\mathrm{d}\mathbf{v} \\ &+ l \sum_{\alpha=1}^{N_n} \boldsymbol{\theta}_\alpha^M \xi_\alpha^{l-1} \int_{\Omega_v} \mathbf{v}^{(N)} \mathfrak{F}(\mathbf{v}|\xi)\Big[\frac{\partial (w_\alpha \xi_\alpha)}{\partial t} + \mathbf{v}(\xi_\alpha)\nabla_{\mathrm{x}}(w_\alpha \xi_\alpha)\Big]\mathrm{d}\mathbf{v} \\ &+ (M) \sum_{\alpha=1}^{N_n} \boldsymbol{\theta}_\alpha^{M-1} \xi_\alpha^l \int_{\Omega_v} \mathbf{v}^{(N)} \mathfrak{F}(\mathbf{v}|\xi)\Big[\frac{\partial (w_\alpha \boldsymbol{\theta}_\alpha)}{\partial t} + \mathbf{v} \cdot \nabla_{\mathrm{x}}(w_\alpha \boldsymbol{\theta}_\alpha)\Big]\mathrm{d}\mathbf{v} \\ &+ \Big( \sum_{\alpha=1}^{N_n} \boldsymbol{\theta}_\alpha^M \xi_\alpha^l - l \sum_{\alpha=1}^{N_n} \boldsymbol{\theta}_\alpha^M \xi^l \\ &- (M) \sum_{\alpha=1}^{N_n} \boldsymbol{\theta}_\alpha^M \xi_\alpha^l \Big) \int_{\Omega_v} \mathbf{v}^{(N)} \mathfrak{F}(\mathbf{v}|\xi)\Big[\frac{\partial w_\alpha}{\partial t} + \mathbf{v} \cdot \nabla_{\mathrm{x}}(w_\alpha)\Big]\mathrm{d}\mathbf{v} \\ = \\ &l \sum_{\alpha=1}^{N_n} w_\alpha \boldsymbol{\theta}_\alpha^M \xi_\alpha^{l-1} \int_{\Omega_v} \mathbf{v}^{(N)} \mathbf{G}\, \mathfrak{F}(\mathbf{v}|\xi)\mathrm{d}\mathbf{v} + \\ &(M) \sum_{\alpha=1}^{N_n} w_\alpha \boldsymbol{\theta}_\alpha^{(M)-1} \xi_\alpha^l \int_{\Omega_v} \mathbf{v}^{(N)} \mathbf{H}\, \mathfrak{F}(\mathbf{v}|\xi)\mathrm{d}\mathbf{v} + \\ &(N) \sum_{\alpha=1}^{N_n} w_\alpha \boldsymbol{\theta}_\alpha^M \xi_\alpha^l \int_{\Omega_v} \mathbf{v}^{(N)-1} \mathbf{F}\, \mathfrak{F}(\mathbf{v}|\xi)\mathrm{d}\mathbf{v}. \end{aligned} \tag{3.31}$$

The integral of the velocity appearing in **Equation** (3.31) is a function of the discrete size considered for each quadrature node and it provides the size-conditional velocity moments:

$$\langle \mathfrak{m}(\xi_\alpha) \rangle^{(N)} = \langle \mathfrak{m} \rangle_\alpha^{(N)} = \int_{\Omega_v} \mathbf{v}^{(N)} \mathfrak{F}(\mathbf{v}|\xi) \mathrm{d}\mathbf{v}, \tag{3.32}$$

which allows rewriting **Equation** (3.31) as

$$\begin{aligned}
&\sum_{\alpha=1}^{N_n} w_\alpha \xi_\alpha^l \boldsymbol{\theta}_\alpha^{(M)} \Big[ \frac{\partial \langle \mathfrak{m} \rangle_\alpha^{(N)}}{\partial t} + \nabla_{\mathrm{x}} \cdot \langle \mathfrak{m} \rangle_\alpha^{(N)+1} - (N) \int_{\Omega_v} \mathbf{v}^{(N)-1} \mathbf{F} \mathfrak{F}(\mathbf{v}|\xi) \mathrm{d}\mathbf{v} \Big] \\
&+ l \sum_{\alpha=1}^{N_n} \boldsymbol{\theta}_\alpha^M \xi_\alpha^{l-1} \Big[ \langle \mathfrak{m} \rangle_\alpha^{(N)} \frac{\partial (w_\alpha \xi_\alpha)}{\partial t} + \langle \mathfrak{m} \rangle_\alpha^{(N)+1} \cdot \nabla_{\mathrm{x}} (w_\alpha \xi_\alpha) - w_\alpha \langle \mathfrak{m} \rangle_\alpha^{(N)} \overline{\mathbf{G}} \Big] \\
&+ (M) \sum_{\alpha=1}^{N_n} \boldsymbol{\theta}_\alpha^{M-1} \xi_\alpha^l \Big[ \langle \mathfrak{m} \rangle_\alpha^{(N)} \frac{\partial (w_\alpha \boldsymbol{\theta}_\alpha)}{\partial t} + \langle \mathfrak{m} \rangle_\alpha^{(N)+1} \cdot \nabla_{\mathrm{x}} (w_\alpha \boldsymbol{\theta}_\alpha) - w_\alpha \langle \mathfrak{m} \rangle_\alpha^{(N)} \overline{\mathbf{H}} \Big] \\
&+ \Big( \sum_{\alpha=1}^{N_n} \boldsymbol{\theta}_\alpha^M \xi_\alpha^l - l \sum_{\alpha=1}^{N_n} \boldsymbol{\theta}_\alpha^M \xi^l - (M) \sum_{\alpha=1}^{N_n} \boldsymbol{\theta}_\alpha^M \xi_\alpha^l \Big) \Big[ \langle \mathfrak{m} \rangle_\alpha^{(N)} \frac{\partial w_\alpha}{\partial t} + \langle \mathfrak{m} \rangle_\alpha^{(N)+1} \cdot \nabla_{\mathrm{x}} (w_\alpha) \Big] \\
&= 0.
\end{aligned} \tag{3.33}$$

The transport velocity for the scalar equations is given in terms of the computed conditional velocity moments as

$$\overline{\mathbf{U}}(\xi_\alpha)^{(N)} = \overline{\mathbf{U}}_\alpha^{(N)} = \frac{\langle \mathfrak{m} \rangle_\alpha^{(N)+1}}{\langle \mathfrak{m} \rangle_\alpha^{(N)}}, \tag{3.34}$$

in which the operation is taken component-wise. Applying this approximation to **Equation** (3.33):

$$\begin{aligned}
&\sum_{\alpha=1}^{N_n} w_\alpha \xi_\alpha^l \boldsymbol{\theta}_\alpha^{(M)} \Big[ \frac{\partial \langle \mathfrak{m} \rangle_\alpha^{(N)}}{\partial t} + \nabla_{\mathrm{x}} \cdot \langle \mathfrak{m} \rangle_\alpha^{(N)+1} - (N) \int_{\Omega_v} \mathbf{v}^{(N)-1} \mathbf{F} \mathfrak{F}(\mathbf{v}|\xi) \mathrm{d}\mathbf{v} \Big] \\
&+ l \sum_{\alpha=1}^{N_n} \boldsymbol{\theta}_\alpha^M \xi_\alpha^{l-1} \langle \mathfrak{m} \rangle_\alpha^{(N)} \Big[ \frac{\partial (w_\alpha \xi_\alpha)}{\partial t} + \overline{\mathbf{U}}_\alpha^{(N)} \cdot \nabla_{\mathrm{x}} (w_\alpha \xi_\alpha) - w_\alpha \langle \mathfrak{m} \rangle_\alpha^{(N)} \overline{\mathbf{G}} \Big] \\
&+ (M) \sum_{\alpha=1}^{N_n} \boldsymbol{\theta}_\alpha^{M-1} \xi_\alpha^l \langle \mathfrak{m} \rangle_\alpha^{(N)} \Big[ \frac{\partial (w_\alpha \boldsymbol{\theta}_\alpha)}{\partial t} + \overline{\mathbf{U}}_\alpha^{(N)} \cdot \nabla_{\mathrm{x}} (w_\alpha \boldsymbol{\theta}_\alpha) - w_\alpha \langle \mathfrak{m} \rangle_\alpha^{(N)} \overline{\mathbf{H}} \Big] \\
&+ \Big( \sum_{\alpha=1}^{N_n} \boldsymbol{\theta}_\alpha^M \xi_\alpha^l - l \sum_{\alpha=1}^{N_n} \boldsymbol{\theta}_\alpha^M \xi^l - (M) \sum_{\alpha=1}^{N_n} \boldsymbol{\theta}_\alpha^M \xi_\alpha^l \Big) \langle \mathfrak{m} \rangle_\alpha^{(N)} \Big[ \frac{\partial w_\alpha}{\partial t} + \overline{\mathbf{U}}_\alpha^{(N)} \cdot \nabla_{\mathrm{x}} (w_\alpha) \Big].
\end{aligned} \tag{3.35}$$

### 3.2.3 Matrix Representation

The structure of **Equation** (3.35) allows representing the system in matrix form. Let,

$$\begin{aligned}
\mathbb{T}[\mathfrak{m}^{(N)}_{\xi_\alpha}] &= \frac{\partial \langle \mathfrak{m} \rangle^{(N)}_{\alpha}}{\partial t} + \nabla_{\mathrm{x}} \cdot \langle \mathfrak{m} \rangle^{(N)+1}_{\alpha} - (N) \int_{\Omega_v} \mathbf{v}^{(N)-1} \mathbf{F}\, \mathfrak{F}(\mathbf{v}|\xi) \mathrm{d}\mathbf{v} \\
\mathbb{T}[w_\alpha \xi_\alpha] &= \frac{\partial (w_\alpha \xi_\alpha)}{\partial t} + \overline{\mathbf{U}}^{(N)}_{\alpha} \cdot \nabla_{\mathrm{x}} (w_\alpha \xi_\alpha) - w_\alpha \langle \mathfrak{m} \rangle^{(N)}_{\alpha} \overline{\mathbf{G}} \\
\mathbb{T}[w_\alpha \boldsymbol{\theta}_\alpha] &= \frac{\partial (w_\alpha \boldsymbol{\theta}_\alpha)}{\partial t} + \overline{\mathbf{U}}^{(N)}_{\alpha} \cdot \nabla_{\mathrm{x}} (w_\alpha \boldsymbol{\theta}_\alpha) - w_\alpha \langle \mathfrak{m} \rangle^{(N)}_{\alpha} \overline{\mathbf{H}} \\
\mathbb{T}[w_\alpha] &= \frac{\partial w_\alpha}{\partial t} + \overline{\mathbf{U}}^{(N)}_{\alpha} \cdot \nabla_{\mathrm{x}} (w_\alpha).
\end{aligned} \tag{3.36}$$

Then **Equation** (3.35) can be written as

$$\begin{aligned}
&\sum_{\alpha=1}^{N_n} w_\alpha \xi^l_\alpha \boldsymbol{\theta}^{(M)}_{\alpha} \mathbb{T}[\mathfrak{m}^{(N)}_{\xi_\alpha}] + l \sum_{\alpha=1}^{N_n} \boldsymbol{\theta}^{M}_{\alpha} \xi^{l-1}_{\alpha} \langle \mathfrak{m} \rangle^{(N)}_{\alpha} \mathbb{T}[w_\alpha \xi_\alpha] \\
&+ (M) \sum_{\alpha=1}^{N_n} \boldsymbol{\theta}^{M-1}_{\alpha} \xi^{l}_{\alpha} \langle \mathfrak{m} \rangle^{(N)}_{\alpha} \mathbb{T}[w_\alpha \boldsymbol{\theta}_\alpha] + \Big( \sum_{\alpha=1}^{N_n} \boldsymbol{\theta}^{M}_{\alpha} \xi^{l}_{\alpha} - \\
&l \sum_{\alpha=1}^{N_n} \boldsymbol{\theta}^{M}_{\alpha} \xi^{l} - (M) \sum_{\alpha=1}^{N_n} \boldsymbol{\theta}^{M}_{\alpha} \xi^{l}_{\alpha} \Big) \mathbb{T}[w_\alpha] = 0,
\end{aligned} \tag{3.37}$$

which, in turn, allows rewriting the equation in matrix form as

$$\left[ \begin{array}{c|c|c|c} \mathbf{A}_{\mathfrak{m}} & \mathbf{A}_{w\xi} & \mathbf{A}_{w\theta} & \mathbf{A}_{w} \end{array} \right] \left[ \begin{array}{c} \mathbb{T}[\mathfrak{m}^{(N)}_{\xi_\alpha}] \\ \mathbb{T}[w_\alpha \xi_\alpha] \\ \mathbb{T}[w_\alpha \boldsymbol{\theta}_\alpha] \\ \mathbb{T}[w_\alpha] \end{array} \right] = \left[ \begin{array}{c} \mathfrak{0}_\alpha \\ \mathfrak{0}_\alpha \\ \mathfrak{0}_\alpha \\ \mathfrak{0}_\alpha \end{array} \right], \tag{3.38}$$

where the matrices

$$\mathbf{A} = \left[ \begin{array}{c|c|c|c} \mathbf{A}_{\mathfrak{m}} & \mathbf{A}_{w\xi} & \mathbf{A}_{w\theta} & \mathbf{A}_{w} \end{array} \right] \tag{3.39}$$

are represented by

$$\begin{aligned}
\mathbf{A}_{\mathfrak{m}} &= \sum_{\alpha=1}^{N_n} w_\alpha \boldsymbol{\theta}^{M}_{\alpha} \xi^{l}_{\alpha} \\
\mathbf{A}_{w\xi} &= l \sum_{\alpha=1}^{N_n} \boldsymbol{\theta}^{M}_{\alpha} \xi^{l-1}_{\alpha} \mathfrak{m}^{(N)}_{\xi_\alpha} \\
\mathbf{A}_{w\theta} &= M \sum_{\alpha=1}^{N_n} \boldsymbol{\theta}^{M-1}_{\alpha} \xi^{l}_{\alpha} \mathfrak{m}^{(N)}_{\xi_\alpha} \\
\mathbf{A}_{w} &= (1 - M - l) \sum_{\alpha=1}^{N_n} \boldsymbol{\theta}^{M}_{\alpha} \xi^{l}_{\alpha} \mathfrak{m}^{(N)}_{\xi_\alpha}.
\end{aligned} \tag{3.40}$$

The size of the matrix $\mathbf{A}$ depends on the size of the joint moment set and the number of quadrature nodes chosen to represent the weights, abscissas, and conditional velocity

moments.[43,61,62] The number of moments needed to close the system of equations is $N_t = N_n(N_s + N_v + 1)$, where $N_n$ is the number of quadrature nodes, $N_s$ is the number of scalar variables, and $N_v$ is the number of conditional velocity moments variables. Assuming that a feasible set of joint moment exist[62] from which it is possible to choose a subset of moments to determine the system of equations, such system is given by **Equation** (3.38). Note that the system in **Equation** (3.38) forms a homogeneous linear system whose minimum norm solution is given by

$$\begin{bmatrix} \mathbb{T}[\mathfrak{m}_{\xi_\alpha}^{(N)}] \\ \mathbb{T}[w_\alpha \xi_\alpha] \\ \mathbb{T}[w_\alpha \boldsymbol{\theta}_\alpha] \\ \mathbb{T}[w_\alpha] \end{bmatrix} = \begin{bmatrix} \mathfrak{V}_\alpha \\ \mathfrak{V}_\alpha \\ \mathfrak{V}_\alpha \\ \mathfrak{V}_\alpha \end{bmatrix}. \tag{3.41}$$

In which case the following set of transport equations are obtained:

$$\begin{aligned} &\frac{\partial \langle \mathfrak{m} \rangle_\alpha^{(N)}}{\partial t} + \nabla_{\mathrm{x}} \cdot \langle \mathfrak{m} \rangle_\alpha^{(N)+1} = (N) \int_{\Omega_{\mathrm{v}}} \mathbf{v}^{(N)-1} \mathfrak{F}(\mathbf{v}|\xi_\alpha) \mathbf{F}(\xi, \mathbf{v}) \mathrm{d}\mathbf{v} \\ &\frac{\partial w_\alpha \xi_\alpha}{\partial t} + \overline{\mathbf{U}}_\alpha^{(N)} \cdot \nabla_{\mathrm{x}}(w_\alpha \xi_\alpha) = w_\alpha \mathbf{G}(\xi, \boldsymbol{\theta}, \mathbf{v}) \\ &\frac{\partial w_\alpha \boldsymbol{\theta}_\alpha}{\partial t} + \overline{\mathbf{U}}_\alpha^{(N)} \cdot \nabla_{\mathrm{x}}(w_\alpha \boldsymbol{\theta}_\alpha) = w_\alpha \mathbf{H}(\xi, \boldsymbol{\theta}, \mathbf{v}) \\ &\frac{\partial w_\alpha}{\partial t} + \overline{\mathbf{U}}_\alpha^{(N)} \cdot \nabla_{\mathrm{x}}(w_\alpha) = 0. \end{aligned} \tag{3.42}$$

The solution shown in **Equation** (3.41) is possible in general whenever a noncollisional system is considered; in this case, particle-particle interactions are neglected and there are no creation or disappearance of particles inside the system. Physical cases involving particle-particle interactions would require the solution of the system in **Equation** (3.38).

## 3.3 Numerical Treatment of Transport Equations

The system of equations proposed in **Equation** (3.42) requires a numerical framework in order to be applicable to CFD codes. The structure of the set of transport equations share many properties with hyperbolic systems[8] and frameworks like finite volumes are suitable to represent them numerically. Among the few unique characteristics inherent to moment transport equations, the flux reconstruction in the computational cell is the one that requires specialized numerical treatment.[29,47,111] The underlying principle of the flux reconstruction is based on the properties of the NDF that the equations are representing; numerical schemes formulated on the basis of the structure of the NDF are called *kinetic*

*schemes*.[126] These schemes were first proposed in the context of Euler and Navier-Stoke equations as a justification of their origins from the Maxwell-Boltzmann equations[127–130] and were recently reintroduced in the context of quadrature-based moment methods.[29,47]

### 3.3.1 Kinetic Advection Schemes and Flux Reconstruction

Numerical schemes based on the properties of the underlying distribution must be *positivity preserving*,[127,129,130] which means that the numerical scheme should produce a nonnegative distribution when evolved. If the numerical scheme is based on the evolution of the moments of the distribution, such moments should be *realizable* which essentially ensures that the computed moments lead to a nonnegative distribution. Starting from an explicit Courant scheme,[126] we explore some of the characteristics of a first order positivity preserving scheme in which the discretized NDF can be written as[a]

$$\mathfrak{F}_i\Big|_{n+1} = \mathfrak{F}_i\Big|_n - \lambda \max(\mathrm{v}_x, 0)(\mathfrak{F}_i\Big|_n - \mathfrak{F}_{i-1}\Big|_n) - \lambda \min(\mathrm{v}_x, 0)(\mathfrak{F}_{i+1}\Big|_n - \mathfrak{F}_i\Big|_n), \tag{3.43}$$

where $\lambda = \Delta t/\Delta x$, $i$ denotes a node in physical space and $n$ represents the time level. The equation can be expanded as

$$\begin{aligned}\mathfrak{F}_i\Big|_{n+1} = (1 - \lambda \max(\mathrm{v}_x, 0) + \lambda \min(\mathrm{v}_x, 0))\mathfrak{F}_i\Big|_n \\ + \lambda \max(\mathrm{v}_x, 0)\mathfrak{F}_{i-1}\Big|_n - \lambda \min(\mathrm{v}_x, 0)\mathfrak{F}_{i+1}\Big|_n.\end{aligned} \tag{3.44}$$

Assuming that the NDF is nonnegative at time level $n$ then $\mathfrak{F}_i\Big|_n \geq 0$, $\mathfrak{F}_{i-1}\Big|_n \geq 0$ and $\mathfrak{F}_{i+1}\Big|_n \geq 0$. Also, the second and third term in the right hand side of **Equation** (3.44) are nonnegative, then, the nonnegativity of the NDF at time level $n+1$ is given by the nonnegativity of the coefficient of the first term in **Equation** (3.44). This gives rise to the condition:

$$\lambda \leq \frac{1}{\max(\mathrm{v}_x, 0) - \min(\mathrm{v}_x, 0)}, \tag{3.45}$$

therefore, the numerical NDF at time level $n+1$ is nonnegative as long as the condition $\lambda \leq \frac{1}{|\mathrm{v}_x|}$ is fulfilled; it also guarantees that the moment set obtained from this NDF will be realizable. Formal proof of these statements can be found elsewhere.[127–131] Extension of this realizability condition to higher order discretization schemes can be found in Kah et

[a] For clarity, only one dimension in physical space is considered.

al.,[121] Vi et al.,[76] and Vikas et al. [132] Starting from **Equation** (3.44), it is possible to justify the use of kinetic schemes for the set in **Equation** (3.42), as long as the numerical schemes for the equations are the result of moment transformations of **Equation** (3.44). For instance, a numerical scheme for the conditional velocity moment can be obtained by replacing the NDF approximation and taking velocity moments of **Equation** (3.44). First, we rewrite the equation as

$$\begin{aligned}\mathfrak{F}_i\Big|_{n+1} = \mathfrak{F}_i\Big|_n - \lambda \Big[ \Big( \min(\mathrm{v}_x, 0)\mathfrak{F}_{i+1}\Big|_n + \max(\mathrm{v}_x, 0)\mathfrak{F}_i\Big|_n \Big) \\ - \Big( \min(\mathrm{v}_x, 0)\mathfrak{F}_i\Big|_n + \max(\mathrm{v}_x, 0)\mathfrak{F}_{i-1}\Big|_n \Big) \Big] .\end{aligned} \tag{3.46}$$

Then, we expand it in terms of the NDF approximation in **Equation** (3.3) and take a velocity moment transformation,

$$\begin{aligned}&\int_{\Omega_\mathrm{v}} \mathrm{v}_x^{(N)} \sum_{\alpha=1}^{N_n} w_\alpha \mathfrak{g}(\xi, \xi_\alpha)\mathfrak{f}(\boldsymbol{\theta}, \boldsymbol{\theta}_\alpha)\mathfrak{F}_i(\mathrm{v}_x|\xi_\alpha)\mathrm{d}\mathrm{v}_x\Big|_{n+1} = \\ &\quad \int_{\Omega_\mathrm{v}} \mathrm{v}_x^{(N)} \sum_{\alpha=1}^{N_n} w_\alpha \mathfrak{g}(\xi, \xi_\alpha)\mathfrak{f}(\boldsymbol{\theta}, \boldsymbol{\theta}_\alpha)\mathfrak{F}_i(\mathrm{v}_x|\xi_\alpha)\mathrm{d}\mathrm{v}_x\Big|_n \\ &\quad - \lambda \Bigg[ \Big( \int_{\Omega_\mathrm{v}} \mathrm{v}_x^{(N)} \min(\mathrm{v}_x, 0) \sum_{\alpha=1}^{N_n} w_\alpha \mathfrak{g}(\xi, \xi_\alpha)\mathfrak{f}(\boldsymbol{\theta}, \boldsymbol{\theta}_\alpha)\mathfrak{F}_{i+1}(\mathrm{v}_x|\xi_\alpha)\mathrm{d}\mathrm{v}_x\Big|_n + \\ &\quad \int_{\Omega_\mathrm{v}} \mathrm{v}_x^{(N)} \max(\mathrm{v}_x, 0) \sum_{\alpha=1}^{N_n} w_\alpha \mathfrak{g}(\xi, \xi_\alpha)\mathfrak{f}(\boldsymbol{\theta}, \boldsymbol{\theta}_\alpha)\mathfrak{F}_i(\mathrm{v}_x|\xi_\alpha)\mathrm{d}\mathrm{v}_x\Big|_n \Big) \\ &\quad - \Big( \int_{\Omega_\mathrm{v}} \mathrm{v}_x^{(N)} \min(\mathrm{v}_x, 0) \sum_{\alpha=1}^{N_n} w_\alpha \mathfrak{g}(\xi, \xi_\alpha)\mathfrak{f}(\boldsymbol{\theta}, \boldsymbol{\theta}_\alpha)\mathfrak{F}_i(\mathrm{v}_x|\xi_\alpha)\mathrm{d}\mathrm{v}_x\Big|_n + \\ &\quad \int_{\Omega_\mathrm{v}} \mathrm{v}_x^{(N)} \max(\mathrm{v}_x, 0) \sum_{\alpha=1}^{N_n} w_\alpha \mathfrak{g}(\xi, \xi_\alpha)\mathfrak{f}(\boldsymbol{\theta}, \boldsymbol{\theta}_\alpha)\mathfrak{F}_{i-1}(\mathrm{v}_x|\xi_\alpha)\mathrm{d}\mathrm{v}_x\Big|_n \Big) \Bigg] ,\end{aligned} \tag{3.47}$$

which, in turn, can be rewritten as

$$\sum_{\alpha=1}^{N_n} w_\alpha \mathfrak{g}(\xi,\xi_\alpha)\mathfrak{f}(\boldsymbol{\theta},\boldsymbol{\theta}_\alpha)\int_{\Omega_v} \mathrm{v}_x^{(N)}\mathfrak{F}_i(\mathrm{v}_x|\xi_\alpha)\mathrm{d}\mathrm{v}_x\Big|_{n+1} = \tag{3.48}$$

$$\begin{aligned}
&\sum_{\alpha=1}^{N_n} w_\alpha \mathfrak{g}(\xi,\xi_\alpha)\mathfrak{f}(\boldsymbol{\theta},\boldsymbol{\theta}_\alpha)\int_{\Omega_v} \mathrm{v}_x^{(N)}\mathfrak{F}_i(\mathrm{v}_x|\xi_\alpha)\mathrm{d}\mathrm{v}_x\Big|_{n} \\
&-\lambda\left[\Big(\sum_{\alpha=1}^{N_n} w_\alpha \mathfrak{g}(\xi,\xi_\alpha)\mathfrak{f}(\boldsymbol{\theta},\boldsymbol{\theta}_\alpha)\int_{\Omega_v} \mathrm{v}_x^{(N)}\min(\mathrm{v}_x,0)\mathfrak{F}_{i+1}(\mathrm{v}_x|\xi_\alpha)\mathrm{d}\mathrm{v}_x\Big|_{n}+\right. \\
&\left.\sum_{\alpha=1}^{N_n} w_\alpha \mathfrak{g}(\xi,\xi_\alpha)\mathfrak{f}(\boldsymbol{\theta},\boldsymbol{\theta}_\alpha)\int_{\Omega_v} \mathrm{v}_x^{(N)}\max(\mathrm{v}_x,0)\mathfrak{F}_i(\mathrm{v}_x|\xi_\alpha)\mathrm{d}\mathrm{v}_x\Big|_{n}\Big)\right. \\
&\left.-\Big(\sum_{\alpha=1}^{N_n} w_\alpha \mathfrak{g}(\xi,\xi_\alpha)\mathfrak{f}(\boldsymbol{\theta},\boldsymbol{\theta}_\alpha)\int_{\Omega_v} \mathrm{v}_x^{(N)}\min(\mathrm{v}_x,0)\mathfrak{F}_i(\mathrm{v}_x|\xi_\alpha)\mathrm{d}\mathrm{v}_x\Big|_{n}+\right. \\
&\left.\sum_{\alpha=1}^{N_n} w_\alpha \mathfrak{g}(\xi,\xi_\alpha)\mathfrak{f}(\boldsymbol{\theta},\boldsymbol{\theta}_\alpha)\int_{\Omega_v} \mathrm{v}_x^{(N)}\max(\mathrm{v}_x,0)\mathfrak{F}_{i-1}(\mathrm{v}_x|\xi_\alpha)\mathrm{d}\mathrm{v}_x\Big|_{n}\Big)\right].
\end{aligned}$$

The system in **Equation** (3.48) can be written in matrix form as

$$\begin{aligned}
[\mathbf{Q}_{gf}][\langle \mathfrak{m}_i\rangle^{(N)}]_{n+1} &= [\mathbf{Q}_{gf}][\langle \mathfrak{m}_i\rangle^{(N)}]_n \\
&-\lambda\left[\Big([\mathbf{Q}_{gf}][\langle \mathfrak{m}_{i+1}^-\rangle^{(N)+1}]_n + [\mathbf{Q}_{gf}][\langle \mathfrak{m}_i^+\rangle^{(N)+1}]_n\Big)\right. \\
&\left.-\Big([\mathbf{Q}_{gf}][\langle \mathfrak{m}_i^-\rangle^{(N)+1}]_n + [\mathbf{Q}_{gf}][\langle \mathfrak{m}_{i-1}^+\rangle^{(N)+1}]_n\Big)\right],
\end{aligned} \tag{3.49}$$

where

$$[\mathbf{Q}_{gf}] = \begin{bmatrix} w_1\mathfrak{g}(\xi,\xi_1)\mathfrak{f}(\boldsymbol{\theta},\boldsymbol{\theta}_1) & 0 & \cdots & 0 \\ 0 & w_2\mathfrak{g}(\xi,\xi_2)\mathfrak{f}(\boldsymbol{\theta},\boldsymbol{\theta}_2) & \cdots & 0 \\ \vdots & \cdots & \ddots & \vdots \\ 0 & 0 & \cdots & w_{N_s}\mathfrak{g}(\xi,\xi_{N_s})\mathfrak{f}(\boldsymbol{\theta},\boldsymbol{\theta}_{N_s}) \end{bmatrix}$$

$$[\langle \mathfrak{m}\rangle^{(N)}] = \begin{bmatrix} \langle \mathfrak{m}\rangle_1^{(N)} \\ \langle \mathfrak{m}\rangle_2^{(N)} \\ \vdots \\ \langle \mathfrak{m}\rangle_{N_s}^{(N)} \end{bmatrix} \quad [\langle \mathfrak{m}_i^-\rangle^{(N)+1}] = \begin{bmatrix} \int_{\Omega_v} \mathrm{v}_x^{(N)}\min(\mathrm{v}_x,0)\mathfrak{F}_i(\mathrm{v}_x|\xi_1)\mathrm{d}\mathrm{v}_x \\ \int_{\Omega_v} \mathrm{v}_x^{(N)}\min(\mathrm{v}_x,0)\mathfrak{F}_i(\mathrm{v}_x|\xi_2)\mathrm{d}\mathrm{v}_x \\ \vdots \\ \int_{\Omega_v} \mathrm{v}_x^{(N)}\min(\mathrm{v}_x,0)\mathfrak{F}_i(\mathrm{v}_x|\xi_{N_s})\mathrm{d}\mathrm{v}_x \end{bmatrix} \tag{3.50}$$

$$[\langle \mathfrak{m}_i^+\rangle^{(N)+1}] = \begin{bmatrix} \int_{\Omega_v} \mathrm{v}_x^{(N)}\max(\mathrm{v}_x,0)\mathfrak{F}_i(\mathrm{v}_x|\xi_1)\mathrm{d}\mathrm{v}_x \\ \int_{\Omega_v} \mathrm{v}_x^{(N)}\max(\mathrm{v}_x,0)\mathfrak{F}_i(\mathrm{v}_x|\xi_2)\mathrm{d}\mathrm{v}_x \\ \vdots \\ \int_{\Omega_v} \mathrm{v}_x^{(N)}\max(\mathrm{v}_x,0)\mathfrak{F}_i(\mathrm{v}_x|\xi_{N_s})\mathrm{d}\mathrm{v}_x \end{bmatrix}.$$

The components of the matrix $[\mathbf{Q}_{gf}]$ are primarily functions that reside in phase space;[b] assuming that the fields are well defined,[43] any particular realization of $\mathfrak{g}$ and $\mathfrak{f}$ has an inverse which can be applied to both sides of **Equation** (3.48) resulting in

$$\begin{aligned}[\langle \mathfrak{m}_i \rangle^{(N)}]_{n+1} = [\langle \mathfrak{m}_i \rangle^{(N)}]_n \\ - \lambda \Big[ \Big( [\langle \mathfrak{m}_{i+1}^- \rangle^{(N)+1}]_n + [\langle \mathfrak{m}_i^+ \rangle^{(N)+1}]_n \Big) \\ - \Big( [\langle \mathfrak{m}_i^- \rangle^{(N)+1}]_n + [\langle \mathfrak{m}_{i-1}^+ \rangle^{(N)+1}]_n \Big) \Big] .\end{aligned} \tag{3.51}$$

**Equation** (3.51) takes the form of a flux splitting method, as in a finite volume discretization of the moment transport equation in **Equation** (3.42). Naturally, it can be rewritten as

$$[\langle \mathfrak{m}_i \rangle^{(N)}]_{n+1} = [\langle \mathfrak{m}_i \rangle^{(N)}]_n - \lambda \Big[ [\mathbf{M}_{i+1/2}] - [\mathbf{M}_{i-1/2}] \Big], \tag{3.52}$$

where

$$\begin{aligned}[\mathbf{M}_{i+1/2}] &= \Big( [\langle \mathfrak{m}_{i+1}^- \rangle^{(N)+1}]_n + [\langle \mathfrak{m}_i^+ \rangle^{(N)+1}]_n \Big) \\ [\mathbf{M}_{i-1/2}] &= \Big( [\langle \mathfrak{m}_i^- \rangle^{(N)+1}]_n + [\langle \mathfrak{m}_{i-1}^+ \rangle^{(N)+1}]_n \Big).\end{aligned} \tag{3.53}$$

The overall numerical scheme uses operator splitting which allows using the same mathematical form for each spatial dimension independently. A similar argument can be applied to **Equation** (3.44) to obtain finite volume discretization in **Equation** (3.42), with the difference that velocity and scalar moment transformations should be simultaneously applied to the discretized NDF. Research on extension to higher order discretization schemes can be found elsewhere.[76,121,132]

### 3.3.2 Conditional Quadrature Method of Moments

Even though a finite volume discretization was obtained for the conditional velocity moment transport equation, further approximations are needed in order to resolve the higher order moments appearing in the flux terms in the moment equations of **Equation** (3.42) and on the flux reconstruction terms in **Equation** (3.51). This shortcoming has been solved by using weights and velocity abscissas in order to approximate higher order

[b] The fields of functions $\mathfrak{g}$ and $\mathfrak{f}$ have not been properly projected onto an Eulerian grid through a moment transformation.

conditional velocity moments. On the other hand, moments should be used to obtain weights and abscissas; as pointed out in **Chapter 2**, this procedure is called *inversion* and there exist several research efforts aimed to the application of these techniques in the context of QBMM.

McGraw [44] first introduced the product-difference algorithm in the context of the quadrature method of moments (QMOM). Essentially, it involved the inversion of a Jacobian matrix relating computed moments with quadrature weights and abscissas. Other related methodologies have been reviewed by John and Thein.[133] A major issue with the *inversion* technique is that it can only be used effectively to compute 1-dimensional transformations; direct extension to higher dimensions is difficult and an open research question.[134] Yoon and McGraw [104] and Desjardins and Fox [47] first introduced a closure for high order moments in terms of a simple two-point quadrature providing algebraic expressions for moments in terms of the weights and velocity abscissas, but extensions to two or three dimensions in physical space resulted in issues with moment realizability.[46] Yuan and Fox [61] proposed the conditional quadrature method of moments (CQMOM) which uses approximations for marginal and conditional *monodisperse* kinetic distributions. Marginal moments are obtained from marginal approximations to the distribution function (in terms of Dirac-delta functions); marginal weights and abscissas are obtained from marginal moments through one-dimensional inversion procedures. Conditional moments are calculated based on the marginal moments by solving Vandermonde type linear systems which in turn allows calculating conditional weights and abscissas through one-dimensional inversion formulas. One key factor in CQMOM is that the number of moments is automatically fixed once the number of quadrature nodes for the approximation of the joint distribution is chosen, unlike the previous inversion procedures, in which high order velocity moments were selected arbitrarily.[29,30,43,46,47,62] In this research, CQMOM has been used to treat the higher order moments appearing in the transport equations.

The conditional velocity moments in **Equation** (3.50) and **Equation** (3.51) can be approximated as [61]

$$\mathfrak{F}(\mathbf{v}|\xi_\alpha) = \sum_{\beta_1=1}^{N_1} \sum_{\beta_2=1}^{N_2} \sum_{\beta_3=1}^{N_3} \rho_{\beta_1} \rho_{\beta_1,\beta_2} \rho_{\beta_1,\beta_2,\beta_3} \delta(\mathbf{v} - \overline{\mathbf{U}}_{\boldsymbol{\beta}}(\xi_\alpha)), \tag{3.54}$$

where

$$\delta(\mathbf{v}-\overline{\mathbf{U}}_{\boldsymbol{\beta}}(\xi_\alpha))=\delta(\mathrm{v}_x-\overline{\mathrm{U}}_{x,\beta_1|\alpha})\delta(\mathrm{v}_y-\overline{\mathrm{U}}_{y,\beta_1,\beta_2|\alpha})\delta(\mathrm{v}_z-\overline{\mathrm{U}}_{z,\beta_1,\beta_2,\beta_3|\alpha}), \tag{3.55}$$

and $\rho_{\beta_1}$ is the velocity weight for direction 1, $\rho_{\beta_1,\beta_2}$ is the velocity weight for direction 2 conditioned on direction 1 and $\rho_{\beta_1,\beta_2,\beta_3}$ is the velocity weight for direction 3 conditioned on directions 1 and 2. In **Equation** (3.54), each successive abscissa is conditioned on the values of the previous ones. The velocity abscissas are functions of the size abscissas, which are evolved in space and time as shown in **Equation** (3.42). The application of a moment transformation to **Equation** (3.54) approximates the conditional velocity moments as

$$\langle \mathfrak{m}\rangle_\alpha^{(N)}=\sum_{\beta_1=1}^{N_1}\sum_{\beta_2=1}^{N_2}\sum_{\beta_3=1}^{N_3}\rho_{\beta_1}\rho_{\beta_1,\beta_2}\rho_{\beta_1,\beta_2,\beta_3}\overline{\mathrm{U}}_{x,\beta_1|\alpha}^{N_1}\overline{\mathrm{U}}_{y,\beta_1,\beta_2|\alpha}^{N_2}\overline{\mathrm{U}}_{z,\beta_1,\beta_2,\beta_3|\alpha}^{N_3}. \tag{3.56}$$

The inversion method used in CQMOM is the Wheeler algorithm[135] which uses the coefficients of orthogonal polynomials basis in order to calculate the weights and abscissas of the Gaussian quadrature from the computed moments in **Equation** (3.56). Now that the connection between weights and abscissas has been established, it is possible to approximate the high-order moments appearing in the transport equations. Extensive details of the inversion algorithm can be found in Marchisio and Fox[8] and Yuan and Fox.[61]

### 3.3.3 Numerical Algorithm

The solution algorithm involves numerical splitting,[8,95] which essentially allows solving separately the convective part (LHS) and the source terms (RHS) of **Equation** (3.42). For instance, for the velocity moment set in **Equation** (3.42), an outline of the discretized equations is

$$\begin{aligned}
&[\langle \mathfrak{m}_i\rangle^{(N)}]_{n+1/2}=[\langle \mathfrak{m}_i\rangle^{(N)}]_n-\lambda\Big[[\mathbf{M}_{i+1/2}]-[\mathbf{M}_{i-1/2}]\Big]\in[t^n,t^{n+1/2}] \\
&[\langle \mathfrak{m}_i^*\rangle^{(N)}]_{n+1}=\overline{\mathfrak{S}}_{\mathfrak{m}}\in[t^n,t^{n+1/2}] \\
&[\langle \mathfrak{m}_i\rangle^{(N)}]_{n+1}=[\langle \mathfrak{m}_i^*\rangle^{(N)}]_n-\lambda\Big[[\mathbf{M}^*_{i+1/2}]-[\mathbf{M}^*_{i-1/2}]\Big]\in[t^{n+1/2},t^{n+1}].
\end{aligned} \tag{3.57}$$

A similar discretization procedure can be applied to the whole set of equations in **Equation** (3.42). A sample of a one-step solution of the algorithm using operator splitting looks like:

1) Calculate $\Delta t$ based on **Equation** (3.45).

2) Use initial conditions to obtain scalar weights, scalar weighted abscissas, and conditional velocity moments.

3) Advance the convective part to obtain scalar weights, scalar weighted abscissas, and conditional moments by $\Delta t/2$.

4) Invert conditional velocity moments to obtain velocity weights and conditional velocities according to CQMOM.

5) Advance drag forces and scalar rate by $\Delta t$ and obtain conditional velocity moments, scalar weights, and scalar weighted abscissas.

6) Advance the convective part with the quantities in Step 5 by $\Delta t/2$.

7) Repeat Steps 1 - 6 until termination.

# CHAPTER 4

# A NOVEL FORMULATION OF THE METHOD OF MOMENTS: PARCELED CONDITIONAL QUADRATURE METHOD OF MOMENTS

Most of the relevant physics concerning particle phenomena in fluid flows are influenced directly or indirectly by the particle size distribution. For instance, particles of different sizes are affected differently by *drag*. In addition, the value of the particle's Stokes number affects the occurrence of PTC and the turbulence in the fluid phase. Size distribution also plays a fundamental role in *mass transfer* (reaction and mass transport) and *heat transfer* (convection, radiation) whose rates are usually dependent on the particle diameter or particle surface.[125,136] The developments in this chapter are focused in the accurate representation of the size coordinate using approximations to the NDF in the framework of the method of moments.

In the same way that Fox and colleagues were exploring McGraw's ideas about moment closures and quadrature methods for kinetic and population balance equations, Laurent and Villedieu and colleagues were exploring the ideas of Tambour[114] on sectional methods to discretize directly variables in phase space. Laurent and Massot[63] first proposed the Eulerian multifluid model in which size space was discretized in an Eulerian grid where conservation of a single moment in size coordinate was guaranteed. The conservation of only one moment leaves out extra information about the correlation of size and other quantities like velocity. Dufour and Villedieu[35] improved the discretization order of the Eulerian-multifluid model in the size coordinate to second order and still guaranteed moment realizability. One of the major drawbacks of this technique is its inability to capture PTC. Schneider at al.[69,70] coupled the Eulerian-multifluid with a quadrature-based moment method for the velocity coordinate in order to capture PTC.[29] The idea developed in this chapter is based on the same concepts of the Eulerian-multifluid model developed

by Schneider et al.[69] with a fundamental difference in the treatment of the size coordinate and the velocity coordinate to capture PTC.

The main idea of the technique presented in this chapter is the accurate representation of the size coordinate of the phase-space. This coordinate contains all the phenomena related to the polydispersity behavior of the particulate system. The concept of *parcel* is used as a mathematical artifact to describe the joint properties of groups of particles in a discrete subdivision of the size coordinate. The core of the concept is to use the joint moments in each parcel in order to approximate the NDF and obtain an accurate description of polydisperse related phenomena: PTC, momentum transfer, mass transfer, and heat transfer. We start with the description of the size coordinate and obtain moment transport equations in terms of a general function that represents the behavior of the particle size distribution. We then describe the reconstruction process based on the transported joint moments and obtain an Eulerian moment method to accurately describe polydispersity behavior of dilute multiphase systems.

## 4.1 Description of the Size Coordinate

The state of a multidimensional (joint) particle distribution can be described by the position in physical space and the variables related to the particle properties. Following Ramkrishna,[94] the *particle state space* can be characterized by *internal coordinates*, that is, particle mass, particle size, particle velocity, particle enthalpy among many others; and *external coordinates*, that is, particle position. The NDF describe the relationship between internal coordinates and external coordinates and the moment transformation must be consistent with this relationship. While external coordinates are evolved using finite volume methods directly in a CFD sense, a specialized treatment might be necessary for the internal coordinates; indeed, many of the techniques previously described are differentiated from each other by their particular treatment of the variables of the internal coordinates. The technique described herein is no different in that aspect.

In the proposed approach, the idea is to calculate joint moments based on a special treatment given to the size coordinate. Some of the concepts for this treatment are built upon similar concepts,[63,69,70] in which essentially the size coordinate is discretized into *sections* or *parcels* of particles; in each parcel joint moments for the phase space variables are

evolved in time and physical space. For a continuous NDF defined in the size coordinate $\Omega_\xi = [s_1, s_{N_\xi+1}]$, with a discretization $s_1 < s_2 < \cdots s_{N_\xi} < s_{N_\xi+1}$, the integral

$$I = \int_{\Omega_\xi} f(\xi)\mathrm{d}\xi \tag{4.1}$$

can be written as

$$I = \sum_{k=1}^{N_\xi} I_k, \qquad I_k = \int_{s_k}^{s_{k+1}} f(\xi)\mathrm{d}\xi. \tag{4.2}$$

This statement assures that the domain $\Omega_\xi$ can be subdivided into a finite set of parcels and the integration process can be carried out in each of them. From this argument, the joint scalar-velocity moments can be now split as

$$\mathfrak{M}^{(l,M,N)} = \sum_{k=1}^{N_\xi} \int_{s_k}^{s_{k+1}} \int_{\mathbb{R}^M} \int_{\mathbb{R}^3} \xi^l \boldsymbol{\theta}^{(M)} \mathbf{v}^{(N)} \mathfrak{F}(\xi, \boldsymbol{\theta}, \mathbf{v})\, \mathrm{d}v\mathrm{d}\theta\mathrm{d}\xi \tag{4.3}$$

The concept of parcel, in principle, allows capturing polydisperse phenomena by classifying the joint moments by particle size and studying the specific behavior of the quantities transported in each of them. This, in turn, improves the physics captured by the method, compared to previous Eulerian moment-based methods.[30,46,61,77]

## 4.2 NDF Approximation and Moment Closure

As in previous moment-based methods, an approximation to the NDF is introduced to handle the issues related to the lack of knowledge of the NDF.[a] For this particular technique, the approximation is formulated in a way that accounts explicitly for particle polydispersity using the concept of a parcel similar to other moment-based techniques.[63,69,70]

$$\begin{aligned}\mathfrak{F}(\xi, \boldsymbol{\theta}, \mathbf{v}) &= \sum_{k=1}^{N_\xi} \ell_k(\xi)\mathfrak{g}_k(\xi)\mathfrak{f}_k(\boldsymbol{\theta}, \mathbf{v}|\xi) \\ &= \sum_{k=1}^{N_\xi} \ell_k(\xi)\mathfrak{g}_k(\xi)\delta(\boldsymbol{\theta} - \overline{\boldsymbol{\theta}}_k(\xi)) \sum_{\alpha=1}^{N_v} \mathbf{w}_{k,\alpha}\delta(\mathbf{v} - \overline{\mathbf{U}}_{k,\alpha}(\xi)),\end{aligned} \tag{4.4}$$

where

$$\begin{aligned}&\sum_{\alpha=1}^{N_v} \mathbf{w}_{k,\alpha}\delta(\mathbf{v} - \overline{\mathbf{U}}_{k,\alpha}(\xi)) \equiv \\ &\quad \sum_{\alpha_1}^{N_1}\sum_{\alpha_2}^{N_2}\sum_{\alpha_3}^{N_3} w_{k,\alpha_1} w_{k,\alpha_2} w_{k,\alpha_3} \delta(v_x - \overline{\mathrm{U}}_{x;k,\alpha_1})\delta(v_y - \overline{\mathrm{U}}_{y;k,\alpha_2})\delta(v_z - \overline{\mathrm{U}}_{z;k,\alpha_3}),\end{aligned} \tag{4.5}$$

[a] Closure problem.

and

$$\ell_k(\xi) = \begin{cases} 1 & \text{if} \quad \xi \in [s_k, s_{k+1}] \\ 0 & \text{otherwise.} \end{cases} \tag{4.6}$$

The approximation used for the velocity of the particles is the same as in Yuan and Fox,[61] more details will be described in **Section 4.5**. Replacing **Equation** (4.4) into **Equation** (4.3),

$$\mathfrak{M}^{(l,M,N)} = \sum_{k=1}^{N_\xi} \int_{s_k}^{s_{k+1}} \ell_k(\xi)\xi^l \mathfrak{g}(\xi) \int_{\mathbb{R}^M} \boldsymbol{\theta}^{(M)} \delta(\boldsymbol{\theta} - \overline{\boldsymbol{\theta}}_k(\xi)) \tag{4.7}$$
$$\int_{\mathbb{R}^3} \mathbf{v}^{(N)} \sum_{\alpha=1}^{N_v} \mathbf{w}_{k,\alpha} \delta(\mathbf{v} - \overline{\mathbf{U}}_{k,\alpha}(\xi)) \mathrm{d}\mathbf{v}\mathrm{d}\boldsymbol{\theta}\mathrm{d}\xi,$$

which after integration becomes

$$\mathfrak{M}^{(l,M,N)} = \sum_{k=1}^{N_\xi} \sum_{\alpha=1}^{N_v} \mathbf{w}_\alpha \int_{s_k}^{s_{k+1}} \ell_k(\xi)\xi^l \mathfrak{g}_k(\xi) [\overline{\boldsymbol{\theta}}_k(\xi)]^{(M)} [\overline{\mathbf{U}}_{k,\alpha}(\xi)]^{(N)} \mathrm{d}\xi. \tag{4.8}$$

Another way to rewrite **Equation** (4.8) is in terms of the moment set per parcel:

$$\mathfrak{M}_k^{(l,M,N)} = \sum_{\alpha=1}^{N_v} \mathbf{w}_{k,\alpha} \int_{s_k}^{s_{k+1}} \xi^l \mathfrak{g}_k(\xi) [\overline{\boldsymbol{\theta}}_k(\xi)]^{(M)} [\overline{\mathbf{U}}_{k,\alpha}(\xi)]^{(N)} \mathrm{d}\xi, \tag{4.9}$$

with the property $\mathfrak{M}^{(l,M,N)} = \sum_{k=1}^{N_\xi} \mathfrak{M}_k^{(l,M,N)}$. The dependency of $\boldsymbol{\theta}$ and $\mathbf{U}$ on the particle size $\xi$ is implicit in **Equation** (4.8).

## 4.3 Moment Transport Equations

In order to deal with the closure issue, **Equation** (2.7) can be rewritten, using the NDF approximation previously presented, as

$$\begin{aligned} \frac{\partial \mathfrak{M}^{(l,M,N)}}{\partial t} + \nabla_{\mathbf{x}} \cdot \mathfrak{M}^{(l,M,N+1)} = & \\ + \sum_{k=1}^{N_\xi} \sum_{\alpha=1}^{N_v} \mathbf{w}_{k,\alpha} \int_{s_k}^{s_{k+1}} \ell_k(\xi)\xi^l \mathfrak{g}_k(\xi) [\overline{\boldsymbol{\theta}}_k]^{(M)} \mathbf{F}(\xi, \overline{\boldsymbol{\theta}}_k, \overline{\mathbf{U}}_{k,\alpha}) \nabla_{\overline{\mathbf{U}}_\alpha} \cdot \left( [\overline{\mathbf{U}}_{k,\alpha}]^{(N)} \right) \mathrm{d}\xi & \\ + l \sum_{k=1}^{N_\xi} \sum_{\alpha=1}^{N_v} \mathbf{w}_{k,\alpha} \int_{s_k}^{s_{k+1}} \ell_k(\xi)\xi^{l-1} \mathfrak{g}_k(\xi) [\overline{\boldsymbol{\theta}}_k]^{(M)} [\overline{\mathbf{U}}_{k,\alpha}]^{(N)} \mathbf{G}(\xi, \overline{\boldsymbol{\theta}}_k, \overline{\mathbf{U}}_{k,\alpha}) \mathrm{d}\xi & \\ + \sum_{k=1}^{N_\xi} \sum_{\alpha=1}^{N_v} \mathbf{w}_{k,\alpha} \int_{s_k}^{s_{k+1}} \ell_k(\xi)\xi^l \mathfrak{g}_k(\xi) [\overline{\mathbf{U}}_{k,\alpha}]^{(N)} \mathbf{H}(\xi, \overline{\boldsymbol{\theta}}_k, \overline{\mathbf{U}}_{k,\alpha}) \nabla_{\overline{\boldsymbol{\theta}}_k} \cdot \left( [\overline{\boldsymbol{\theta}}_k]^{(M)} \right) \mathrm{d}\xi. & \end{aligned} \tag{4.10}$$

A more compact way to present the moment transport equations is to represent the moment set per parcel or section as

$$\begin{aligned}\frac{\partial \mathfrak{M}_k^{(l,M,N)}}{\partial t} + \nabla_{\mathbf{x}} \cdot \mathfrak{M}_k^{(l,M,N+1)} = \\ + \sum_{\alpha=1}^{N_v} \mathbf{w}_{k,\alpha} \int_{s_k}^{s_{k+1}} \xi^l \mathfrak{g}_k(\xi) [\overline{\boldsymbol{\theta}}_k]^{(M)} \mathbf{F}(\xi, \overline{\boldsymbol{\theta}}_k, \overline{\mathbf{U}}_{k,\alpha}) \nabla_{\overline{\mathbf{U}}_\alpha} \cdot \left( [\overline{\mathbf{U}}_{k,\alpha}]^{(N)} \right) \mathrm{d}\xi \\ + l \sum_{\alpha=1}^{N_v} \mathbf{w}_{k,\alpha} \int_{s_k}^{s_{k+1}} \xi^{l-1} \mathfrak{g}_k(\xi) [\overline{\boldsymbol{\theta}}_k]^{(M)} [\overline{\mathbf{U}}_{k,\alpha}]^{(N)} \mathbf{G}(\xi, \overline{\boldsymbol{\theta}}_k, \overline{\mathbf{U}}_{k,\alpha}) \mathrm{d}\xi \\ + \sum_{\alpha=1}^{N_v} \mathbf{w}_{k,\alpha} \int_{s_k}^{s_{k+1}} \xi^l \mathfrak{g}_k(\xi) [\overline{\mathbf{U}}_{k,\alpha}]^{(N)} \mathbf{H}(\xi, \overline{\boldsymbol{\theta}}_k, \overline{\mathbf{U}}_{k,\alpha}) \nabla_{\overline{\boldsymbol{\theta}}_k} \cdot \left( [\overline{\boldsymbol{\theta}}_k]^{(M)} \right) \mathrm{d}\xi,\end{aligned} \tag{4.11}$$

again, with the property $\mathfrak{M}^{(l,M,N)} = \sum_{k=1}^{N_\xi} \mathfrak{M}_k^{(l,M,N)}$.

## 4.4 Moment-Based Size Reconstruction

In order to completely approximate the NDF and determine the set of moment transport equations, the functional $\mathfrak{g}_k(\xi)$ must be established. $\mathfrak{g}_k(\xi)$, is a representation of the distribution of particle sizes in the size coordinate, whose exact mathematical form is not known; It is possible, however, to approximate it based on joint lower order size moments. John et al.[137] introduced a technique to reconstruct 1-dimensional distribution functions using spline polynomials and lower order moments. The concept is very similar to spline interpolation,[138] with the difference that actual values of the NDF are not used (not known), but instead, lower order moments of the NDF are used. As in regular spline interpolation, the reconstruction yields a set of polynomial coefficients from which it is possible to approximate the distribution function in each discretized parcel.

### 4.4.1 Spline Reconstruction

Following the ideas of John et al.[137] and de Souza et al.,[139] let $\Omega = [s_1, s_{N_\xi+1}] \in \mathbb{R}$ be a finite size interval divided in $N_\xi$ size subintervals. In each subinterval $[s_k, s_{k+1}]$, a polynomial of order $l_s$

$$S_k^{(l_s)} = \sum_{j=0}^{l_s} C_{k,j} (\xi - s_k)^j, \tag{4.12}$$

with $S_k^{(l_s)}$ being of class $\mathrm{C}^{l_s-1}$, is used to approximate the distribution function. A priori knowledge of the distribution shape is not necessary, only an appropriate subinterval

where the values of the distribution are known to be positive. In order to obtain the polynomial coefficients $C_{k,j}$ for the reconstruction, a linear system of equations is generated in terms of an arbitrary number of moments and regular continuity conditions for the splines. In the following section we describe in detail the formulation of such system.

### 4.4.2 Linear System Formulation

Given that $N_\xi$ polynomials are needed for the reconstruction (one in each subinterval), there are $(l_s+1)N_\xi$ unknown coefficients and *at least* $N_\xi$ equations are needed in order to determine them. The equations needed for the formulation of the linear system are

- $N_\xi - 1$ equations of continuity at the nodes $s_{k+1}$ with $k = 1 \dots k-1$ of the form $S_k^{(l_s)}(s_{k+1}) = S_{k+1}^{(l_s)}(s_{k+1})$.

- $(l_s - 1)(N_\xi - 1)$ equations of continuity of the $n^{\text{th}}$ derivative at the nodes $s_{k+1}$ of the form $S_k^{(l_s-n)}(s_{k+1}) = S_{k+1}^{(l_s-n)}(s_{k+1})$.

- Assuming that the distribution function vanishes at the tails, the left boundary would have $l$ equations of the form

$$\begin{aligned} S_1^{(l_s)}(s_1) &= 0 \\ S_1^{(l_s-1)}(s_1) &= 0 \\ &\vdots \\ S_1^{(1)}(s_1) &= 0. \end{aligned} \tag{4.13}$$

- Similarly, the right boundary would have $l_s$ equations of the form

$$\begin{aligned} S_{N_\xi}^{(l_s)}(s_{N_\xi+1}) &= 0 \\ S_{N_\xi}^{(l_s-1)}(s_{N_\xi+1}) &= 0 \\ &\vdots \\ S_{N_\xi}^{(1)}(s_{N_\xi+1}) &= 0. \end{aligned} \tag{4.14}$$

The total number of equations are $l_s(N_\xi + 1)$, and the number of unknown coefficients are $(l_s+1)N_\xi$, this means that at least $N_\xi - l_s$ additional equations are needed in order to obtain a determined or overdetermined linear system of equations. These equations

must come from the computed moments. The fundamental assumption of this technique is that $\mathfrak{g}_k$ can be represented by polynomial splines as an approximation for the NDF in each parcel:

$$\mathfrak{g}_k(\xi) = \sum_{j=0}^{l_s} C_{k,j}(\xi - s_k)^j, \tag{4.15}$$

where $l_s$ determines the order of the polynomial. The marginal size moments can be written as

$$\begin{aligned}\mathfrak{M}_k^{(l,\mathbf{0},\mathbf{0})} &= \sum_{\alpha=1}^{N_v} \mathbf{w}_{k,\alpha} \int_{s_k}^{s_{k+1}} \xi^l \mathfrak{g}_k(\xi)[\overline{\boldsymbol{\theta}}_k(\xi)]^{(0)}[\overline{\mathbf{U}}_{k,\alpha}(\xi)]^{(0)}\mathrm{d}\xi \\ &= \sum_{\alpha=1}^{N_v} \mathbf{w}_{k,\alpha} \int_{s_k}^{s_{k+1}} \xi^l \mathfrak{g}_k(\xi)\mathrm{d}\xi \\ &= \int_{s_k}^{s_{k+1}} \xi^l \mathfrak{g}_k(\xi)\mathrm{d}\xi,\end{aligned} \tag{4.16}$$

with the velocity weights normalized to one. By having a representation in terms of polynomials, the marginal size moments can be defined in each parcel as

$$\begin{aligned}\mathfrak{M}_k^l &= \int_{s_k}^{s_{k+1}} \xi^l \sum_{j=0}^{2} C_{k,j}(\xi - \xi_k)^j \mathrm{d}\xi \\ &= C_{k,0} I_{\Delta k}^{(l+1)} + C_{k,1} T_{1,\Delta k}^{(l)} + C_{k,2} T_{2,\Delta k}^{(l)},\end{aligned} \tag{4.17}$$

where $\Delta k = \xi_{k+1} - \xi_k$ and

$$\begin{aligned} I_{\Delta k}^{(l+z)} &= \frac{\xi_{k+1}^{l+z} - \xi_k^{l+z}}{l+z} \quad z \in [1,2,3] \\ T_{1,\Delta k}^{(l)} &= I_{\Delta k}^{(l+2)} - \xi_k I_{\Delta k}^{(l+1)} \\ T_{2,\Delta k}^{(l)} &= I_{\Delta k}^{(l+3)} - 2\xi_k I_{\Delta k}^{(l+2)} + \xi_k^2 I_{\Delta k}^{(l+1)}. \end{aligned} \tag{4.18}$$

The structure of **Equation** (4.17) suggests that the coefficients can be found if the values of $\mathfrak{M}_k^l$ and $T_{1,\Delta k}^{(l)}$, $T_{2,\Delta k}^{(l)}$ are available. It is possible to formulate a linear system in order to find the values of $C_{k,j}$. Assuming that the size coordinate is discretized into 5 parcels, and the NDF in each parcel is represented by a quadratic spline, the linear system $[\mathbf{A}][\mathbf{C}] = [\mathfrak{M}]$ can be represented as

$$
[\mathbf{A}] = \begin{bmatrix}
0 & 0 & (\Delta 1)^2 & -1 & 0 & 0 & 0 & \cdots & 0 & 0 & 0 \\
0 & 0 & 2(\Delta 1) & 0 & -1 & 0 & 0 & \cdots & 0 & 0 & 0 \\
I^1_{\Delta 1} & T^0_{1,\Delta 1} & T^0_{2,\Delta 1} & 0 & 0 & 0 & 0 & \cdots & 0 & 0 & 0 \\
I^2_{\Delta 1} & T^1_{1,\Delta 1} & T^1_{2,\Delta 1} & 0 & 0 & 0 & 0 & \cdots & 0 & 0 & 0 \\
\vdots & \vdots & \vdots & & & & & \cdots & & & \\
I^{l+1}_{\Delta 1} & T^l_{1,\Delta 1} & T^l_{2,\Delta 1} & 0 & 0 & 0 & 0 & \cdots & 0 & 0 & 0 \\
0 & 0 & 0 & 1 & (\Delta 2) & (\Delta 2)^2 & -1 & 0 & \cdots & 0 & 0 \\
0 & 0 & 0 & 0 & 1 & 2(\Delta 2) & 0 & -1 & \cdots & 0 & 0 \\
0 & 0 & 0 & I^1_{\Delta 2} & T^0_{1,\Delta 2} & T^0_{2,\Delta 2} & 0 & 0 & \cdots & 0 & 0 \\
0 & 0 & 0 & I^2_{\Delta 2} & T^1_{1,\Delta 2} & T^1_{2,\Delta 2} & 0 & 0 & \cdots & 0 & 0 \\
 & & & \vdots & \vdots & \vdots & & & \cdots & & \\
0 & 0 & 0 & I^{l+1}_{\Delta 2} & T^l_{1,\Delta 2} & T^l_{2,\Delta 2} & 0 & 0 & \cdots & 0 & 0 \\
0 & 0 & 0 & 0 & 0 & \cdots & \ddots & \ddots & \cdots & 0 & 0 \\
0 & 0 & 0 & 0 & 0 & 0 & 0 & \cdots & 1 & (\Delta 5) & (\Delta 5)^2 \\
0 & 0 & 0 & 0 & 0 & 0 & 0 & \cdots & 0 & 1 & 2(\Delta 5) \\
0 & 0 & 0 & 0 & 0 & 0 & 0 & \cdots & I^1_{\Delta 5} & T^{(0)}_{1,\Delta 5} & T^{(0)}_{2,\Delta 5} \\
0 & 0 & 0 & 0 & 0 & 0 & 0 & \cdots & I^2_{\Delta 5} & T^{(1)}_{1,\Delta 5} & T^{(1)}_{2,\Delta 5} \\
0 & 0 & 0 & 0 & 0 & 0 & 0 & \cdots & \vdots & \vdots & \vdots \\
0 & 0 & 0 & 0 & 0 & 0 & 0 & \cdots & I^{l+1}_{\Delta 5} & T^{(l)}_{1,\Delta 5} & T^{(l)}_{2,\Delta 5}
\end{bmatrix}, \tag{4.19}
$$

$$
[\mathbf{C}] = \begin{bmatrix} C_{1,0} & C_{1,1} & C_{1,2} & C_{2,0} & C_{2,1} & C_{2,2} & \cdots & \cdots & C_{5,0} & C_{5,1} & C_{5,2} \end{bmatrix}^T, \tag{4.20}
$$

$$
[\mathfrak{M}] = \begin{bmatrix} 0 & 0 & \mathfrak{M}^0_1 & \mathfrak{M}^1_1 & \cdots & \mathfrak{M}^l_1 & \cdots & \cdots & 0 & 0 & \mathfrak{M}^0_5 & \mathfrak{M}^1_5 & \cdots & \mathfrak{M}^l_5 \end{bmatrix}. \tag{4.21}
$$

The block-diagonal structure of matrix $[\mathbf{A}]$ in **Equation** (4.19) arises due to the discrete nature of the size coordinate; each block represents the moment evolution of each parcel and is used to reconstruct that portion of the NDF. In principle, this structure allows for optimization at run time and parallelization as an added benefit. In their original papers John et al.[137] and de Souza et al.[139] have proposed an iterative scheme for the reconstruction using an equally constrained system of equations. We have found that solving an overdetermined system of equations using the moments in each section to form the linear system uses fewer iterations under the same framework. The overdetermined system is in general ill-conditioned, however, we have found that the minimum norm solution via singular value decomposition (SVD) and very low tolerances produce reasonable results for several types of reconstruction as shown in **Section 5.2.1**.

## 4.5 Physical Space Transport

As in **Section 3.3**, specialized numerical techniques are necessary to reconstruct the advection fluxes in each computational cell. The relationship between the joint moment transport equation and the kinetic equation allow using the underlying properties of the NDF to formulate *kinetic schemes* to represent the discretized fluxes in the Eulerian grid.

### 4.5.1 Flux Reconstruction in Physical Space

Numerical schemes based on the properties of the underlying distribution must be positivity preserving,[127,129,130] which means that the numerical scheme should produce a nonnegative distribution when evolved. If the numerical scheme is based on the evolution of the moments of the distribution, such moments should be *realizable* which basically ensures that the computed moments lead to a nonnegative distribution. For first order schemes, an outline of the necessary conditions for preserving positivity was given in **Section 3.3**; formal proof of those statements can be found elsewhere.[127–131]

A moment transformation over **Equation** (3.44) is given by

$$\begin{aligned}\mathfrak{M}_i^{(l,M,N)}|_{n+1} = \mathfrak{M}_i^{(l,M,N)}|_n - \lambda\Big\{ &\int_{\Omega_\xi}\int_{\Omega_\theta}\int_{\Omega_\mathrm{v}} \xi^l \boldsymbol{\theta}^{(M)} \mathrm{v}_x^{(N)} \max(\mathrm{v}_x,0)\mathfrak{F}_i \mathrm{d}\mathrm{v}_x \mathrm{d}\boldsymbol{\theta}\mathrm{d}\xi + \\ &\int_{\Omega_\xi}\int_{\Omega_\theta}\int_{\Omega_\mathrm{v}} \xi^l \boldsymbol{\theta}^{(M)} \mathrm{v}_x^{(N)} \min(\mathrm{v}_x,0)\mathfrak{F}_{i+1} \mathrm{d}\mathrm{v}_x \mathrm{d}\boldsymbol{\theta}\mathrm{d}\xi\Big]_n \\ &- \Big[\int_{\Omega_\xi}\int_{\Omega_\theta}\int_{\Omega_\mathrm{v}} \xi^l \boldsymbol{\theta}^{(M)} \mathrm{v}_x^{(N)} \max(\mathrm{v},0)\mathfrak{F}_{i-1} \mathrm{d}\mathrm{v}_x \mathrm{d}\boldsymbol{\theta}\mathrm{d}\xi \\ &+ \int_{\Omega_\xi}\int_{\Omega_\theta}\int_{\Omega_\mathrm{v}} \xi^l \boldsymbol{\theta}^{(M)} \mathrm{v}_x^{(N)} \min(\mathrm{v}_x,0)\mathfrak{F}_i \mathrm{d}\mathrm{v}_x \mathrm{d}\boldsymbol{\theta}\mathrm{d}\xi\Big]_n\Big\},\end{aligned} \tag{4.22}$$

where $n$ is the time level corresponding to $t^n$. Replacing the approximation to the NDF taken at the computational cell $i$,

$$\mathfrak{F}_i\,|_n = \Big[\sum_{k=1}^{N_\xi} \mathfrak{g}_{k,i}(\xi)\delta(\boldsymbol{\theta}-\boldsymbol{\theta}_{k,i}) \sum_{\alpha=1}^{N_v} w_{\alpha,k,i}\delta(\mathrm{v}_x - \overline{\mathrm{U}}_{\alpha,k,i})\Big]_n. \tag{4.23}$$

Carrying out the integrations, the discretized moment equation can be written as[b]

[b]The moment order index is dropped for clarity. Although not specified in the equation, all the RHS is evaluated at time level $n$. For clarity, the transport equation is analyzed only in one physical space dimension.

$$\begin{aligned}\mathfrak{M}_{k,i}|_{n+1} = \mathfrak{M}_{k,i}|_n - \lambda\Big\{\Big[\int_{s_k}^{s_{k+1}} \xi^l \mathfrak{g}_{k,i}(\xi) \sum_{\alpha}^{N_v} w_{\alpha,k,i} \max(\overline{\mathrm{U}}_{\alpha,k,i}, 0)\overline{\mathrm{U}}_{\alpha,k,i}^{(N)} \mathrm{d}\xi \\ + \int_{s_k}^{s_{k+1}} \xi^l \mathfrak{g}_{k,i+1}(\xi) \sum_{\alpha}^{N_v} w_{\alpha,k,i+1} \min(\overline{\mathrm{U}}_{\alpha,k,i+1}, 0)\overline{\mathrm{U}}_{\alpha,k,i+1}^{(N)} \mathrm{d}\xi\Big]_n \\ - \Big[\int_{s_k}^{s_{k+1}} \xi^l \mathfrak{g}_{k,i-1}(\xi) \sum_{\alpha}^{N_v} w_{\alpha,k,i-1} \max(\overline{\mathrm{U}}_{\alpha,k,i-1}, 0)\overline{\mathrm{U}}_{\alpha,k,i-1}^{(N)} \mathrm{d}\xi \\ + \int_{s_k}^{s_{k+1}} \xi^l \mathfrak{g}_{k,i}(\xi) \sum_{\alpha}^{N_v} w_{\alpha,k,i} \min(\overline{\mathrm{U}}_{\alpha,k,i}, 0)\overline{\mathrm{U}}_{\alpha,k,i}^{(N)} \mathrm{d}\xi\Big]_n\Big\}.\end{aligned} \tag{4.24}$$

If **Equation** (4.24) is written as

$$\mathfrak{M}_{k,i}|_{n+1} = \mathfrak{M}_{k,i}|_n - \lambda[\langle \mathfrak{M}_k \rangle_{i+1/2}|_n - \langle \mathfrak{M}_k \rangle_{i-1/2}|_n], \tag{4.25}$$

it naturally takes the form of a flux splitting descretization method in the finite volume methodology in which

$$\begin{aligned}\langle \mathfrak{M}_k \rangle_{i+1/2}|_n = \Big[\int_{s_k}^{s_{k+1}} \xi^l \mathfrak{g}_{k,i}(\xi) \sum_{\alpha}^{N_v} w_{\alpha,k,i} \max(\overline{\mathrm{U}}_{\alpha,k,i}, 0)\overline{\mathrm{U}}_{\alpha,k,i}^{(N)} \mathrm{d}\xi \\ + \int_{s_k}^{s_{k+1}} \xi^l \mathfrak{g}_{k,i+1}(\xi) \sum_{\alpha}^{N_v} w_{\alpha,k,i+1} \min(\overline{\mathrm{U}}_{\alpha,k,i+1}, 0)\overline{\mathrm{U}}_{\alpha,k,i+1}^{(N)} \mathrm{d}\xi\Big]_n \\ \langle \mathfrak{M}_k \rangle_{i-1/2}|_n = \Big[\int_{s_k}^{s_{k+1}} \xi^l \mathfrak{g}_{k,i-1}(\xi) \sum_{\alpha}^{N_v} w_{\alpha,k,i-1} \max(\overline{\mathrm{U}}_{\alpha,k,i-1}, 0)\overline{\mathrm{U}}_{\alpha,k,i-1}^{(N)} \mathrm{d}\xi \\ + \int_{s_k}^{s_{k+1}} \xi^l \mathfrak{g}_{k,i}(\xi) \sum_{\alpha}^{N_v} w_{\alpha,k,i} \min(\overline{\mathrm{U}}_{\alpha,k,i}, 0)\overline{\mathrm{U}}_{\alpha,k,i}^{(N)} \mathrm{d}\xi\Big]_n.\end{aligned} \tag{4.26}$$

The overall algorithm can be incorporated seamlessly into a finite volume framework due to the similarities and could make use of operator splitting for stability purposes as explained in **Chapter 3**.

### 4.5.2 Conditional Quadrature Method of Moments

Even though a finite volume discretization was obtained for the joint moment transport equation, further approximations are needed in order to resolve the higher order moments appearing in the numerical flux in **Equation** (4.24); these high order moments are due to the particle velocity transport in physical space. This shortcoming is solved if weights and abscissas are used to approximate higher order moments and, in turn, conditional velocity moments are used to obtain weights and abscissas as in the inversion procedure explained in **Section 3.3**. An approximation to conditional velocity moments can be obtained as

$$\langle \mathfrak{m}_k \rangle^{(N)} = \frac{\int_{s_k}^{s_{k+1}} \xi^l \mathfrak{g}_k(\xi) [\overline{\theta}_k(\xi)]^{(M)} \sum_{\alpha=1}^{N_v} \mathbf{w}_{k,\alpha} [\overline{\mathbf{U}}_{k,\alpha}(\xi)]^{(N)} \mathrm{d}\xi}{\int_{s_k}^{s_{k+1}} \xi^l \mathfrak{g}_k(\xi) [\overline{\theta}_k(\xi)]^{(M)} \mathrm{d}\xi}. \tag{4.27}$$

Once the value of the conditional velocity moments are known (from **Equation** (4.27)), it is possible to obtain an approximation to the conditional weights and velocity abscissas needed in order to compute the joint moments. This is accomplished via the inversion algorithm proposed for CQMOM explained in **Section 3.3**. In this technique, as well, CQMOM has been used to treat higher order moments appearing in the joint moment transport equations. Now that the connection between weights and abscissas has been established, it is possible to approximate the high order moments appearing in the transport equations. Extensive details of the inversion algorithm can be found in Marchisio and Fox[8] and Yuan and Fox.[61]

### 4.5.3 Solution Algorithm

An example of a one-time step solution of the proposed algorithm using operator splitting is as follows:

1) Calculate $\Delta t$ based on **Equation** (3.45).

2) Using initial conditions for weights, velocities, and polynomial size-coefficients, calculate joint moments.

3) Advance joint moments by $\Delta t/2$.

4) Obtain conditional velocity moments from **Equation** (4.27).

5) Obtain weighs and abscissas from the conditional velocity moments using an inversion algorithm.

6) Obtain polynomial coefficients by solving linear system in **Equation** (4.19), **Equation** (4.20), **Equation** (4.21) from the marginal size moments.

7) Obtain any other scalar property by averaging with the corresponding conditional scalar moments in each parcel.

8) Using the weights, abscissas, and moments obtained from Steps 1, 2, and 3, reconstruct the fluxes in physical space.

9) Using the fluxes from Step 8 and the joint moments from the previous time step, evolve the joint moments by $\Delta t/2$.

10) Calculate and advance drag force by $\Delta t$.

11) Calculate and advance scalar rates for the particles by $\Delta t$.

12) Compute joint moments as in Step 2.

13) Repeat Steps 5 - 9 with the joint moment from Step 12.

# CHAPTER 5

# NUMERICAL APPLICATIONS

In the methodologies described in **Chapter 3** and **Chapter 4**, the set of transport equations in **Equation** (3.42) and **Equation** (4.10) are general enough to allow the introduction of detailed physics and the complexities of polydisperse systems; however, in order to test the capability of the model at the most basic level, several approximating assumptions have been made. As new methodologies, the main objective is to capture characteristic behaviors at the core physics rather than model all the complexities present in multiphase systems. These relaxing assumptions include: (i) only one and two dimensional representations in physical space; (ii) the Stokes number is either of $\mathbb{O}(1)$ or infinity, reducing the drag model to very simple approximations[a]; and (iii) turbulence interactions between particles and the fluid have not been taken into account. In the conditional quadrature method of moments (DQCMOM) one of the main characteristics we are trying to capture is PTC, given that this model transport conditional velocity moments along with scalar properties of the particles explicitly. On the other hand, for the parceled method of moments (PMOM), the most important characteristic to test first is the performance in the reconstruction of the particle size distribution, followed by the ability of the method to capture PTC, given that conditional velocity moments that describe these characteristics can be computed from the joint moments.

## 5.1 Example Applications in DQCMOM

We first describe some applications for the direct quadrature of conditional moments, DQCMOM, in one and two dimensions.

---

[a] For instance, Schiller-Neumann drag law.

### 5.1.1 Particle Trajectory Crossing

The complex interactions between the fluid and the particles cause particles to move with a broad spectrum of Stokes numbers, with some of these particles being able to cross between eddies and interact with other clouds of particles; this phenomena is best explained from the stochastic point of view.[4,9,84,110,140,141] Most of the Eulerian methods based on the Navier-Stokes equations fail to explain or capture it for dilute multiphase systems.[8] On the other hand, previously formulated Eulerian moment-based techniques[29,43,47,61] for monodisperse systems use multinode quadratures that allow them to capture clouds of different characteristics crossing each other and the particular polydisperse formulation presented in this paper should not be an exception. In the first test, three packets with a specific concentration are located in different positions in a one dimensional physical space. The three packets have different sizes and each packet is controlled by three quadrature nodes, which means that it is possible to capture crossing not only among particle of the same size but also among particles of different sizes. The first packet is located between $0.2 \leq x \leq 0.25$, the second between $0.3 \leq x \leq 0.35$, and the third between $0.4 \leq x \leq 0.45$. **Figure 5.1** and **Figure 5.2** show the evolution of the weights (packet particle concentration per size) and the zeroth joint moment (total particle concentration). Time and physical space are nondimensional; size is also nondimensional and scaled in order to represent the order of magnitude of the real sizes. The top plot in each subfigure explains the evolution of the concentration of particles of each individual size and the interaction among the three different sizes is depicted in the bottom plot, along with the evolution of the mean particle velocity of the three packets. The packets located at $x < 0.4$ move to the right of the domain, with velocities 0.4 and 0.2 and with sizes $65 \times 10^{-6}$ and $98 \times 10^{-6}$. The packet located at $x > 0.4$ moves to the left with velocity $-0.4$ and size $131 \times 10^{-6}$. The particles are moving in a vacuum advected by their own velocity[b] and they cross several times during the simulation due to the periodicity of the left and right boundaries of the domain. The number density of the packets are: 182.72, 644.30, and 170.12. The sizes and the number densities were chosen from the moments of a Gaussian particle size distribution (PSD) in the interval $[40 \times 10^{-6}, 160 \times 10^{-6}]$. The Wheeler algorithm was used to select the weights

[b] Infinity Stokes number.

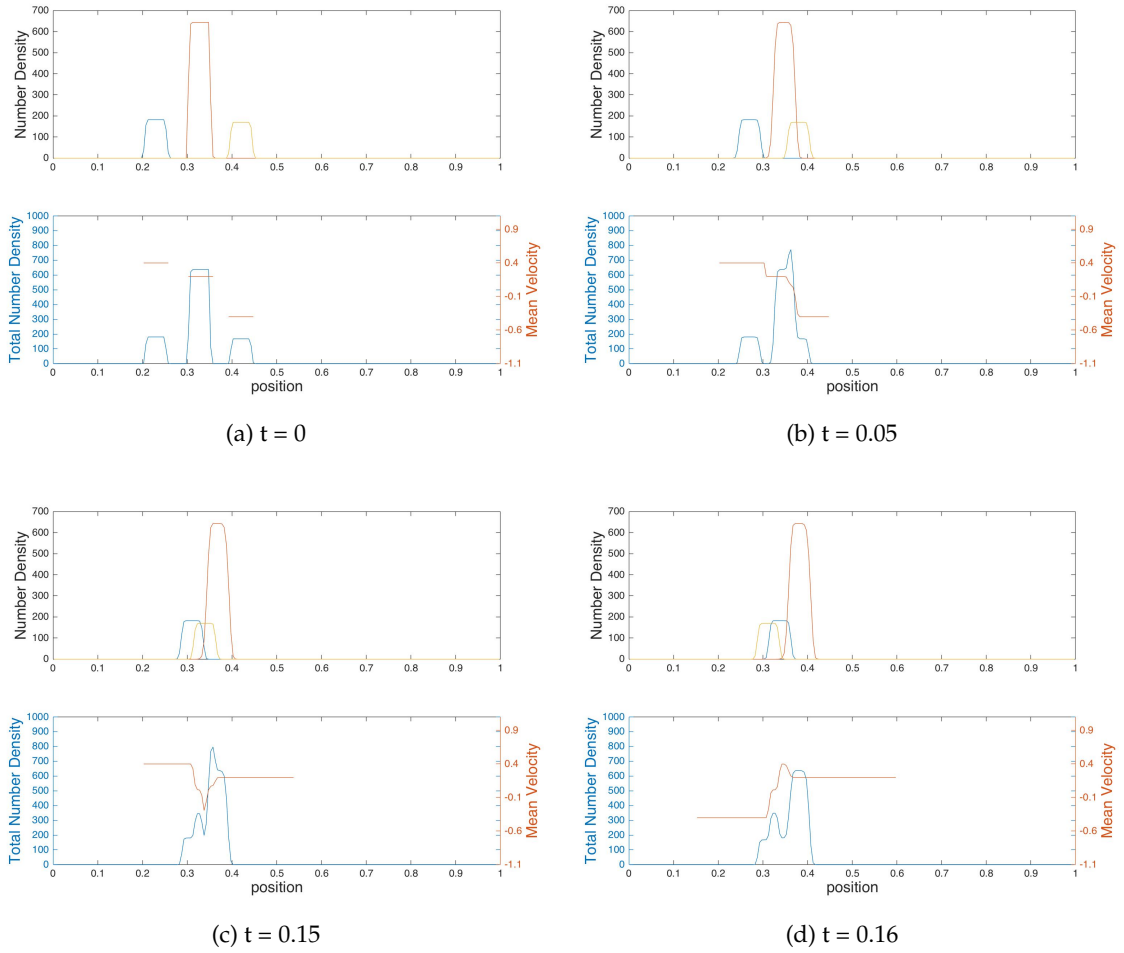


(a) t = 0

(b) t = 0.05

(c) t = 0.15

(d) t = 0.16

**Figure 5.1**: Trajectory crossing for particles of different sizes at initial times. (a) and (b) represent the initial condition and the crossing between Packets 2 and 3; the bottom plot shows the evolution of the total concentration and the mean velocity of the system. (c) and (d) represent the first interaction of Packets 1 and 3 and their respective total concentration evolution.

and size abscissas as initial conditions for all simulations.

The figures focus on the crossing events occurring during the simulation, up to $t = 0.2$. The three packets have mutually crossed each other as can be seen by the increase in number concentration in the bottom plots for the joint moments. At $t = 0.3$, particles with size $131 \times 10^{-6}$ have left the domain through the left and have entered it again through the right to cross again with the small particles (size $65 \times 10^{-6}$). Between times $t = 0.3$ and $t = 2$ the packets have left and reentered the domain several times and multiple crossing events have taken place. The ramifications of these results in modeling

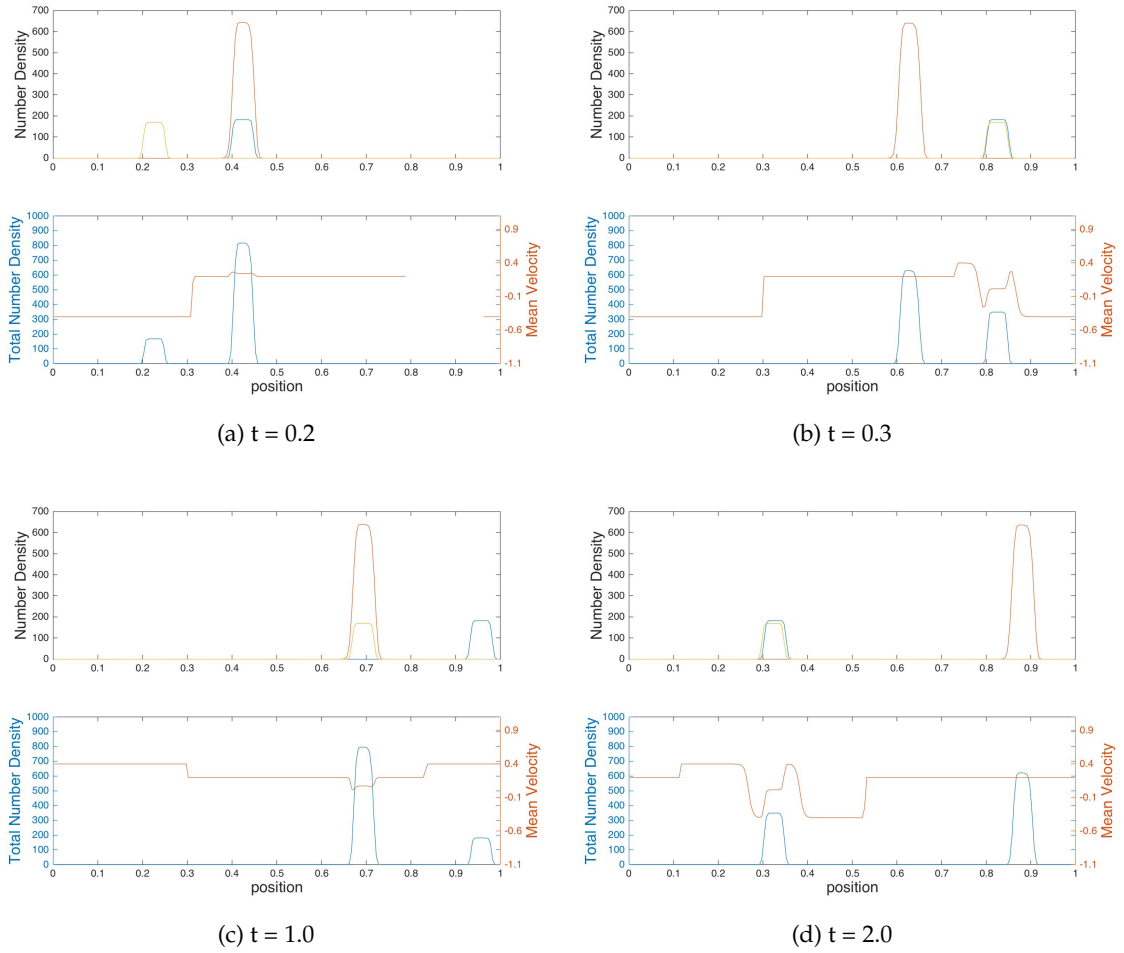


(a) t = 0.2

(b) t = 0.3

(c) t = 1.0

(d) t = 2.0

**Figure 5.2**: Trajectory crossing for particles of different sizes at later times. (a) represents a full interaction between Packets 1 and 2. In (b), Packet 3 has left the domain through the left and reentered through the right of the periodic domain to interact with Packet 1. In (c) and (d) the packets have left and reentered the domain several times; mean velocity and total concentration at these instances are shown in the bottom plots.

of polydisperse systems are important, since many of the current hydrodynamic-based Eulerian models lack the capability of capturing crossing of particles with a large Stokes number, especially particles with different sizes. Effects such as segregation in dilute systems can now be better approximated using these Eulerian methodologies resulting in a less expensive alternative to Lagrangian methods.

### 5.1.2 Advection With Drag

In most gas-particle systems, the dispersed phase experiences body forces exerted by the interaction with the fluid, the most common in many unit operations is the drag force.

Depending on the flow regime,[8] particles have a wide spectrum of Stoke numbers which becomes even more significant in polydisperse systems. It is possible to estimate the Stokes number based on the attributes[6] of the fluid and the particles and identify the regimes in which the particles are inertial and in which the particles follow closely the fluid. In turbulent flow, zones with high strain are common, when particles reach these zones they might follow the fluid patterns or they might cross the strained zone and their behavior will be determined by the Stokes regime of the particles, among other factors. In these zones, the solution of any Eulerian system for the particle velocity might become multivalued and hydrodynamic-based multiphase models are incapable of capturing these effects. This issue is represented by unphysical accumulation of mass in the zones of high strain,[29] which numerically correspond to *shocks* in the hydrodynamic model for the case of multivalued solutions.

For this analysis, a laminar Taylor-Green vortex has been chosen to represent the fluid solution. Although it is a laminar flow, it shares many of the most simple characteristics of turbulent systems, including high strain zones and vortex zones where particles and fluid interact according to the their regime of motion, but allowing a simpler treatment from a numerical and mathematical point of view. For the Taylor-Green flow, it has been shown through linearization around the locations of the high strain zones that the Stokes number for which particles would begin to cross[c] is approximately $\mathbb{S}t \approx 0.04$.[6] Hydrodynamic models (for instance, two fluid models) that represent particle regimes below $\mathbb{S}t \approx 0.04$ can represent well the particle velocity field which follows closely that of the fluid flow. On the contrary, mass accumulation will be predicted by the two-fluid models in zones where particles regimes are above $\mathbb{S}t \approx 0.04$, most likely where crossing is happening. **Figure 5.3**, **Figure 5.4** and **Figure 5.5** show simulations for three different particle sizes in a Taylor-Green vortex at Stokes numbers in the range $0.1 < \mathbb{S}t < 0.3$.

The previous results for the Stokes regime $0.1 < \mathbb{S}t < 0.3$ have been labeled *low Stokes regime*, the initial particle velocities for this regime is close to the gas velocity and the biggest effect on the Stokes number comes from the particle sizes. A *high Stokes regime* simulation has been run with Stokes numbers in the range $0.4 < \mathbb{S}t < 0.7$ and the con-

[c] At the corner of the vortex.

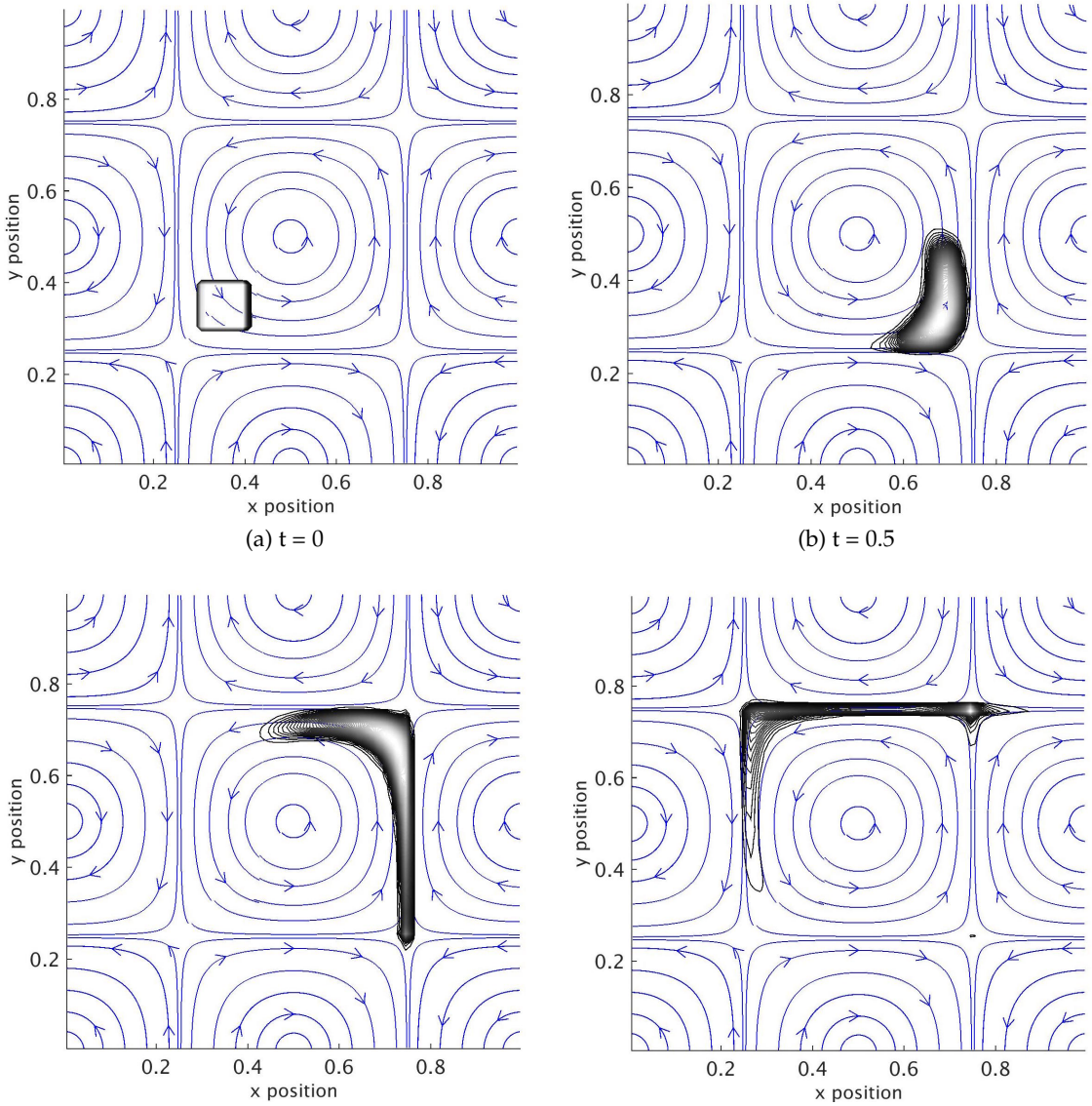


(a) t = 0 (b) t = 0.5

(c) t = 1.0 (d) t = 1.7

**Figure 5.3**: Zeroth moment (particle concentration) for 65 micron particles in a Taylor-Green vortex at low Stokes numbers. In this case, the initial velocity of the particles is the fluid velocity, which allows the Stokes number to be mainly influenced by the particle size.

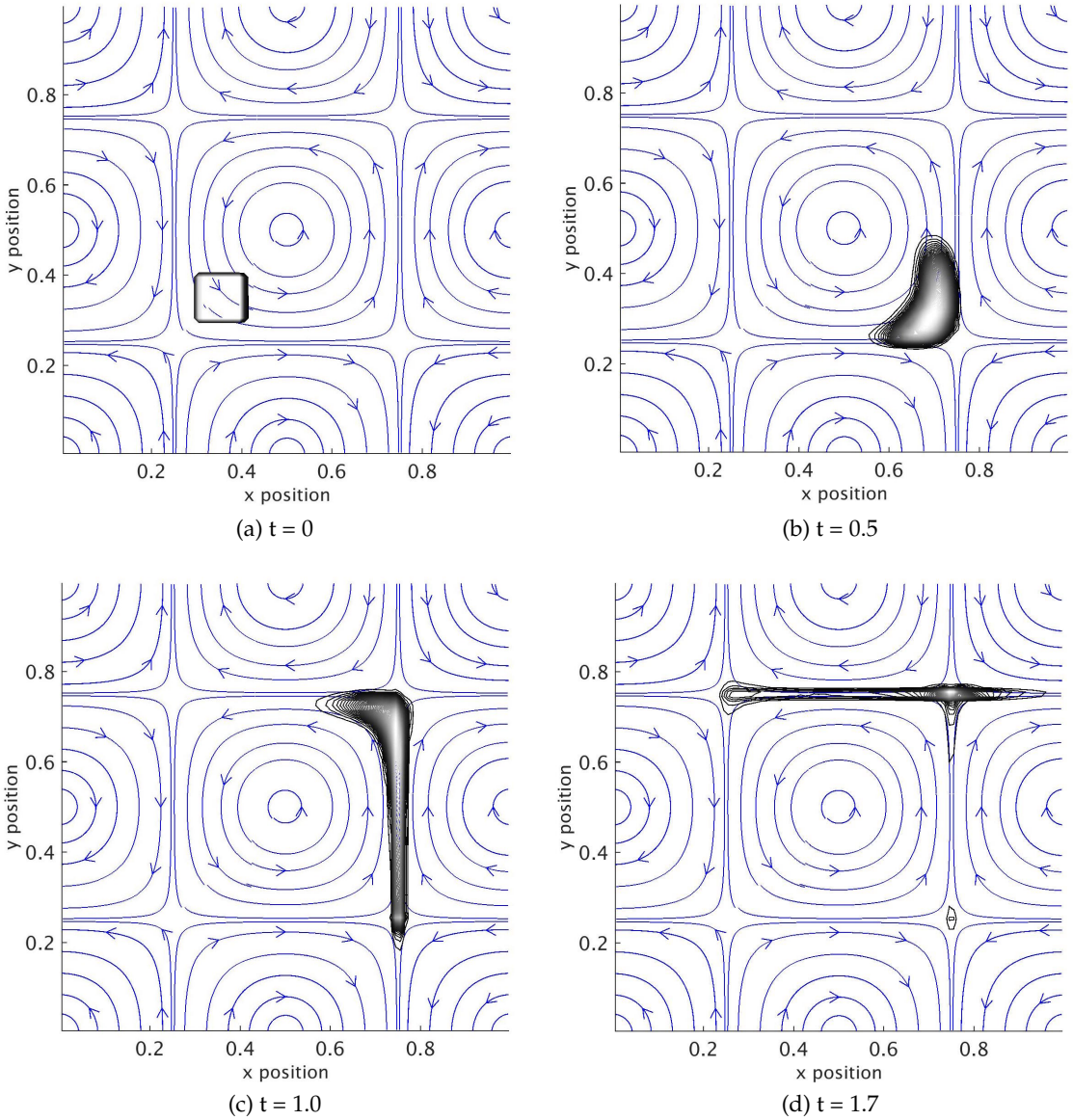


(a) t = 0 (b) t = 0.5

(c) t = 1.0 (d) t = 1.7

**Figure 5.4**: Zeroth moment (particle concentration) for 98 micron particles in a Taylor-Green vortex at low Stokes numbers. In this case, the initial velocity of the particles is the fluid velocity, which allows the Stokes number to be mainly influenced by the particle size.

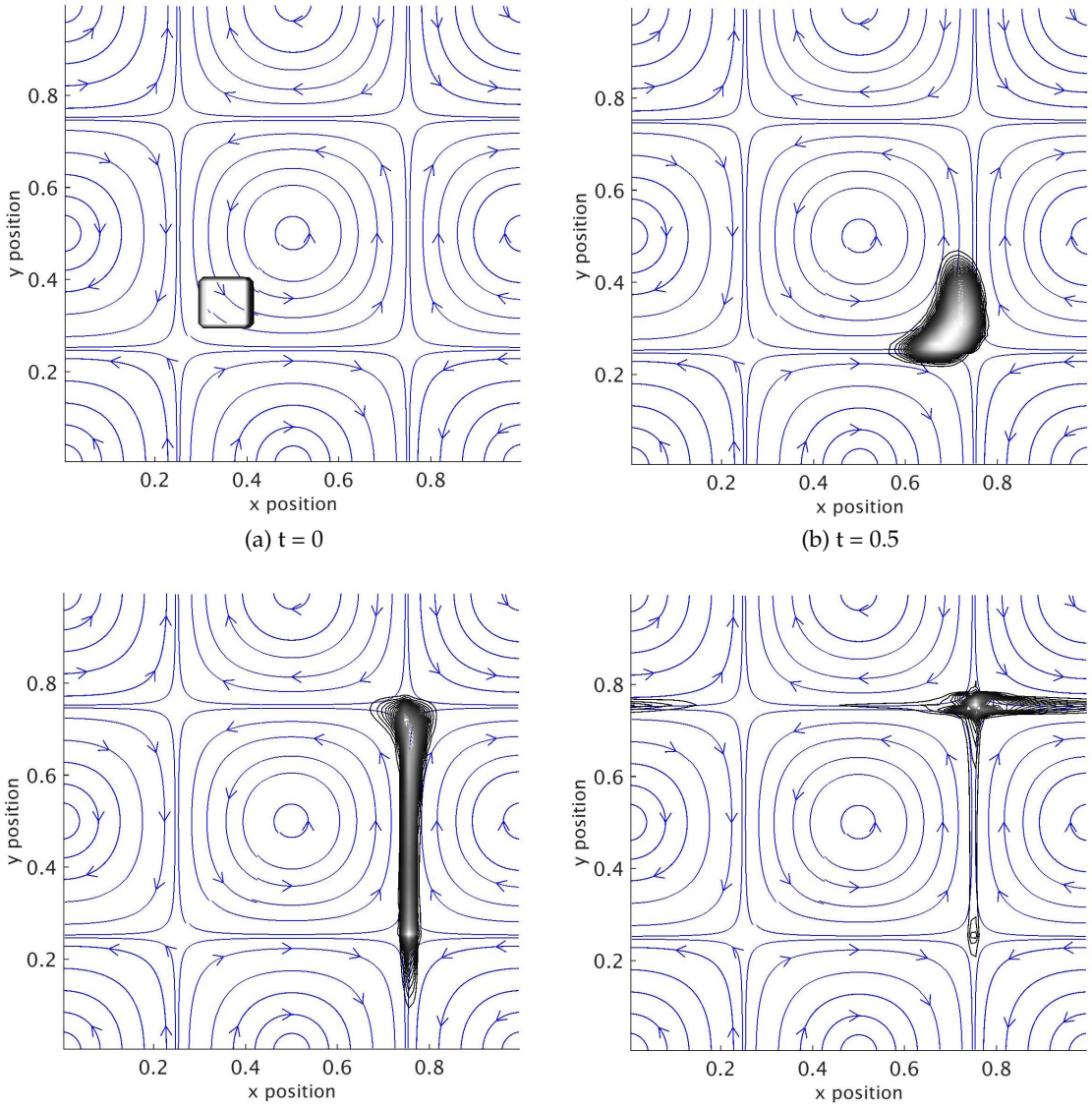


(a) t = 0 (b) t = 0.5

(c) t = 1.0 (d) t = 1.7

**Figure 5.5**: Zeroth moment (particle concentration) for 131 micron particles in a Taylor-Green vortex at low Stokes numbers. In this case, the initial velocity of the particles is the fluid velocity, which allows the Stokes number to be mainly influenced by the particle size.

tribution to the Stokes regimes comes from both the size and the velocity of the particles. In both simulations the effects of particle crossing were more pronounced near the corner of the vortex. The particles at *low Stokes* regime have a faster response time and follow the fluid sooner as shown in **Figure 5.3** compared with **Figure 5.6** in the *high Stokes* regime. **Figure 5.7** and **Figure 5.8** present simulations at *high Stokes* for medium and large particles.

The method captured the differences between the particles with low Stokes numbers and high Stokes numbers. For instance, for the big particles in range of high Stokes numbers at $t = 1.7$, some particles cross to the right at the upper right vortex due to their inertia and their velocity while the opposite behavior occurs for the particles in the low Stokes regime. For comparison, a Lagrangian simulation for particles around $98 \times 10^{-6}$ was run in the high range of Stokes numbers in order to verify the patterns presented by the Eulerian simulation. Results are presented in **Figure 5.9**. Differences between Lagrangian and Eulerian simulations are essentially due to the numerical diffusion present in the first order discretization scheme used in the Eulerian method, second or higher order discretization schemes would better represent the patterns of the Lagrangian simulations.

## 5.2 Example Applications in PMOM

As in **Section 5.1**, similar applications were tested for the proposed technique presented in **Chapter 4** (parceled method of moments, PMOM); these include PTC in one spatial dimension, advection with drag in two spatial dimensions, and a direct comparison with data from a char oxidation experiment. All these applications require the reconstruction of the PSD in the size coordinate; it is then necessary test the accuracy of the reconstruction even before the proposed examples.

### 5.2.1 Goodness of the Particle Size Reconstruction

We have tested the accuracy of the reconstruction using a unimodal distribution. For this test, 1000 normally distributed particles are evolving in time according to the growth law

$$\frac{\mathrm{d}D_p}{\mathrm{d}t} = 0.5\sqrt{D_p}. \tag{5.1}$$

Although this growth model might not represent any particular real system, it provides valuable information about the accuracy of the reconstruction. The rate in **Equation** (5.1)

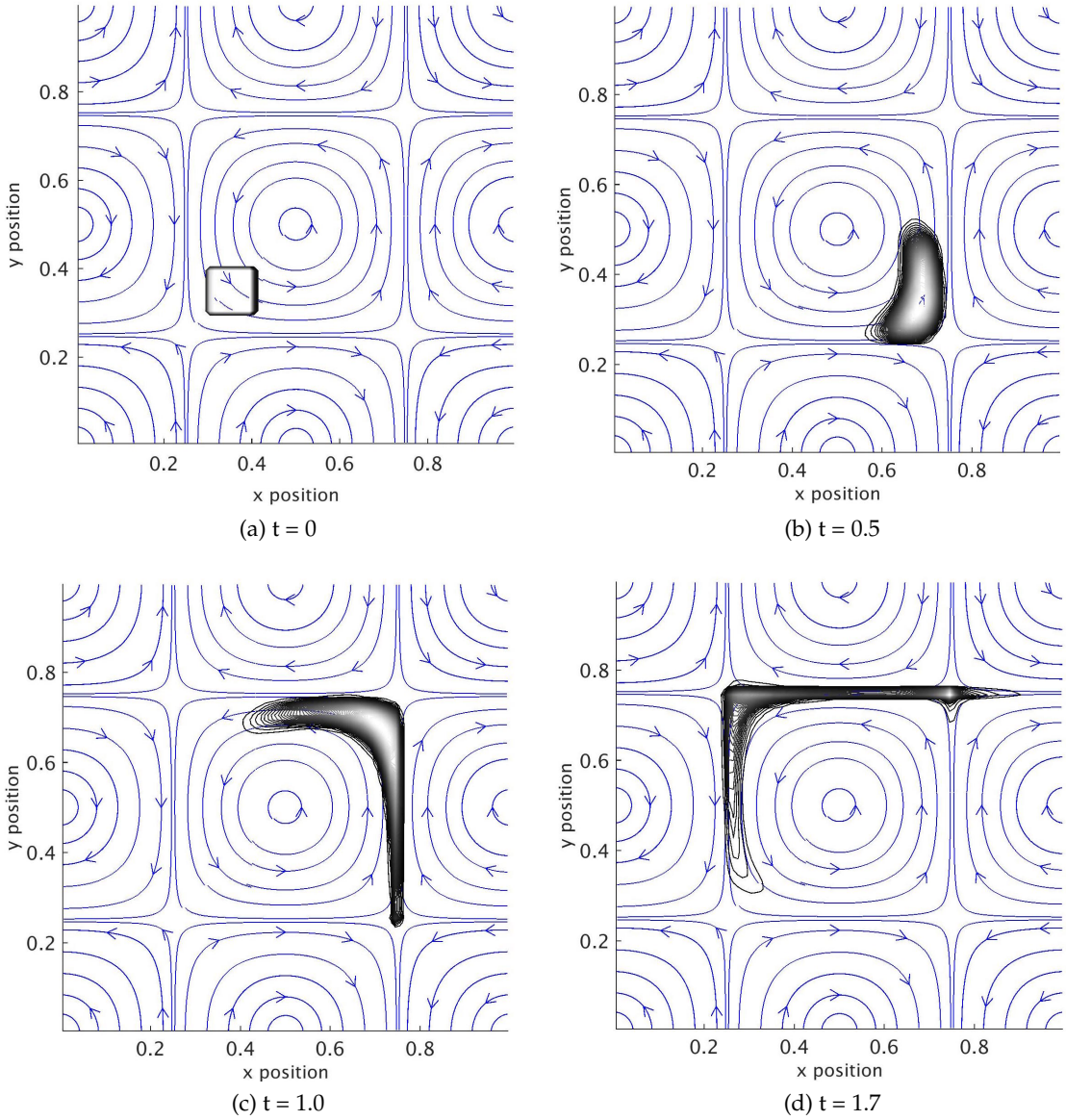


(a) t = 0 (b) t = 0.5

(c) t = 1.0 (d) t = 1.7

**Figure 5.6**: Zeroth moment (particle concentration) for 65 micron particles in a Taylor-Green vortex at high Stokes numbers. The initial velocity of the particles is higher than the local velocity of the fluid; the Stokes number is controlled by both size and velocity of the particle.

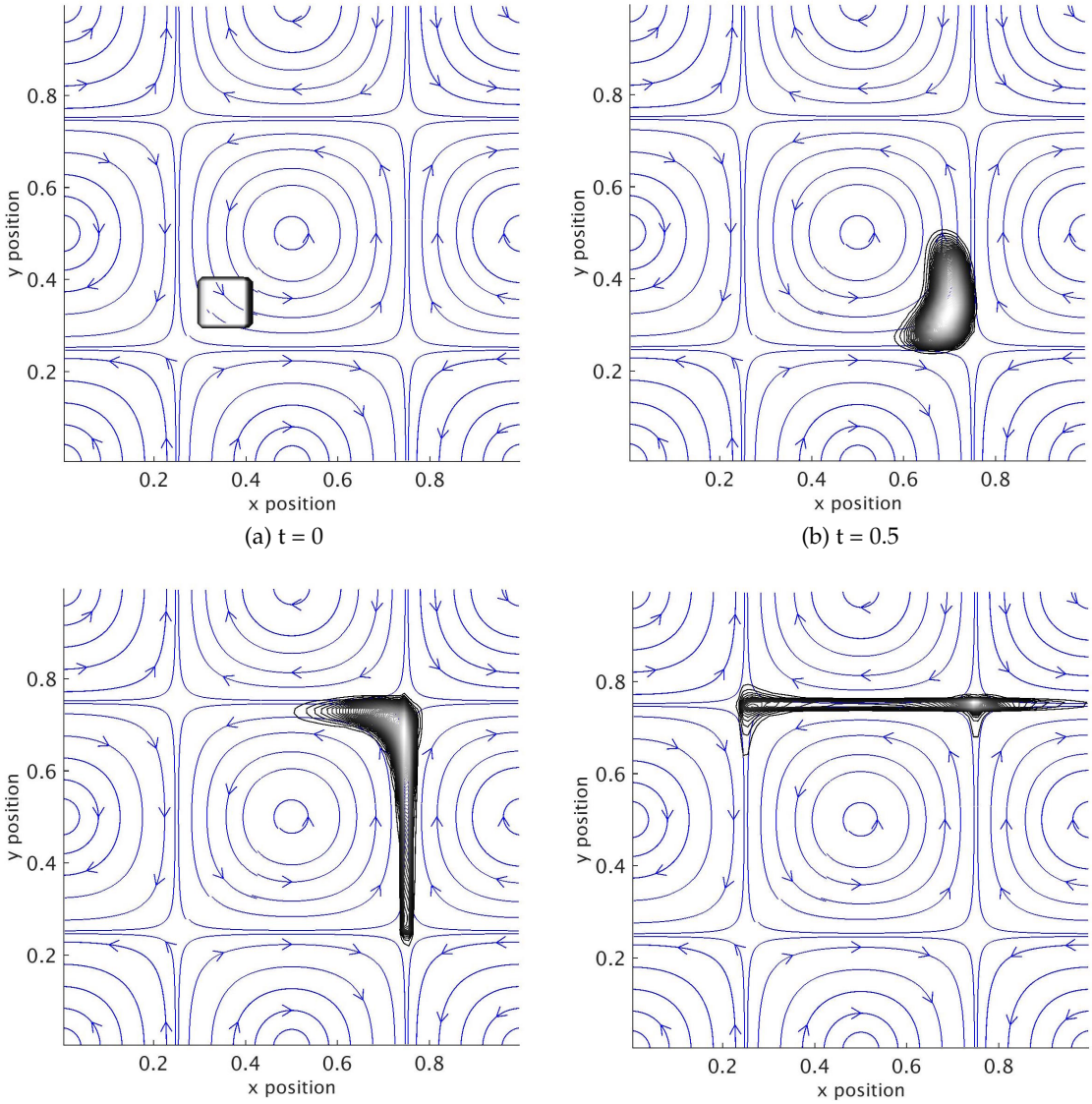


(a) t = 0 (b) t = 0.5

(c) t = 1.0 (d) t = 1.7

**Figure 5.7**: Zeroth moment (particle concentration) for 98 micron particles in a Taylor-Green vortex at high Stokes numbers. The initial velocity of the particles is higher than the local velocity of the fluid; the Stokes number is controlled by both size and velocity of the particle.

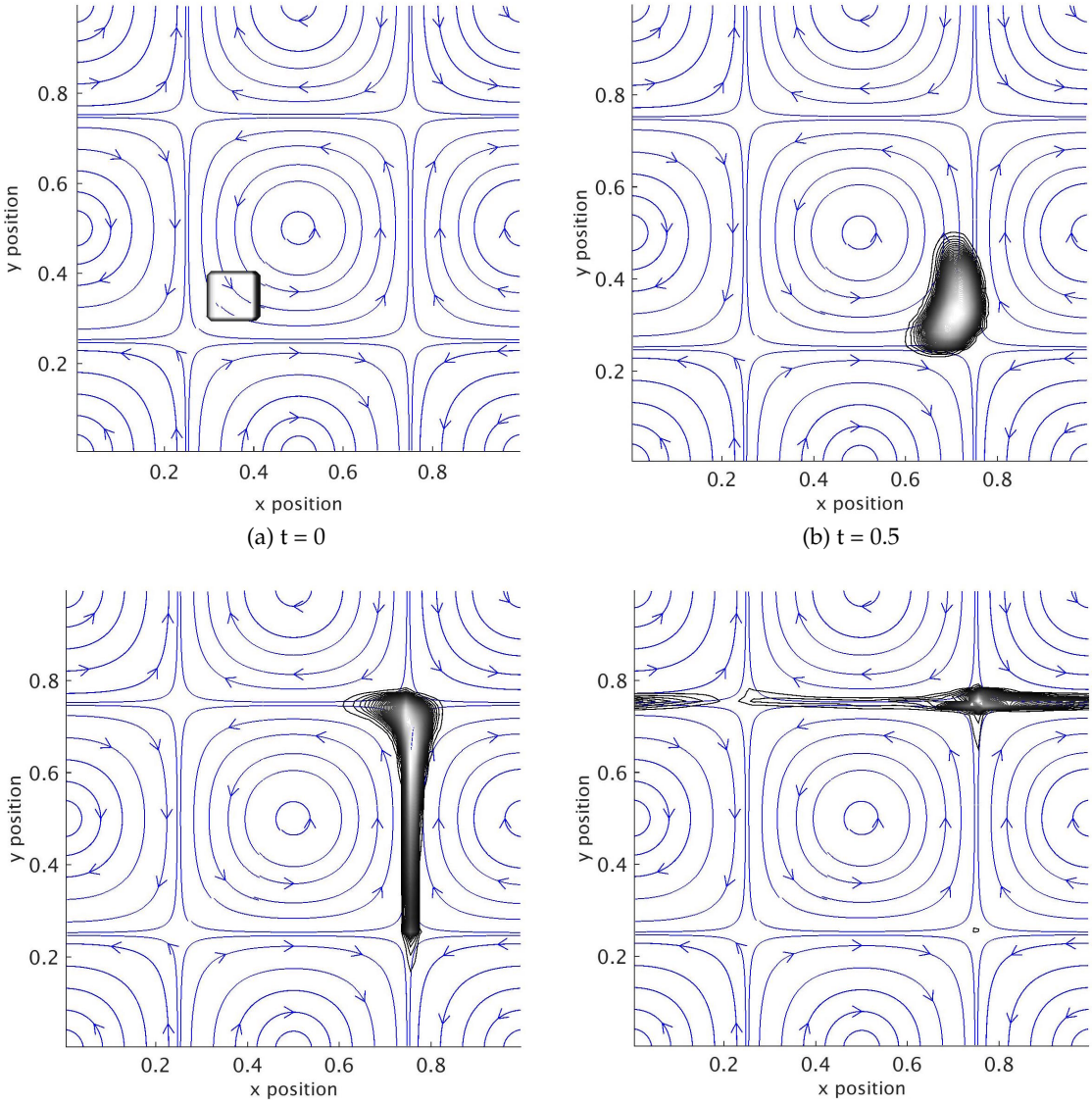


(a) t = 0 (b) t = 0.5

(c) t = 1.0 (d) t = 1.7

**Figure 5.8**: Zeroth moment (particle concentration) for 131 micron particles in a Taylor-Green vortex at high Stokes numbers. The initial velocity of the particles is higher than the local velocity of the fluid; the Stokes number is controlled by both size and velocity of the particle.

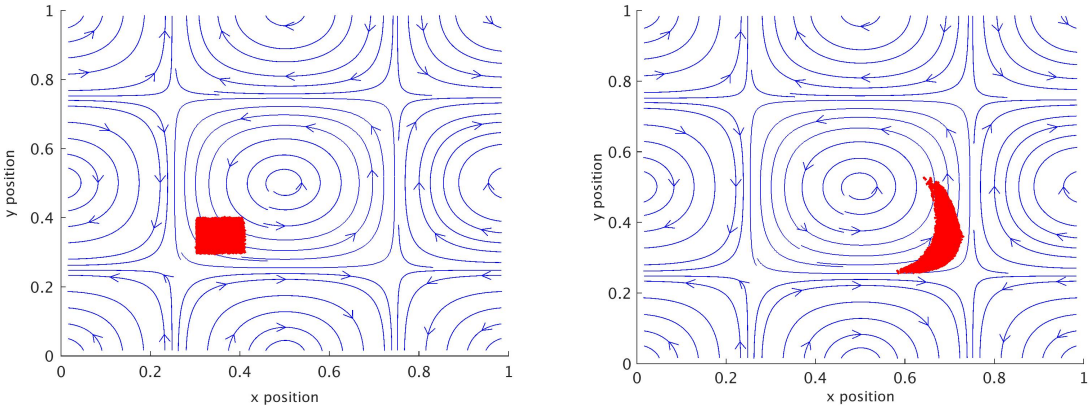


(a) t = 0

(b) t = 0.5

(c) t = 1.0

(d) t = 1.7

**Figure 5.9**: Particle concentration for 98 micron Lagrangian particles in a Taylor-Green vortex at high Stokes numbers. This is a direct comparison with **Figure 5.7** and the differences are due to the numerical in the Eulerian moment-based method.

advects the particles in size space. In physical space, this would be represented by particles suspended in a fluid, growing in diameter. Initial raw moments were obtained from the distributed particles and were used to formulate the reconstruction as described in **Section 4.4**. As time evolves, the sample moments of the data are used to reconstruct the distribution of particles with PMOM at each time step, the *real* distribution based on maximum likelihood estimates is also obtain at each time step for comparison. **Figure 5.10** presents the comparison between the particle distribution and the reconstructed distribution at $t = 0$ ms and $t = 20$ ms. For this case, only one iteration of the linear solver was needed and 5 parcels were used at each time step.

It is more common than not for particle distributions to be bimodal; the same test has been run to represent 2000, initially binormal distributed particles, assuming the same growth law. Results are presented in **Figure 5.11**. This results were obtained using six

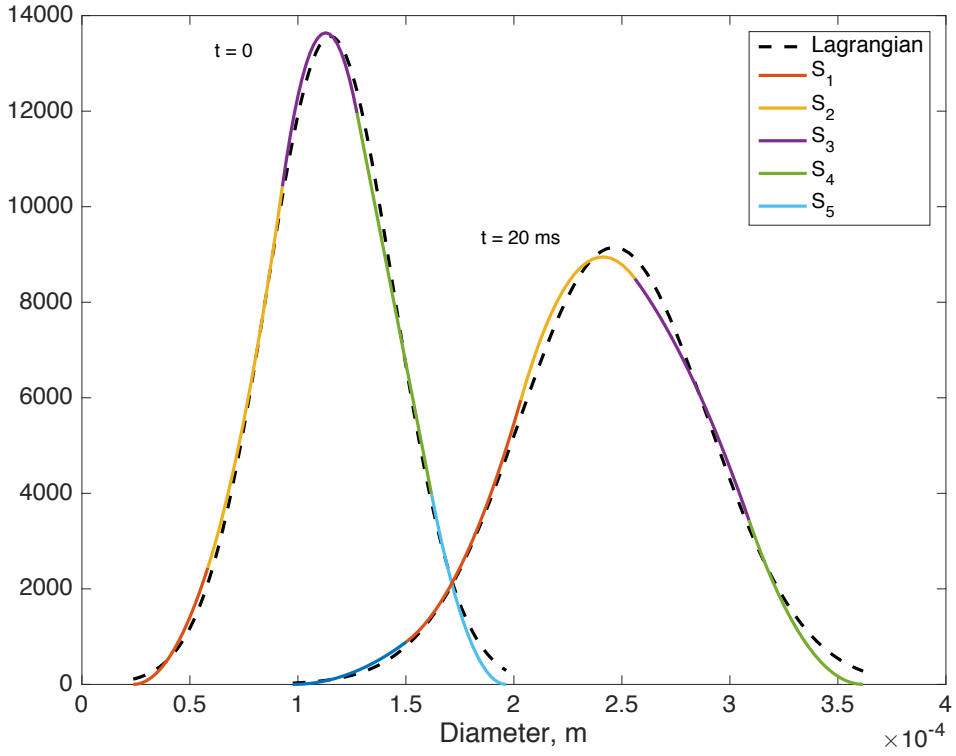


**Figure 5.10**: Comparison between particle distribution and reconstructed distribution at the beginning and at the end of the simulation. The dashed lines represent the particle distribution obtained via maximum likelihood estimation based on the distributed data. The continuous lines represent the polynomial approximations of the particle distribution based on the raw moments of the data.

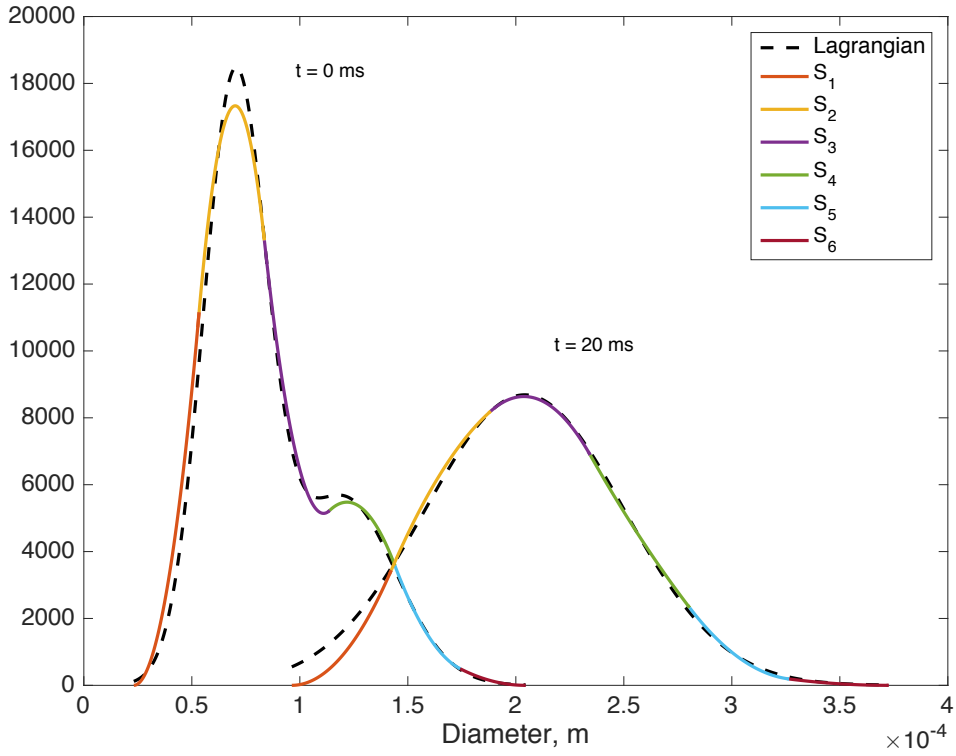


**Figure 5.11**: Comparison between particle distribution and reconstructed distribution at the beginning and at the end of the simulation. The dashed lines represent the particle distribution obtained via maximum likelihood estimation based on the bimodal data. The continuous lines represent the polynomial approximations of the particle distribution based on the raw moments of the bimodal data.

parcels and only one iteration of the linear solver.

In order to asses the accuracy of the reconstruction, the relative error between the moments of the original distribution and the moments of the reconstructed distribution was measured. The error is defined as

$$\text{error} = \frac{\int_{\mathbb{R}} \xi^l \mathfrak{F} d\xi - \int_{\mathbb{R}} \xi^l \mathfrak{F}_r d\xi}{\int_{\mathbb{R}} \xi^l \mathfrak{F} d\xi}, \tag{5.2}$$

where $\mathfrak{F}_r$ is the reconstructed distribution and $\mathfrak{F}$ is the Lagrangian particle distribution. **Figure 5.12** shows the error for the unimodal and bimodal distribution at $t = 0$ ms and $t = 20$ ms; the error was measured for combinations of number of moments and number of parcels. The general trends in **Figure 5.12** shows that the error incurred in the reconstruction of the unimodal distribution is smaller than the error of the reconstruction of the bimodal distribution. In theory, fewer moments are required to reconstruct a unimodal distribution than a bimodal distribution.[142,143] Also, the trend indicates that accuracy is

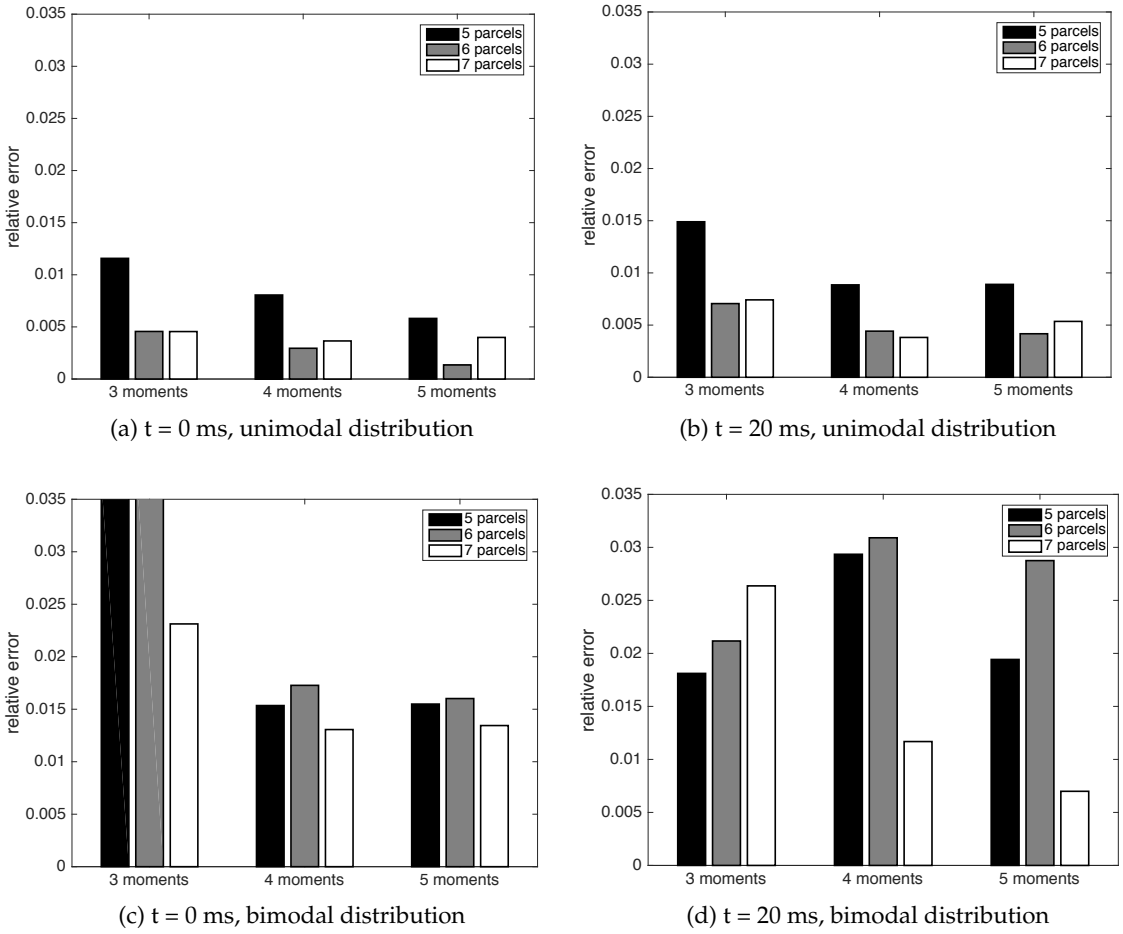


(a) t = 0 ms, unimodal distribution

(b) t = 20 ms, unimodal distribution

(c) t = 0 ms, bimodal distribution

(d) t = 20 ms, bimodal distribution

**Figure 5.12**: Relative error for combinations of 3, 4, and 5 moments with 5, 6, and 7 parcels. For instance, each of three bars over the label *moment* corresponds to 5, 6, and 7 parcels used in the reconstruction of both unimodal and bimodal distributions. The vertical axis shows the relative error of each combination.

increased by using more than 5 parcels with 5 moments or more. The technique allows increasing the number of moments and parcels arbitrarily to increase the accuracy of the reconstruction, but at an increased cost on the computational loop presented in **Section 4.5.3**.

### 5.2.2 Particle Trajectory Crossing

The complex interactions between the fluid and the particles produce particles that move with a broad spectrum of Stokes numbers, with some of these particles being able to cross between eddies and interact with other clouds of particles; this phenomena is best explained from the stochastic point of view.[4,9,84,110,140,141] Unfortunately, most of the Eulerian methods based on the Navier-Stokes equations fail to explain or capture it for dilute multiphase systems.[8] On the other hand, previously formulated Eulerian moment-based techniques[29,43,47,61] use multinode quadratures that allow them to capture clouds of different characteristics crossing each other. The methodology presented in this dissertation is essentially a moment-based method and it is important to test its ability to also capture particle trajectory crossing. The proposed test is similar to those proposed in Desjardins and Fox[47] and Desjardins et al.[29] in which two waves or "packets" represented by two quadrature velocity abscissas travelling at opposing velocities interact with each other in a spatial grid. The results are shown in **Figure 5.13** and **Figure 5.14**.

Initially, each cell in the Eulerian grid contains an NDF that represents approximately 1000 normally distributed particles, similar to that reconstructed in **Figure 5.10**. Each NDF is divided into 6 parcels with particle size ranges as shown in **Table 5.1**.

The method successfully tracks the evolution of these distributions in each cell at each time step. As in the previous section, time and space are nondimensional; size is also nondimensional but properly scaled to represent the order of magnitude of the sizes. The top panels in **Figure 5.13** and **Figure 5.14** show the evolution of the distribution at a position $x = 0.5$, very close to the point of the crossing of the packets for the first time. The velocity weights are $w_\alpha = 0.5$ for each packet and they have opposite velocities of $|U| = 0.2$. The particles are advected in physical space at their own velocity[d] and no other rate is affecting the behavior of the particles; ultimately, the NDF is not being advected in size space, but its value (related to particle concentration) is changing according to the

[d] St is infinite.

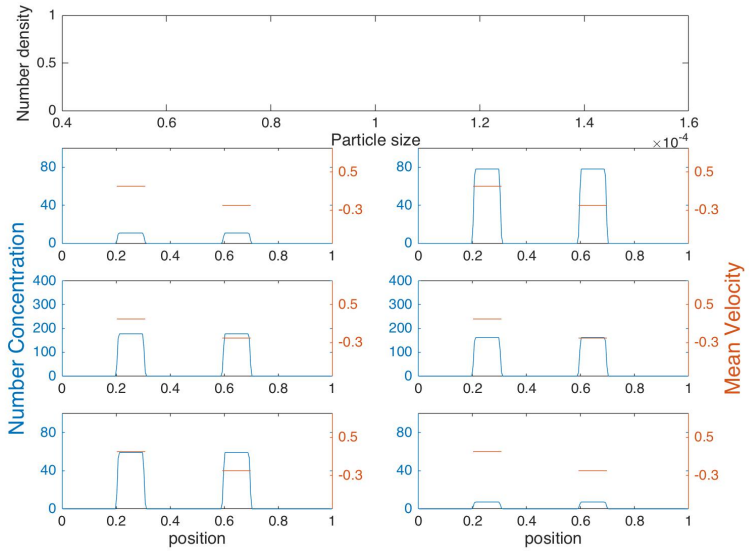


(a) t = 0

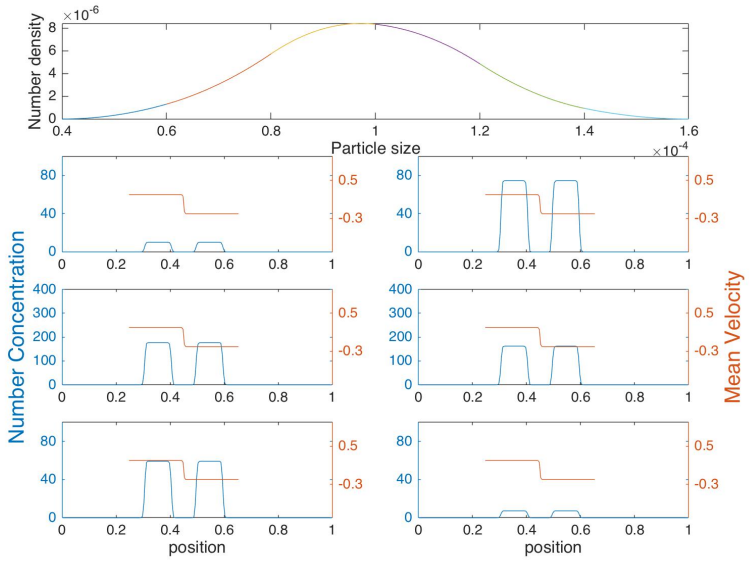


(b) t = 0.25

**Figure 5.13**: Trajectory crossing for distributed particles in a 1-dimensional Eulerian grid with the NDF reconstruction at $x = 0.5$. Each pair of packets represents a parcel projected onto the computational cells. In (a) there are no numerical moments at the beginning of the simulation; in (b) PMOM reconstructs the distribution as soon as numerical moments are advected in the computational cells. This can be seen in the numerical value of the NDF.

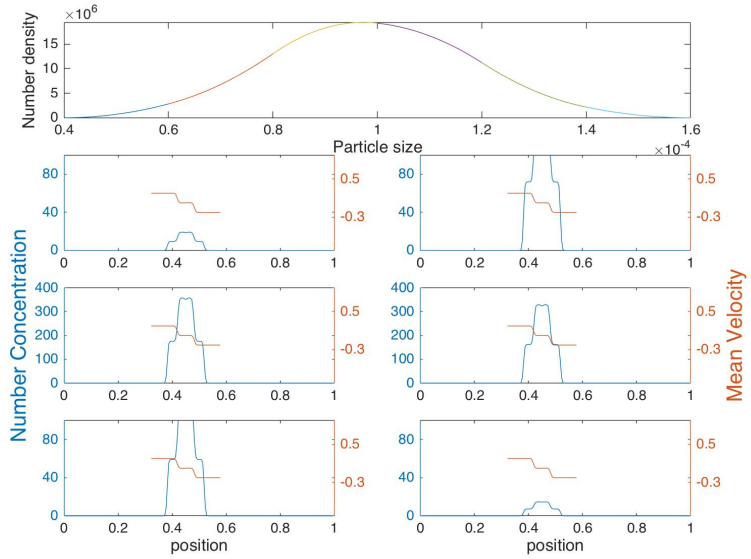


(a) t = 0.45

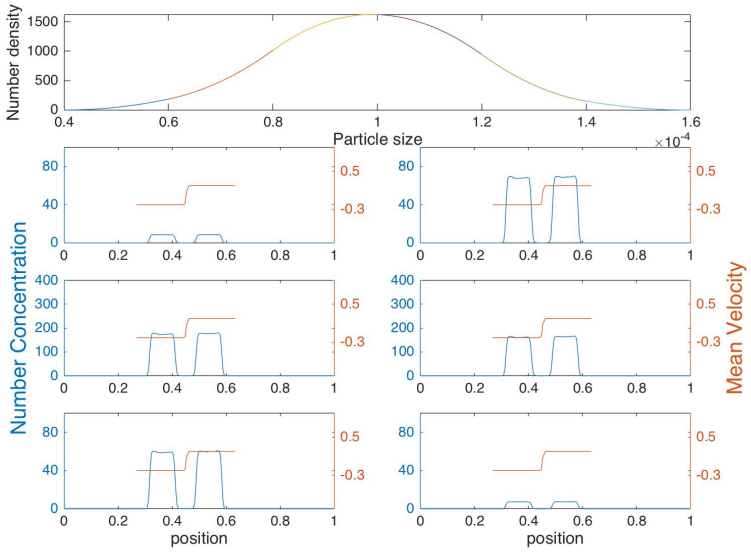


(b) t = 0.7

**Figure 5.14**: Trajectory crossing for distributed particles in a 1-dimensional Eulerian grid with the NDF reconstruction at $x = 0.5$. In (a) the value of the NDF is maximum, coinciding with the full interaction of the packets at the point of crossing, once the packets pass through each other the value of the NDF diminishes again, as shown in (b).

**Table 5.1**: Particle size ranges for each parcel

| Parcel | Particle size range |
|---|---|
| Parcel 1 | $[40 \times 10^{-6}, 60 \times 10^{-6}]$ |
| Parcel 2 | $[60 \times 10^{-6}, 80 \times 10^{-6}]$ |
| Parcel 3 | $[80 \times 10^{-6}, 100 \times 10^{-6}]$ |
| Parcel 4 | $[100 \times 10^{-6}, 120 \times 10^{-6}]$ |
| Parcel 5 | $[120 \times 10^{-6}, 140 \times 10^{-6}]$ |
| Parcel 6 | $[140 \times 10^{-6}, 160 \times 10^{-6}]$ |

interaction of the packets. The bottom panels show the evolution of the zeroth moment (mean total concentration) and mean velocity for each parcel. At time $t = 0.25$, the method detects numerical particles at the sampled position and reconstruct a distribution with very low values for the NDF. At $t = 0.45$ where the two packets have almost completely superimposed, the NDF reaches its maximum value and after $t = 0.7$ the NDF decreases until there are no more numerical particles in the sampled cell. As expected, the crossing behavior is similar to that presented in early works with monodisperse particles.[29,47,61,111] Although this is a very simple example, it is very important, because it represents a method that can potentially reconstruct a statistical distribution without the need of statistical particles (Lagrangian method) at a lower computational cost and in an Eulerian method.

### 5.2.3 Advection With Drag

In this example we have also chosen a laminar Taylor-Green vortex for the fluid solution. The reason behind this choice was explained in **Section 5.1**. In turbulent flow, zones with high strain are common and when particles reach these zones they might follow the fluid patterns or they might cross the strained zone, in this case the particle behavior will be determined by their Stokes regime, among other factors. In these zones, the solution of any Eulerian system for the particle velocity might become multivalued and hydrodynamic-based multiphase models are incapable of capturing the effects produced by the crossing. This issue is represented by unphysical accumulation of mass in the zones of high strain,[29] which numerically, corresponds to *shocks* in the hydrodynamic model for the case of multivalued solutions. For the Taylor-Green flow, it has been shown through linearization around the locations of the high strain zones that the Stokes number for which

particles would begin to cross[e] is approximately $\mathbb{S}t \approx 0.04$.[6] Hydrodynamic models (for instance, two fluid models) that represent particle regimes below $\mathbb{S}t \approx 0.04$ can represent well the particle velocity field which follows closely that of the fluid flow. On the contrary, mass accumulation will be predicted by the two-fluid models in zones where particle regimes are above $\mathbb{S}t \approx 0.04$, most likely where crossing events are happening. The interval of Stokes numbers simulated in this example covers the range $0.1 < \mathbb{S}t < 0.4$, which is affected by both size and velocity of the particles. The interval includes particle sizes that might follow the fluid and might cross the high strained zones as shown in **Figure 5.15** and **Figure 5.16**.

As in the 1-dimensional example, the method is reconstructing the distribution in each cell at each time step and the evolution of the distribution is tracked at position $x = 0.4, y = 0.4$. The top panels in the figures show how the particle size distribution shifts when Eulerian particles are advected in the computational grid. As before, each cell starts with a normally distributed NDF, as the simulation progresses, small particles respond faster to the fluid time scales due to their low Stokes regime and leave the computational cell faster. This effect makes the reconstructed distribution shift its mean towards bigger particles, as can be seen in **Figure 5.15** and **Figure 5.16** as time increases. Once the particles have traveled all around the domain, small particles arrive first to the computational cell and the distribution start shifting back towards its original mean.

### 5.2.4 Char Oxidation

So far we have discussed rates that affect the particle distribution in velocity space (i.e., drag) due to our interest in capturing PTC, which is essentially driven by body and superficial forces over the particles. Other scalar rates also affect the particle distribution in different coordinates of the phase-space: particle mass, particle temperature, and particle size as was explained in **Chapter 2**. In order to describe some of these rates in a real application, a detailed characterization of the heat and mass transfer process occurring during char oxidation is simulated. An entrained flow reactor was used to burn the particles and measurements of temperature and char mass fraction were taken during the evolution of the combustion process.[144] Particle temperature, particle mass, particle

[e] At the corner of the vortex.

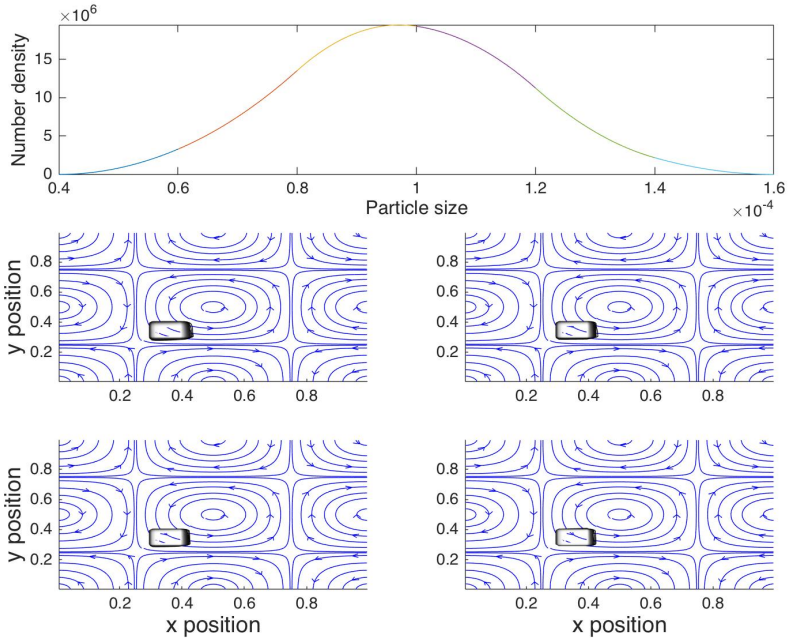


(a) t = 0

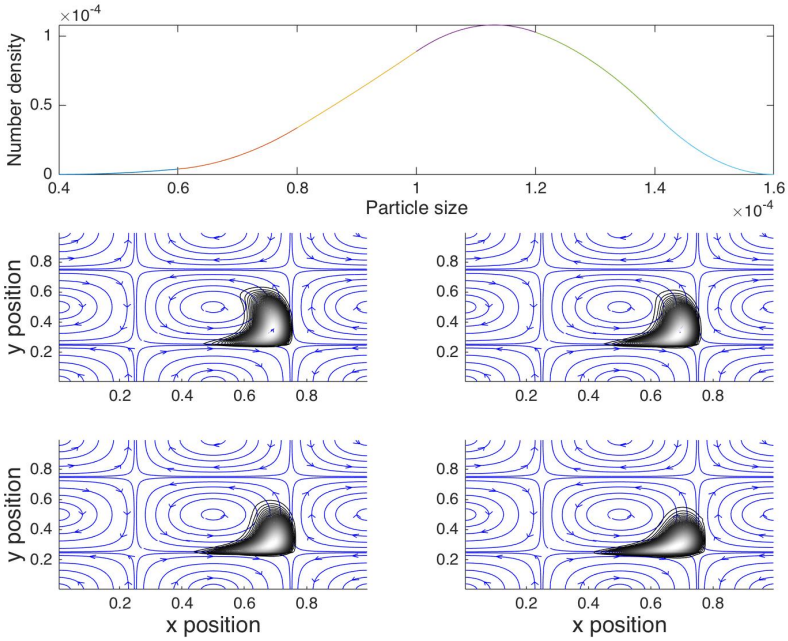


(b) t = 0.5

**Figure 5.15**: Advection of parcels 1, 3, 4, and 6 in a Taylor-Green vortex. Particles started with a slightly greater velocity than the fluid, small particles in Parcel 1 will respond faster to the fluid forces compared to particles in Parcel 6.

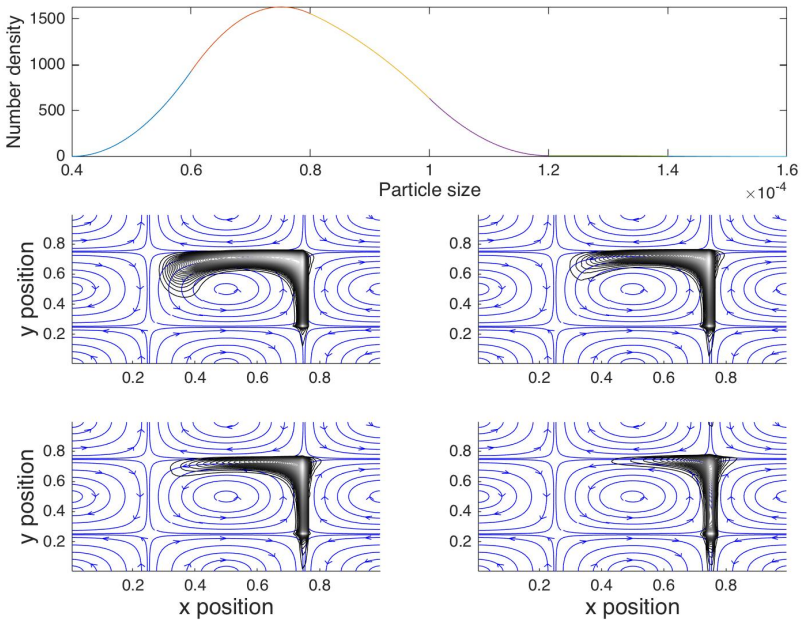


(a) t = 1.0

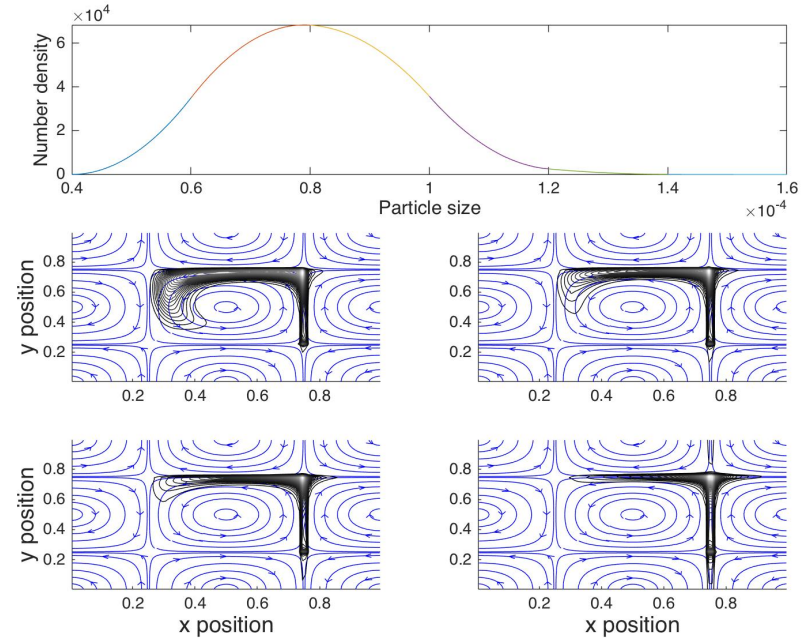


(b) t = 1.2

**Figure 5.16**: Advection of parcels 1, 3, 4, and 6 in a Taylor-Green vortex. Note the shift in the distributions in the top plots; large particles from each parcel are left behind which shifts the mean of the distribution when evolved in time.

velocity, and particle size were the variables tracked during the combustion process. The moment equations for this particular process can be written as

$$\begin{aligned}\frac{\partial \mathfrak{M}_k^{(l,M,T,N)}}{\partial t} + \frac{\partial \mathfrak{M}_k^{(l,M,T,N+1)}}{\partial x} = \\ + M \sum_{\alpha=1}^{N_v} w_{k,\alpha} \int_{s_k}^{s_{k+1}} \xi^l \mathfrak{g}_k(\xi) \left( [\mathrm{U}_{k,\alpha}(\xi)]^N [\overline{m}_k(\xi)]^{M-1} [\overline{\theta}_k(\xi)]^T \mathrm{G}(\xi, \overline{m}_k(\xi), \overline{\theta}_k(\xi)) \right) \mathrm{d}\xi \\ + T \sum_{\alpha=1}^{N_v} w_{k,\alpha} \int_{s_k}^{s_{k+1}} \xi^l \mathfrak{g}_k(\xi) \left( [\mathrm{U}_{k,\alpha}(\xi)]^N [\overline{m}_k(\xi)]^{M} [\overline{\theta}_k(\xi)]^{T-1} \mathrm{H}(\xi, \overline{m}_k(\xi), \overline{\theta}_k(\xi)) \right) \mathrm{d}\xi \\ + N \sum_{\alpha=1}^{N_v} w_{k,\alpha} \int_{s_k}^{s_{k+1}} \xi^l \mathfrak{g}_k(\xi) [\overline{m}_k(\xi)]^M [\overline{\theta}_k(\xi)]^T [\mathrm{U}_{k,\alpha}(\xi)]^{N-1} \frac{1}{\overline{m}_k} \mathrm{F}_\alpha(\xi, \overline{\theta}_k(\xi), \mathrm{U}_\alpha(\xi)) \mathrm{d}\xi,\end{aligned} \tag{5.3}$$

where the indexing correspond to: $l$ size, $M$ mass, $T$ temperature, and $N$ velocity. F, G, and H are the rates of change of particle velocity ($\xi$), particle mass ($\overline{m}_p$), and particle temperature ($\overline{\theta}$), respectively. Particle acceleration (advection in velocity coordinate) due to drag forces can be written as

$$\mathrm{F} = \frac{3\overline{m}_k \rho_g}{4\rho_p \xi} \mathrm{C}_d |\mathrm{U}_{k,r}| \mathrm{U}_{k,r}, \tag{5.4}$$

where

$$\mathrm{U}_{k,r} = \mathrm{U}_g - \mathrm{U}_{k,\alpha}. \tag{5.5}$$

The drag coefficient is given by Schiller-Naumann correlation

$$\mathrm{C}_d = \frac{24}{\mathbb{R}\mathrm{e}_p} \left( 1 + 0.15 \mathbb{R}\mathrm{e}_p^{0.687} \right), \tag{5.6}$$

in which

$$\mathbb{R}\mathrm{e}_p = \frac{\rho_g \xi |\mathrm{U}_{k,r}|}{\mu_f}, \tag{5.7}$$

$\mu_f$ being the dynamic viscosity of the gas phase and $\mathrm{U}_{k,\alpha}$ is the velocity of particle $\alpha$ in the parcel $k$.

The rate of change of particle temperature includes heat transfer due to radiation exchange, heat transfer by convection due to mass transfer from the particle to the fluid

phase, and heat generation due to chemical reactions occurring inside and at the surface of the particle. The mathematical expression can be written as[144]

$$\mathrm{H}(\xi, \overline{m}_p, \overline{\theta}) = -\frac{6\varepsilon\sigma_h}{\xi C_p \rho_p}(\theta^4 - T_w^4) - \frac{12\gamma_h}{\xi^2 C_p \rho_p}\left[\frac{\kappa/2}{\exp(\kappa/2) - 1}\right](\theta - T_g) + q\Delta h, \tag{5.8}$$

where the quantity,

$$\kappa = \frac{-q\xi}{\gamma}\sum_{i=1}^{N_{spe}} v_i C_{g,i} \tag{5.9}$$

corresponds to the ratio of convective velocity of the net mass leaving the particle surface to the diffusive velocity of heat leaving the surface (Peclet number), where $v_i$ are the stoichiometric coefficients defined in terms of the oxidizer-fuel ratio given by an Arrhenius-like expression,[144,145] and $q$ is the burning rate calculated based on the kinetic expression for the heterogeneous reaction occurring at the particle surface.[144] The rate of mass change is given in terms of the burning rate as

$$\mathrm{G}(\xi, \overline{m}_p, \overline{\theta}) = \pi\xi^2 q \mathrm{M}_c, \tag{5.10}$$

where $\mathrm{M}_c$ is the molecular weight of carbon. The heat transfer parameters were taken as in the original paper from Murphy and Shaddix.[144]

**Equation** (5.3) was used with the described rates to represent a plug flow reactor with specified gas temperature profiles and a constant initial velocity at the inlet for all the particles.[144] The initial particle size distribution is normal, with a mean size of $\overline{\xi} = 115$ microns and a standard deviation of $\sigma = 30$ microns. Initial particle mass and temperatures are $M_0 = 2.15 \times 10^{-9}$ kg and $T_0 = 1900$ K for all particles. Five parcels with their respective transport equations were used to discretize the size coordinate and three joint size moments were used to reconstruct the particle size distribution at each time step. **Figure 5.17** shows the temporal evolution of the particle temperature and char mass fraction for each parcel. The comparison with the experimental results show qualitative agreement with the data and refinement of the physics used might further improve the results of the model.[f] The purpose of the test was to show how this polydispersity technique captured the essential features of the results without the need of the Lagrangian, single particle

[f] For instance, the abrupt drop in the temperature profile happens when the particle runs out of organic matter and everything is left is mineral matter.

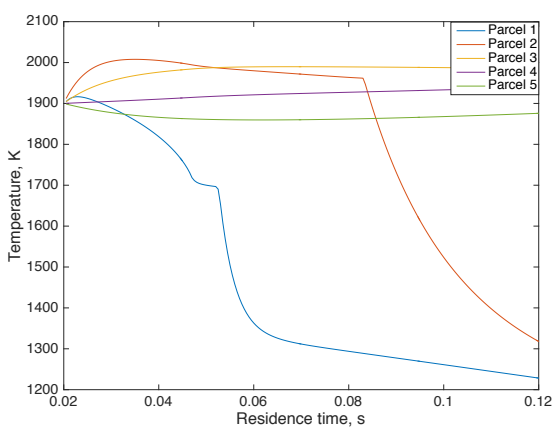


(a) Evolution of temperature per parcel

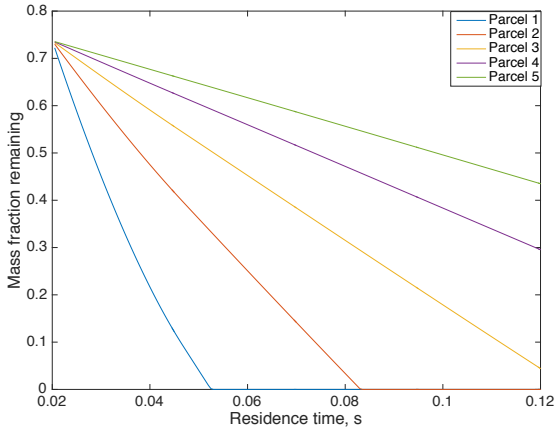


(b) Evolution of mass fraction per parcel

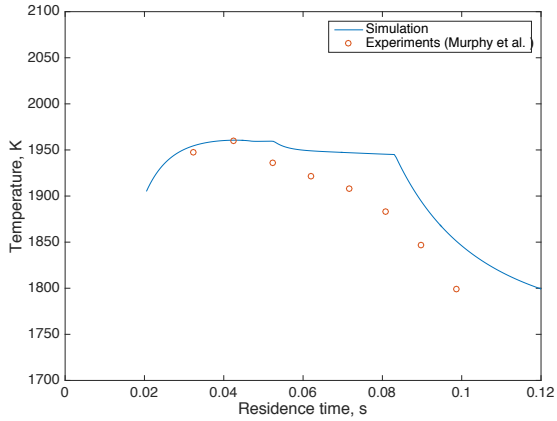


(c) Evolution of mean temperature for all particles

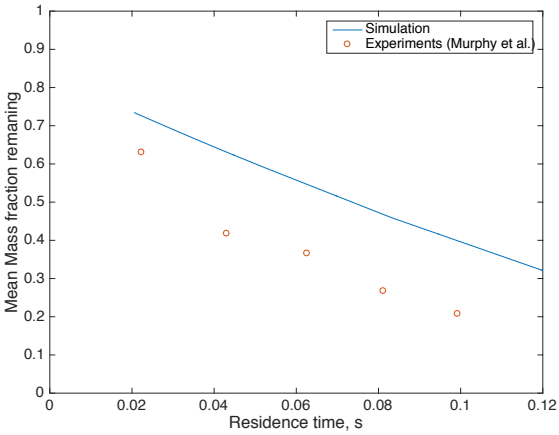


(d) Evolution of mean mass fraction for all particles

**Figure 5.17**: Mass and temperature results from the simulation of a char oxidation laminar reactor.

treatment presented in the original reference,[144] highlighting the importance of capturing and treating polydispersity in multiphase gas-solid flows. Although the tests and the physical system represented are simple in nature, the technique is readily formulated to handle more complex flows involving strong coupling with the fluid phase, topics that will become material for future work.

# CHAPTER 6

# CONCLUSIONS AND FUTURE WORK

The research reported in this dissertation has covered 2 formalism to simulate *polydisperse* multiphase systems, the mathematical models were developed under the hypothesis of the Eulerian moment-based methods previously proposed in the literature and sufficiently verified.[29,43,47,61,69,70] The first formalism has been coined *direct quadrature of conditional moments* DQCMOM. Working examples in one and two physical space dimensions were proposed in order to show its capabilities at core and fundamental physics. The second formalism was coined *parceled method of moments*, PMOM, and its methodology was demonstrated with different examples in polydisperse system. Finally, in **Appendix A** a brief discussion on closures based on ME will be given. This chapter opens up the discussion for alternative and possibly more powerful Eulerian moment-based methods.

## 6.1 Eulerian-Based Moment Method Techniques

Some general conclusions can be drawn from the two formalisms developed in **Chapter 3** and **Chapter 4**, revolving around the novelty on the formulation of the mathematical model and its performance in simplified systems.

### 6.1.1 Direct Quadrature of Conditional Moments, DQCMOM

An Eulerian moment-based model was formulated on the basis of DQMOM[43] and CQMOM[61] in order to expand their capabilities to polydisperse multiphase systems in a natural way, specifying explicitly the transport of conditional velocity moments and the transport of scalar properties. The novelty in this approach resides in the mathematical formulation that allows coupling the transport of the scalars to the transport of velocity moments; this coupling comply with the effects of crossing (PTC) that can be present in dilute multiphase flows.

The model was essentially formulated for dilute and very dilute multiphase systems

in which particle effects are negligible, allowing us to obtain a weakly coupled set of transport equations. However, this is by no means restricted to these kind of flows; a quick review on **Equation** (3.35) allows us to partially conclude that it is possible to lump the particulate effects of moderately dense systems into the equation for the weights enabling the weights and the other scalars to change in situations of moderate collision effects: breakage, aggregation, coalescence, and so forth. A study in moderately dense systems was reported by Fox and Vedula.[90]

The structure of the mathematical model requires us to use numerical schemes that are based on the structure of the NDF; regular numerical schemes within the finite volume framework would probably fail at preserving the realizability of the moment space.[8] **Section 3.3** and **Section 4.5** were devoted to explaining how these *kinetic schemes* work. In this dissertation, kinetic schemes are used for both the transport of conditional velocity moments as in Yuan and Fox[61] and the transport of scalar properties. The formulation of these schemes for scalar equations are based on the early works of Estivalezes and Villedieu[131] and Perthame,[128,129] they were formulated and valid for first order discretizations, extensions to higher second order was only performed in the 1-dimensional cases.

Verification of the methodology was achieved via 1- and 2-dimensional cases; the main focus was on capturing PTC on polydisperse systems allowing the crossing between different sizes at different Stokes regimes affected simultaneously by size and velocity. A simple, deterministic drag law (Schiller-Neumann) was used in order to simulate the effect of the fluid on the particles; this does not hinder the capability of the model to capture PTC from the mathematical point of view, but tests in turbulent flows with more complex drag laws are required to asses this statement.

### 6.1.2 Parceled Method of Moments, PMOM

A second Eulerian moment-based method was developed built on the concept of *section* proposed by Tambour,[114] Laurent at al.,[115] and Schneider et al.[69,70] The novelty of the approach in this dissertation resides on the treatment to approximate the marginal size-NDF, which allows reconstructing the particle size distribution from a set of low order moments. This approach modifies kernel-based reconstruction algorithms[137,139] in order to efficiently reconstruct the size distribution.

An augmented inversion algorithm was proposed that essentially invert moment in two different coordinates of phase space: size and velocity. In size coordinate, marginal size moments are used to obtain the particle size distribution in velocity coordinate, the conditional velocity moments are used in CQMOM in order to obtain the velocity weights and velocity abscissas at each *parcel* of the obtained size-NDF.

In **Section 4.5** it was shown that it is possible to use the structure of the NDF in order to formulate numerical schemes to transport the equations in the finite volume framework. The kinetic schemes formulated take into account the discretization in velocity and size coordinates yielding realizable moments for first order-type schemes. Extension to second order is possible but requires the formulation of second order fluxes that preserve the realizability of the moment space.[35] Yet, some questions that require further exploration still remain open to discussion, namely uniqueness of the formulation and higher order extension of the numerical schemes.

#### 6.1.2.1 Uniqueness of the Formulation

This kind of spline-based reconstruction falls into the category of nonparametric density estimation and more specifically into polynomial-based kernel density estimation techniques. Essentially, these methodologies require distributed data in order to estimate the shape of the distribution. Unfortunately, not only values of the NDF are unknown, but only a finite set of moments is available.

In general it is only possible to have complete knowledge of a distribution if all of its moments are known.[a] There are several variations of this problem, among them: i) moments of distribution functions defined in the real line or the *Hamburger moment problem*, ii) moments of distribution functions defined on the positive real line or the *Stieltjes moment problem*, and iii) moments of distribution functions defined in a closed interval of the real line or the *Hausdorff moment problem*. While the first two are in general ill-condition problems, the third, if solvable, has a unique solution. The framework of the Hausdorff problem is of interest for this work, because it is *also* defined in finite, closed intervals. Athanassoulis and Gavriliadis[142] gives solution to the Hausdorff problem in terms of kernel density representations, which in principle can be extended to polynomial kernels.

[a] This is known as the *Moment Problem*.

de Souza et al.[139] described the uniqueness of the reconstruction for finite intervals when all the moments are known. Even though only a handful of moments are known, the presented reconstruction gives a good approximation for common particle size-NDF, like the ones for experimental particle size distributions (PSD). Indeed, the more complex the distributions, the more moments are needed for an accurate reconstruction.[137,139]

Consider a parcel in size space in a closed interval $[s_k, s_k + 1] = [a, b]$. Kinetic moments reconstructed using CQMOM or any quadrature-based moment inversion,[74] are guaranteed to preserve, at least, first order realizability conditions, namely

$$\begin{aligned} \mathfrak{M}_k^{(0,0,0)} &> 0 \\ \mathfrak{M}_k^{(0,0,0)} \mathfrak{M}_k^{(0,0,2)} &\geq \left( \mathfrak{M}_k^{(0,0,1)} \right)^2 \end{aligned} \tag{6.1}$$

Moreover, increasing the number of quadrature nodes allows the discrete approximation to match an arbitrary number of moments of a continuous distribution.[61] Along with the conservation of the moment realizability by the inversion procedure, physical transport for each parcel must preserve the moment space. Desjardins et al.[29] showed that first order kinetic schemes used for the flux reconstruction guarantee the conservation of the moment space. Vié et al.[76] extended the principle for higher order discretization schemes. From the studies of Vi et al.,[76] de Souza et al.,[139] and Athanassoulis and Gavriliadis[142] it is possible to speculate about the overall conservation of the moment space, using the parceled method of moments (PMOM).

#### 6.1.2.2 High Order Discretization Schemes

The numerical results presented so far are only first order accurate. Although they follow the expected behavior at a qualitative level, high order discretization schemes are necessary in order to produce results capable of predicting behaviors at a quantitative level. The development of conservative discretization methods that are capable of producing realizable, joint conditional and marginal moments are necessary especially when polydispersity is introduced explicitly as in this method. Several works in the literature[35,63,76,111] have shown this realizability issue for monodisperse systems and their extension to higher order. Dufour and Villedieu[35] proposed a second order extension to the Eulerian-multifluid method that compares in similarities to the model developed in this research; in principle, it is entirely possible to accomplish this extension.

### 6.1.3 Future Perspectives

The models developed in this dissertation will become a stepping stone for more resolved and accurate Eulerian moment-based methods. There are several areas that need to be completely defined before these models might be effectively used in real CFD applications; among them:

a) *Introduction of turbulence* especially for the particulate phase. Although the treatment of turbulence in Eulerian moment-based methods is relatively new, excellent reviews exist on turbulence closures for the source terms of the moment transport equations,[5,8] which can be used as a starting point to develop more accurate Eulerian LES-based models for the dispersed phase.

b) *High order discretization schemes* need to be developed and implemented in the methods in order to prevent spurious predictions due to excessive numerical diffusion. As shown in Desjardins et al.,[29] only first order discretization schemes are guaranteed to preserve the convexity of the moment space. François and François[146] have developed second order schemes in the context of the pressureless Euler equations but more research is needed in regards to moment transport equations. Vikas et al.[132] have developed "pseudo" high order methods, in which the weights are discretized using high order schemes, but the velocity is treated using first order schemes. Some of these methods have been implemented in this dissertation, but only for the 1-dimensional cases.

c) *Introduction of complex physics* is a requirement in order to predict realistic scenarios. For instance, most of the examples treated in this dissertation described mass transfer between the particulate phases and the gas, or none at all. In realistic scenarios, mass and heat transfer can also happen between the particulate phases and the model should be able to represent this kind of processes.

# APPENDIX A

# MAXIMUM ENTROPY AND MOMENT-BASED METHOD

Exploring the ideas about Eulerian moment-based methods has taken many tours and detours, one of those detours will form the contents of this appendix; as such, these ideas are not completely developed but I believe their further exploration is worthy and the possible benefits of these advanced methods might allow the introduction of more complexity into Eulerian moment-based methods.

In the various applications discussed throughout this dissertation, a common problem has been faced: based on a particular set of moments, roughly approximate the distribution were they came from; this is a particular instance of an inverse problem.[a] Inverse problems are present in many scientific and engineering fields: communication, tomography, computer vision, natural language processing, and machine learning, in which causal factors have to be determined from the observations. The abundance of these problems allows research on techniques to relate effects and causes. One of such techniques is maximum entropy (ME).

In one of his seminal papers, Jaynes[147] explained why and how the principles from statistical mechanics can be recovered from the principles of information theory, specifically, how the statistical approach of ME principle can, in fact, predict thermodynamic states. Since then, many other fields have adopted the principles of ME in order to give solution to their specific problems. In this particular research, we used theory of orthogonal polynomials and kernel density estimation in order to relate moments to approximated distribution functions.[b] The purpose of this appendix is to explore the properties of ME principles in order to determine its feasibility in inversion procedures and its use in

---

[a] The moment problem as discussed in **Chapter 6**.

[b] In the form of inversion algorithms.

moment-based methods. The continuous entropy of a pdf is given by

$$H = -\int_{\mathbb{R}} f(\mathrm{z}) \ln(f(\mathrm{z}))\mathrm{dz}. \tag{A.1}$$

This concept of entropy is intrinsically related to the moment problem, since it helps in providing an appropriate solution to the statement: *Given a finite set of moments, is it possible to find a distribution that satisfies them?* It turn out that the function $f(\mathrm{z})$ that maximizes the entropy $H$ is the least unbiased function that can represent the set of given moments. A formal statement to this problem is

$$\begin{aligned} \underset{f}{\text{Max}} \quad & \left( H(f) = -\int_{\mathbb{R}} f(\mathrm{z}) \ln(f(\mathrm{z}))\mathrm{dz} \right) \\ \text{s. t.} \quad & \int_{\mathbb{R}} f(\mathrm{z})\mathrm{dz} = \mu_0 \\ & \int_{\mathbb{R}} \mathrm{z} f(\mathrm{z})\mathrm{dz}i = \mu_1 \\ & \int_{\mathbb{R}} \mathrm{z}^2 f(\mathrm{z})\mathrm{dz} = \mu_2 \\ & \vdots \\ & \int_{\mathbb{R}} \mathrm{z}^m f(\mathrm{z})\mathrm{dz} = \mu_m. \end{aligned} \tag{A.2}$$

The classical solution to this problem is given in terms of Lagrangian multipliers[148] and is represented by

$$f(\mathrm{z}) = \exp[-\chi_0 - \sum_{k=1}^{m} \chi_k \mathrm{z}^k]. \tag{A.3}$$

In the following we explore a possible formulation of moment transport equations based on ME solutions in **Equation** (A.3) (**Section A.1**); we also explore methodologies that could use **Equation** (A.3) as closure approximation (**Section A.2**).

## A.1 Hyperbolicity of Entropy-Based Transport Equations

Consider the monodisperse kinetic equation

$$\frac{\partial \mathfrak{F}}{\partial t} + \mathbf{v} \cdot \nabla_{\mathrm{x}} \mathfrak{F} = \mathfrak{S}, \tag{A.4}$$

where $\mathfrak{F} = \mathfrak{F}(\mathbf{v}; \mathbf{x}, t)$. Let $\mathbf{V}^{(N)} = [1, \mathbf{v}, \mathbf{vv}, \cdots]$. The moment transformation can be written as

$$\left\langle \mathbf{V}^{(N)} \mathfrak{F} \right\rangle = \mathfrak{m}^{(N)} = \iiint_{\mathbb{R}^3} \mathbf{V}^{(N)} \mathfrak{F} \mathrm{d}^3\mathbf{v}. \tag{A.5}$$

Applying **Equation** (A.5) to **Equation** (A.4), moment transport equations are obtained:

$$\frac{\partial}{\partial t}\left\langle \mathbf{V}^{(N)}\mathfrak{F}\right\rangle + \nabla_{\mathrm{x}}\cdot\left\langle \mathbf{v}\mathbf{V}^{(N)}\mathfrak{F}\right\rangle = \left\langle \mathbf{V}^{(N)}\mathfrak{S}\right\rangle. \tag{A.6}$$

Assume now that $\mathfrak{F}$ is a function that maximizes the entropy for a given finite set of moments

$$\mathfrak{F} = \exp[\mathbb{P}^{(N)}] = \exp[\boldsymbol{\lambda}^T\mathbf{V}^{(N)}], \tag{A.7}$$

where $\mathbb{P}^{(N)}$ is a polynomial in the velocity variable and $\boldsymbol{\lambda}^T = [\lambda_0, \lambda_1, \lambda_2, \cdots]^T$ are the coefficients of the polynomial. One of the most desirable properties of ME is that it is strictly positive, which is a necessary condition for the realizability of the moment space. Levermore[149] analyzed the mathematical structure of **Equation** (A.6) by dissecting each term separately:

$$\begin{aligned}\frac{\partial}{\partial t}\left\langle \mathbf{V}^{(N)}\mathfrak{F}\right\rangle &= \frac{\mathrm{d}}{\mathrm{d}\boldsymbol{\lambda}}\left\langle \mathbf{V}^{(N)}\mathfrak{F}\right\rangle\frac{\partial\boldsymbol{\lambda}}{\partial t}\\ \nabla_{\mathrm{x}}\cdot\left\langle \mathbf{v}\mathbf{V}^{(N)}\mathfrak{F}\right\rangle &= \frac{\mathrm{d}}{\mathrm{d}\boldsymbol{\lambda}}\left\langle \mathbf{v}\mathbf{V}^{(N)}\mathfrak{F}\right\rangle\cdot\nabla_{\mathrm{x}}\boldsymbol{\lambda}.\end{aligned} \tag{A.8}$$

In each expression the first term represents the flux and density potentials respectively.

$$\begin{aligned}\frac{\mathrm{d}}{\mathrm{d}\boldsymbol{\lambda}}\left\langle \mathbf{V}^{(N)}\mathfrak{F}\right\rangle &= \iiint_{\mathbb{R}^3}\mathbf{V}^{(N)}\frac{\mathrm{d}}{\mathrm{d}\boldsymbol{\lambda}}\exp[\boldsymbol{\lambda}^T\mathbf{V}^{(N)}]\mathrm{d}^3\mathbf{v}\\ &= \iiint_{\mathbb{R}^3}\mathbf{V}^{(N)}[\mathbf{V}^{(N)}]^T\exp[\boldsymbol{\lambda}^T\mathbf{V}^{(N)}]\mathrm{d}^3\mathbf{v}\\ \frac{\mathrm{d}}{\mathrm{d}\boldsymbol{\lambda}}\left\langle \mathbf{v}\mathbf{V}^{(N)}\mathfrak{F}\right\rangle &= \iiint_{\mathbb{R}^3}\mathbf{v}\mathbf{V}^{(N)}\frac{\mathrm{d}}{\mathrm{d}\boldsymbol{\lambda}}\exp[\boldsymbol{\lambda}^T\mathbf{V}^{(N)}]\mathrm{d}^3\mathbf{v}\\ &= \iiint_{\mathbb{R}^3}\mathbf{v}\mathbf{V}^{(N)}[\mathbf{V}^{(N)}]^T\exp[\boldsymbol{\lambda}^T\mathbf{V}^{(N)}]\mathrm{d}^3\mathbf{v}\end{aligned} \tag{A.9}$$

From **Equation** (A.8), **Equation** (A.6) can be written as

$$\frac{\mathrm{d}}{\mathrm{d}\boldsymbol{\lambda}}\left\langle \mathbf{V}^{(N)}\mathfrak{F}\right\rangle\frac{\partial\boldsymbol{\lambda}}{\partial t} + \frac{\mathrm{d}}{\mathrm{d}\boldsymbol{\lambda}}\left\langle \mathbf{v}\mathbf{V}^{(N)}\mathfrak{F}\right\rangle\cdot\nabla_{\mathrm{x}}(\boldsymbol{\lambda}) = \langle\mathfrak{S}\rangle. \tag{A.10}$$

These are now transport equations for the coefficients of the ME function.

For the following analysis only one spatial dimension is considered, but its extension to higher dimensions is straight forward. First, for notation purposes, let $\mathbf{V}^{(N)} = [1, v, v^2, \cdots]$

where $v = v_x$. Second, the term $\mathbf{V}^{(N)}[\mathbf{V}^{(N)}]^T$ can be expanded into a matrix of velocity fields as

$$\mathbf{V}^{(N)}[\mathbf{V}^{(N)}]^T = \begin{bmatrix} 1 & v & v^2 & \cdots \\ v & v^2 & v^3 & \cdots \\ v^2 & v^3 & v^4 & \cdots \\ \vdots & \vdots & \vdots & \ddots \end{bmatrix}. \tag{A.11}$$

The first integral in **Equation** (A.9) can be resolved as

$$\begin{aligned} \frac{\mathrm{d}}{\mathrm{d}\boldsymbol{\lambda}} \left\langle \mathbf{V}^{(N)} \mathfrak{F} \right\rangle &= \int_{\mathbb{R}} \begin{bmatrix} 1 & v & v^2 & \cdots \\ v & v^2 & v^3 & \cdots \\ v^2 & v^3 & v^4 & \cdots \\ \vdots & \vdots & \vdots & \ddots \end{bmatrix} \exp[\boldsymbol{\lambda}^T \mathbf{V}^{(N)}] \mathrm{d}v \\ &= \begin{bmatrix} \mathfrak{m}^{(0)} & \mathfrak{m}^{(1)} & \mathfrak{m}^{(2)} & \cdots \\ \mathfrak{m}^{(1)} & \mathfrak{m}^{(2)} & \mathfrak{m}^{(3)} & \cdots \\ \mathfrak{m}^{(2)} & \mathfrak{m}^{(3)} & \mathfrak{m}^{(4)} & \cdots \\ \vdots & \vdots & \vdots & \ddots \end{bmatrix}. \end{aligned} \tag{A.12}$$

and the extension to the second integral is straightforward. The transport equation for the coefficient can now be written as

$$\begin{aligned} &\begin{bmatrix} \mathfrak{m}^{(0)} & \mathfrak{m}^{(1)} & \mathfrak{m}^{(2)} & \cdots \\ \mathfrak{m}^{(1)} & \mathfrak{m}^{(2)} & \mathfrak{m}^{(3)} & \cdots \\ \mathfrak{m}^{(2)} & \mathfrak{m}^{(3)} & \mathfrak{m}^{(4)} & \cdots \\ \vdots & \vdots & \vdots & \ddots \end{bmatrix} \frac{\partial}{\partial t} \begin{bmatrix} \lambda_0 \\ \lambda_1 \\ \lambda_2 \\ \vdots \end{bmatrix} + \begin{bmatrix} \mathfrak{m}^{(1)} & \mathfrak{m}^{(2)} & \mathfrak{m}^{(3)} & \cdots \\ \mathfrak{m}^{(2)} & \mathfrak{m}^{(3)} & \mathfrak{m}^{(4)} & \cdots \\ \mathfrak{m}^{(3)} & \mathfrak{m}^{(4)} & \mathfrak{m}^{(5)} & \cdots \\ \vdots & \vdots & \vdots & \ddots \end{bmatrix} \nabla_{\mathrm{x}} \begin{bmatrix} \lambda_0 \\ \lambda_1 \\ \lambda_2 \\ \vdots \end{bmatrix} \\ &= \begin{bmatrix} \langle \mathfrak{S} \rangle \\ \langle v\mathfrak{S} \rangle \\ \langle v^2\mathfrak{S} \rangle \\ \vdots \end{bmatrix}. \end{aligned} \tag{A.13}$$

Note the structure of the matrices premultiplying the terms in **Equation** (A.13); they are matrices of moments with the property:

$$\{\mathfrak{m}_{i,j}^{(N)}\} = \{\mathfrak{m}_{i+1,j-1}^{(N)}\} = m_{i+j-2}^{(N)}, \tag{A.14}$$

where

$$\frac{\mathrm{d}}{\mathrm{d}\boldsymbol{\lambda}} \left\langle \mathbf{V}^{(N)} \mathfrak{F} \right\rangle = \{\mathfrak{m}^{(N)}\} = \begin{bmatrix} \mathfrak{m}^{(0)} & \mathfrak{m}^{(1)} & \mathfrak{m}^{(2)} & \cdots \\ \mathfrak{m}^{(1)} & \mathfrak{m}^{(2)} & \mathfrak{m}^{(3)} & \cdots \\ \mathfrak{m}^{(2)} & \mathfrak{m}^{(3)} & \mathfrak{m}^{(4)} & \cdots \\ \vdots & \vdots & \vdots & \ddots \end{bmatrix}. \tag{A.15}$$

They share the same structure and properties of the Hankel matrices, common in Markov and moment problems. It would be ideal to factor out the moment matrices premultiplying

the terms in the transport equations for the coefficients; currently two approaches might achieve this: the first one corresponds to using the Jensen inequality,[150] which basically allows finding a function over convex spaces, such that

$$\phi(\mathbb{E}[X]) \leq \mathbb{E}[\phi(X)], \tag{A.16}$$

and the second one corresponds to expressing high order moments as a linear combination of low order moments.

### A.1.1 Jensen Inequality

Let

$$X = v^{i-1} \exp[\boldsymbol{\lambda}^T \mathbf{V}^{(N)}], \tag{A.17}$$

and

$$\phi(X) = vX. \tag{A.18}$$

Then,

$$\begin{aligned} \frac{\mathfrak{m}^i}{\mathfrak{m}^{i-1}} &= \frac{\int_{\mathbb{R}} v^i \exp[\boldsymbol{\lambda}^T \mathbf{V}^{(N)}] \mathrm{d}v}{\int_{\mathbb{R}} v^{i-1} \exp[\boldsymbol{\lambda}^T \mathbf{V}^{(N)}] \mathrm{d}v} \\ &= \frac{\mathbb{E}[\phi(X)]}{\mathbb{E}[X]} \\ \phi &\leq \frac{\mathbb{E}[\phi(X)]}{\mathbb{E}[X]}. \end{aligned} \tag{A.19}$$

Now $\phi$ is a linear function in phase space, which is not strictly a convex function, rendering the inequality to an equality that only depends on physical space and time.

$$\overline{\mathrm{U}}_p(x,t) = \frac{\mathfrak{m}^i}{\mathfrak{m}^{i-1}} \tag{A.20}$$

The matrices in **Equation** (A.13) can be now factored out as

$$\begin{aligned} &\begin{bmatrix} \mathfrak{m}^{(0)} & \mathfrak{m}^{(1)} & \mathfrak{m}^{(2)} & \cdots \\ \mathfrak{m}^{(1)} & \mathfrak{m}^{(2)} & \mathfrak{m}^{(3)} & \cdots \\ \mathfrak{m}^{(2)} & \mathfrak{m}^{(3)} & \mathfrak{m}^{(4)} & \cdots \\ \vdots & \vdots & \vdots & \ddots \end{bmatrix} \left( \frac{\partial}{\partial t} \begin{bmatrix} \lambda_0 \\ \lambda_1 \\ \lambda_2 \\ \vdots \end{bmatrix} + \begin{bmatrix} \overline{\mathrm{U}}_0 & \overline{\mathrm{U}}_1 & \overline{\mathrm{U}}_2 & \cdots \\ \overline{\mathrm{U}}_1 & \overline{\mathrm{U}}_2 & \overline{\mathrm{U}}_3 & \cdots \\ \overline{\mathrm{U}}_2 & \overline{\mathrm{U}}_3 & \overline{\mathrm{U}}_4 & \cdots \\ \vdots & \vdots & \vdots & \ddots \end{bmatrix} \cdot \nabla_{\mathrm{x}} \begin{bmatrix} \lambda_0 \\ \lambda_1 \\ \lambda_2 \\ \vdots \end{bmatrix} \right) \\ &= \begin{bmatrix} \langle \mathfrak{S} \rangle \\ \langle v\mathfrak{S} \rangle \\ \langle v^2\mathfrak{S} \rangle \\ \vdots \end{bmatrix}. \end{aligned} \tag{A.21}$$

### A.1.2 Linear Combination of Low Order Moments

Using the properties of Hankel matrices a factorization can be achieved as

$$\begin{bmatrix} \mathfrak{m}^{(0)} & \mathfrak{m}^{(1)} & \mathfrak{m}^{(2)} & \cdots \\ \mathfrak{m}^{(1)} & \mathfrak{m}^{(2)} & \mathfrak{m}^{(3)} & \cdots \\ \mathfrak{m}^{(2)} & \mathfrak{m}^{(3)} & \mathfrak{m}^{(4)} & \cdots \\ \vdots & \vdots & \vdots & \ddots \end{bmatrix} \begin{bmatrix} 0 & 0 & \cdots & \beta_0 \\ 1 & 0 & \cdots & \beta_1 \\ 0 & 1 & \cdots & \beta_2 \\ \vdots & \vdots & \vdots & \vdots \\ 0 & \cdots & 1 & \beta_N \end{bmatrix} \begin{bmatrix} \mathfrak{m}^{(1)} & \mathfrak{m}^{(2)} & \mathfrak{m}^{(3)} & \cdots \\ \mathfrak{m}^{(2)} & \mathfrak{m}^{(3)} & \mathfrak{m}^{(4)} & \cdots \\ \mathfrak{m}^{(3)} & \mathfrak{m}^{(4)} & \mathfrak{m}^{(5)} & \cdots \\ \vdots & \vdots & \vdots & \ddots \end{bmatrix}. \tag{A.22}$$

The coefficients $\beta_i$ are obtained as

$$\beta_0 \mathfrak{m}^0 + \beta_1 \mathfrak{m}^1 + \beta_2 \mathfrak{m}^2 + \cdots + \beta_N \mathfrak{m}^N = \mathfrak{m}^{N+1}. \tag{A.23}$$

Additional factorization can be applied[c] in order to simplify the system and find the coefficients. The system of transport equations can be written as

$$\begin{bmatrix} \mathfrak{m}^{(0)} & \mathfrak{m}^{(1)} & \mathfrak{m}^{(2)} & \cdots \\ \mathfrak{m}^{(1)} & \mathfrak{m}^{(2)} & \mathfrak{m}^{(3)} & \cdots \\ \mathfrak{m}^{(2)} & \mathfrak{m}^{(3)} & \mathfrak{m}^{(4)} & \cdots \\ \vdots & \vdots & \vdots & \ddots \end{bmatrix} \left( \frac{\partial}{\partial t} \begin{bmatrix} \lambda_0 \\ \lambda_1 \\ \lambda_2 \\ \vdots \end{bmatrix} + \begin{bmatrix} 0 & 0 & \cdots & \beta_0 \\ 1 & 0 & \cdots & \beta_1 \\ 0 & 1 & \cdots & \beta_2 \\ \vdots & \vdots & \vdots & \vdots \\ 0 & \cdots & 1 & \beta_N \end{bmatrix} \cdot \nabla_{\mathrm{x}} \begin{bmatrix} \lambda_0 \\ \lambda_1 \\ \lambda_2 \\ \vdots \end{bmatrix} \right) = \begin{bmatrix} \langle \mathfrak{S} \rangle \\ \langle v \mathfrak{S} \rangle \\ \langle v^2 \mathfrak{S} \rangle \\ \vdots \end{bmatrix}. \tag{A.24}$$

To put this analysis into perspective, consider an Eulerian computational mesh in physical space. Assume that some of the cells are initially distributed in velocity coordinate according to a normal distribution. For a normal distribution, a minimum of three moments are required to reconstruct the distribution using ME. The system of equations reads as

$$\begin{bmatrix} \mathfrak{m}^{(0)} & \mathfrak{m}^{(1)} & \mathfrak{m}^{(2)} \\ \mathfrak{m}^{(1)} & \mathfrak{m}^{(2)} & \mathfrak{m}^{(3)} \\ \mathfrak{m}^{(2)} & \mathfrak{m}^{(3)} & \mathfrak{m}^{(4)} \end{bmatrix} \left( \frac{\partial}{\partial t} \begin{bmatrix} \lambda_0 \\ \lambda_1 \\ \lambda_2 \end{bmatrix} + \begin{bmatrix} \mathfrak{m}^{(1)} & \mathfrak{m}^{(2)} & \mathfrak{m}^{(3)} \\ \mathfrak{m}^{(2)} & \mathfrak{m}^{(3)} & \mathfrak{m}^{(4)} \\ \mathfrak{m}^{(3)} & \mathfrak{m}^{(4)} & \mathfrak{m}^{(5)} \end{bmatrix} \cdot \nabla_{\mathrm{x}} \begin{bmatrix} \lambda_0 \\ \lambda_1 \\ \lambda_2 \end{bmatrix} \right) = \begin{bmatrix} 0 \\ 0 \\ 0 \end{bmatrix}, \tag{A.25}$$

for which collisionless flow has been assumed. It is clear that six moments are needed in order to formulate and close the system of equations. In general, if $N$ are the number

[c] Vandermonde factorization to be precise if the moments can be expressed as polynomial functions (weights and abscissas).

of moments needed to reconstruct the distribution, $N+3$ are the number of moments needed to close the system of equations. The exact form of the system of equations after factorization (Jensen or linear combination) requires further analysis and justification; for now, assume that the convection coefficients are available from the Jensen factorization, reducing **Equation** (A.25) to

$$\frac{\partial}{\partial t}\begin{bmatrix}\lambda_0\\ \lambda_1\\ \lambda_2\end{bmatrix}+\begin{bmatrix}\mathrm{U}_0 & \mathrm{U}_1 & \mathrm{U}_2\\ \mathrm{U}_1 & \mathrm{U}_2 & \mathrm{U}_3\\ \mathrm{U}_2 & \mathrm{U}_3 & \mathrm{U}_4\end{bmatrix}\cdot\nabla_{\mathrm{x}}\begin{bmatrix}\lambda_0\\ \lambda_1\\ \lambda_2\end{bmatrix}=\begin{bmatrix}0\\ 0\\ 0\end{bmatrix}. \tag{A.26}$$

The matrix of coefficients $\mathrm{U}_i$ is symmetric and positive-definite, with real eigenvalues and can be diagonalized as

$$\mathbf{U}=\mathbf{R}\boldsymbol{\Lambda}\mathbf{R}^{-1}, \tag{A.27}$$

where $\mathbf{R}$ is the matrix whose columns are the eigenvectors of $\mathbf{U}$, and $\boldsymbol{\Lambda}$ is the diagonal matrix of eigenvalues of $\mathbf{U}$. The system in **Equation** (A.26) can be now rewritten as

$$\frac{\partial}{\partial t}\begin{bmatrix}\tilde{w}_0\\ \tilde{w}_1\\ \tilde{w}_2\end{bmatrix}+\begin{bmatrix}\boldsymbol{\Lambda}_0 & 0 & 0\\ 0 & \boldsymbol{\Lambda}_1 & 0\\ 0 & 0 & \boldsymbol{\Lambda}_2\end{bmatrix}\cdot\nabla_{\mathrm{x}}\begin{bmatrix}\tilde{w}_0\\ \tilde{w}_1\\ \tilde{w}_2\end{bmatrix}=\begin{bmatrix}0\\ 0\\ 0\end{bmatrix}, \tag{A.28}$$

where $\tilde{\mathbf{w}}=\mathbf{R}^{-1}\boldsymbol{\lambda}$. The transformation in **Equation** (A.28) allows writing the system as a set of decoupled PDEs of the form

$$\frac{\partial\tilde{w}_0}{\partial t}+\Lambda_0\nabla_{\mathrm{x}}\tilde{w}_0=0 \tag{A.29}$$

$$\frac{\partial\tilde{w}_1}{\partial t}+\Lambda_1\nabla_{\mathrm{x}}\tilde{w}_1=0 \tag{A.30}$$

$$\frac{\partial\tilde{w}_2}{\partial t}+\Lambda_2\nabla_{\mathrm{x}}\tilde{w}_2=0. \tag{A.31}$$

The system in **Equation** (A.26) is strictly hyperbolic, thanks to the structure of $\mathbf{U}$. The reduced system in **Equation** (A.28) corresponds to a set of linear equations easily implemented within the finite volume framework, without the need of specialized numerical schemes.[d] In principle, **Equation** (A.29) is a transformation for the original moment equation, that preserves the essential mathematical structure in velocity coordinate when ME is used as an approximation for the NDF.

A question that is important to ask at this point is *Can this reduced system capture PTC?* Assume a 1-dimensional computational mesh in physical space in the nondimensional

[d] Compared to the moment transport equations that use kinetic schemes to reconstruct the advective fluxes.

interval $[-1, 1]$. The distribution of velocities is located initially in $-0.40 \leq x \leq -0.35$ and $0.35 \leq x \leq 0.4$. In these intervals, the moments of the distribution can be calculated and a ME function can be reconstructed; after this process, the coefficients of ME are available and the system **Equation** (A.29) can be obtained.[e] **Figure A.1** shows the evolution of transformed system. In principle, it is possible to substitute the transport of moment (**Equation** (A.5)) by the transport of reduced coefficients (**Equation** (A.26)), from which it is possible to capture PTC at the level of the characteristics of the system (eigenvalues) without the need of specialized discretization schemes. More research needs to be devoted to the matrix factorization and to testing the limits of the model.

## A.2 Closures Based on Maximum entropy

Another way to tackle the closure problem is dealing directly with the approximation of the NDF. For instance, consider **Equation** (A.6) and its unclosed convection term. All the research presented so far (original and reviewed) uses some kind of functional approximation to the joint NDF in order to treat the high order term; in all the cases, a general form for these functions corresponds to

$$\mathfrak{F}(\mathbf{z}) = \sum_{\alpha=1}^{N} w_\alpha \delta(\mathbf{z}, \mathbf{z}_\alpha, \boldsymbol{\chi}), \tag{A.32}$$

in which $\mathbf{z}$ are generic variables that represent velocity, size, and other scalars. Concrete representations of $\delta(\mathbf{z}, \mathbf{z}_\alpha, \boldsymbol{\chi})$ can be found in DQCMOM (**Chapter 3**), where it was characterized as

$$\delta(\mathbf{z}, \mathbf{z}_\alpha, \boldsymbol{\chi}) = \delta(\mathbf{z} - \mathbf{z}_\alpha), \tag{A.33}$$

a Dirac-delta function in the different variables of phase space, following mostly the research of Fox and coworkers.[29,30,43,46,47,61] It was also found in PMOM (**Chapter 4**), where it was loosely presented as

$$\delta(\mathbf{z}, \mathbf{z}_\alpha, \boldsymbol{\chi}) = \ell_\alpha(\mathbf{z}) \mathfrak{g}_\alpha(\mathbf{z}, \boldsymbol{\chi}) \mathfrak{f}_\alpha(\mathbf{z}). \tag{A.34}$$

It can also be found in Chalons et al.,[71] Yuan et al.,[77] and Marchisio and Fox[8] where it was represented by the canonical distributions: Normal, Beta, and Gamma. For instance, for

[e] Time and physical space are nondimensional quantities.

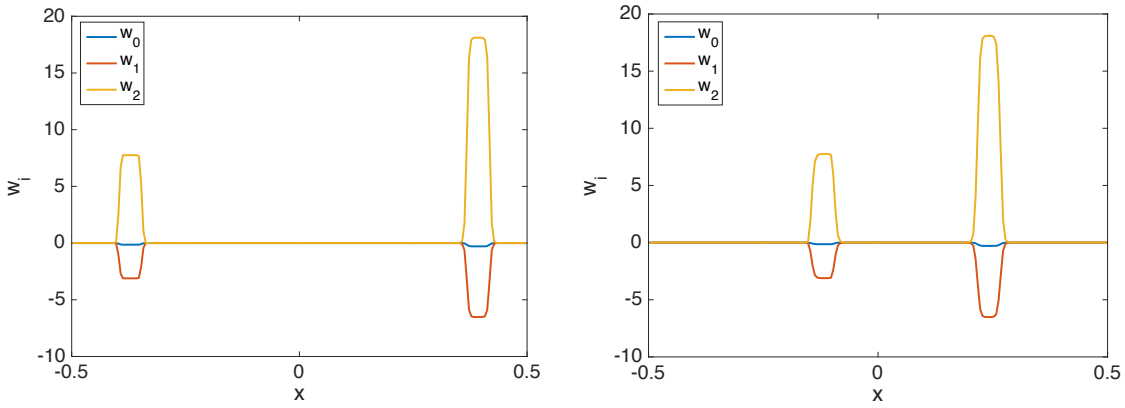


(a) t = 0 (b) t = 0.6

(c) t = 1.05 (d) t = 1.5

**Figure A.1**: Evolution of the decoupled system of transport equations. (a) Initial position of the fields. (b) The packets move in opposite direction towards each other. (c) Point of crossing. (d) The characteristics have successfully crossed each other

the Beta distribution with z in only one dimension of the phase space the representation is

$$\delta(z, z_\alpha, \chi) = \frac{z^{z_\alpha/(\chi-1)}(1-z)^{1-z_\alpha/(\chi-1)}}{\mathbf{B}(z_\alpha/\chi, (1-z_\alpha)/\chi)}, \tag{A.35}$$

where **B** is the beta function.[151]

Following the same concepts, we propose a closure approximation of the form of **Equation** (A.32) where

$$\delta(z, z_\alpha, \chi) = \exp[-\chi_0 - \chi_1 z - \chi_2 z^2] \tag{A.36}$$

is a ME solution of **Equation** (A.2) with 3 moment constraints. Assume that an approximation to the NDF in one dimension of the phase space, can be written as

$$\begin{aligned}\mathfrak{F}(\xi) &= \sum_{\alpha=1}^{N_\xi} w_\alpha \delta_\alpha(\xi, \boldsymbol{\lambda}) \\ &= \sum_{\alpha=1}^{N_\xi} w_\alpha \exp[-\lambda_0^{(\alpha)} - \lambda_1^{(\alpha)}\xi - \lambda_2^{(\alpha)}\xi^2].\end{aligned} \tag{A.37}$$

Specifying the problem requires us to formulate a system of equations to find $w_\alpha, \lambda_i^{(\alpha)}$. In order to find $\lambda_i^{(\alpha)}$ a nonlinear system of equations is formulated as

$$\begin{aligned}&\int_{\mathbb{R}} \exp[-\lambda_0^{(\alpha)} - \lambda_1^{(\alpha)}\xi - \lambda_2^{(\alpha)}\xi^2]\mathrm{d}\xi = \mu_0 \\ &\int_{\mathbb{R}} \xi^j \exp[-\lambda_0^{(\alpha)} - \lambda_1^{(\alpha)}\xi - \lambda_2^{(\alpha)}\xi^2]\mathrm{d}\xi = \mu_j \\ &\int_{\mathbb{R}} \xi^k \exp[-\lambda_0^{(\alpha)} - \lambda_1^{(\alpha)}\xi - \lambda_2^{(\alpha)}\xi^2]\mathrm{d}\xi = \mu_k.\end{aligned} \tag{A.38}$$

The system **Equation** (A.38) can be solved with very efficient algorithms,[152] similar to those used to improve the solutions in ME optimization. The exponents $j$ and $k$ are arbitrary, so we focus on using lower order moments in order to approximate higher order moments and ultimately the NDF. Now, taking the moments in **Equation** (A.35) we obtain

$$\begin{aligned}\int_{\mathbb{R}} \xi^i \mathfrak{F}\mathrm{d}\xi &= \int_{\mathbb{R}} \xi^i \sum_{\alpha=1}^{N_\xi} w_\alpha \delta_\alpha(\xi, \boldsymbol{\lambda})\mathrm{d}\xi \\ \mu_i &= \sum_{\alpha=1}^{N_\xi} w_\alpha \int_{\mathbb{R}} \xi^i \delta_\alpha(\xi, \boldsymbol{\lambda})\mathrm{d}\xi.\end{aligned} \tag{A.39}$$

Once the value of each $\delta_\alpha(\xi, \boldsymbol{\lambda}) = \exp[-\lambda_0^{(\alpha)} - \lambda_1^{(\alpha)}\xi - \lambda_2^{(\alpha)}\xi^2]$ is obtained from the solution of the nonlinear system **Equation** (A.39) is used to formulate a linear system to find the values of $w_\alpha$. The availability of $w_\alpha, \lambda_i^{(\alpha)}$ will allow finding $\mathfrak{F}(\xi)$ and approximate higher order moments to close the transport equations. This procedure is useful whenever a handful of moments are available through a moment transport equation and higher order moments need to be approximated in order to close the transport equations.

In order to test the validity of this technique, a test has been conducted in which a Gaussian and Beta distributions are reconstructed using four of its moments. For the Gaussian distribution, a set of a thousand random normally distributed numbers were computed and the first four sample moments were calculated from these data. Similarly, a thousand numbers were computed from a sample distributed with a beta distribution,

and the sample moments were calculated. **Table A.1** shows the calculated moments from the raw data. Using those moments, the distributions will be approximated as

$$\mathfrak{F}(\xi) = w_1\delta_1(\xi, \boldsymbol{\lambda}) + w_2\delta_2(\xi, \boldsymbol{\lambda}) + w_3\delta_3(\xi, \boldsymbol{\lambda}), \tag{A.40}$$

where

$$\delta_\alpha(\xi, \boldsymbol{\lambda}) = \exp[-\lambda_0^{(\alpha)} - \lambda_1^{(\alpha)}\xi - \lambda_2^{(\alpha)}\xi^2]. \tag{A.41}$$

In order to find the coefficients $\boldsymbol{\lambda}^{(\alpha)}$, 3 nonlinear systems of the form of **Equation** (A.38) need to be solved, in which the triplets of moments $(0, j, k)$ are given by

$$(\mu_0, \mu_j, \mu_k) = \{(\mu_0, \mu_1, \mu_2), (\mu_0, \mu_1, \mu_3), (\mu_0, \mu_2, \mu_3)\}. \tag{A.42}$$

With the computed coefficients, it is possible to completely characterize the functions $\delta_\alpha(\xi, \boldsymbol{\lambda})$ and propose the linear system

$$\begin{bmatrix} \int_{\mathbb{R}} \delta_1(\xi, \boldsymbol{\lambda})\mathrm{d}\xi & \int_{\mathbb{R}} \delta_2(\xi, \boldsymbol{\lambda})\mathrm{d}\xi & \int_{\mathbb{R}} \delta_3(\xi, \boldsymbol{\lambda})\mathrm{d}\xi \\ \int_{\mathbb{R}} \xi\delta_1(\xi, \boldsymbol{\lambda})\mathrm{d}\xi & \int_{\mathbb{R}} \xi\delta_2(\xi, \boldsymbol{\lambda})\mathrm{d}\xi & \int_{\mathbb{R}} \xi\delta_3(\xi, \boldsymbol{\lambda})\mathrm{d}\xi \\ \int_{\mathbb{R}} \xi^2\delta_1(\xi, \boldsymbol{\lambda})\mathrm{d}\xi & \int_{\mathbb{R}} \xi^2\delta_2(\xi, \boldsymbol{\lambda})\mathrm{d}\xi & \int_{\mathbb{R}} \xi^2\delta_3(\xi, \boldsymbol{\lambda})\mathrm{d}\xi \end{bmatrix} \begin{bmatrix} w_1 \\ w_2 \\ w_3 \end{bmatrix} = \begin{bmatrix} \mu_1 \\ \mu_2 \\ \mu_3 \end{bmatrix}. \tag{A.43}$$

The results are presented in **Figure A.2**.

**Table A.1**: First 4 moments of a Gaussian and Beta distribution

| | Gaussian | Beta |
|---|---|---|
| $\mu_0$ | 1 | 1 |
| $\mu_1$ | 0.2478 | 0.2888 |
| $\mu_2$ | 0.0658 | 0.1081 |
| $\mu_3$ | 0.0185 | 0.0480 |

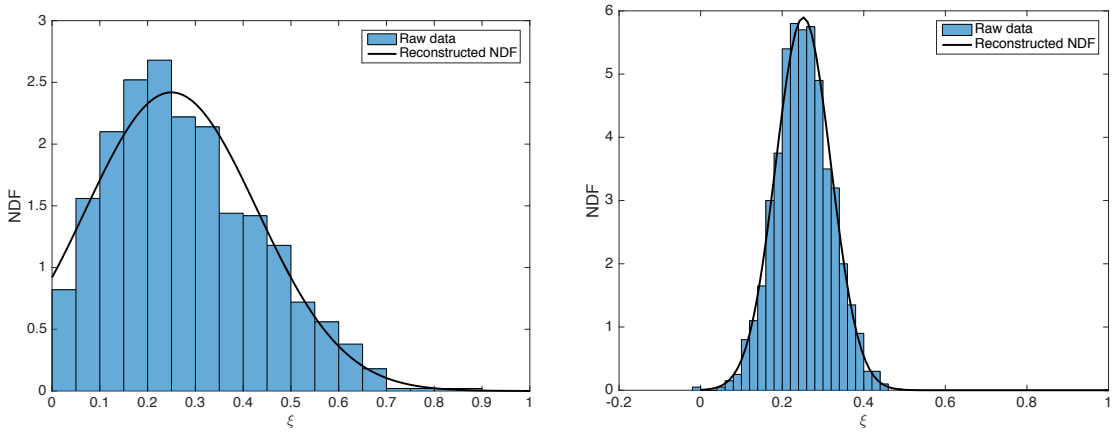


(a) Beta distribution

(b) Gaussian distribution

**Figure A.2**: Reconstruction of the data using the ME-based closure. (a) Reconstruction of the distribution using moments from a beta distributed samples. (b) Reconstruction of a distribution using moments from normally distributed samples.

# APPENDIX B

# NDF RECONSTRUCTION USING SPLINE POLYNOMIALS

```
function [Ms,P,Dpn,Ebinn] = PolyReconst(Ebin,Dp,M,N1,nI,nE,k,ks,tol,BC)

% first reconstruction
[zt,toln] = SolveCoefAuto(Ebin,M,N1,nI,k,tol,BC);

% Reconstructed polynomials
P = zeros(nI-1,nE);
for i = 1:nI-1
    P(i,:) = zt(1,i) + zt(2,i)*(Dp(i,:)-Ebin(i)) +
     zt(3,i)*(Dp(i,:)-Ebin(i)).^2;
end

figure(1)
plot(Dp(1,:),P(1,:),Dp(2,:),P(2,:),Dp(3,:),P(3,:),Dp(4,:),P(4,:),...
    Dp(5,:),P(5,:),Dp(6,:),P(6,:));
Dp1 = Dp(1,1);
Dpend = Dp(end,end);

% analytical moments
mr = [0.10,0.15,0.25,0.25,0.15,0.10]; % mass redistribution vector
Mb = AnalMom(Ebin,zt,ks,nI);
b = any(Mb(1,:) < 0);
if (b == 1)
    while (b == 1)
        pmax = zeros(1,nI-1);
        for h = 1:nI-1
            pmax(h) = max(P(h,:));
        end
        [~,Ip] = sort(pmax);
        [~,Im] = sort(Mb(1,:));
        Is = Ip - Im;
%         [~,Is] = ismember(Ip,Im);
        [~,col] = find(~Is);
        Et1 = Ebin(col(1)); Et2 = Ebin(col(end));
        Ebin = linspace(Et1,Et2,nI);
        for h = 1:nI-1
```

```
            Dp(h,:) = linspace(Ebin(h),Ebin(h+1),nE);
        end
        Mt = sum(M,2);
        Mr = zeros(length(ks),nI-1);
        for h = 1:nI-1
           for h2 = 1:length(ks)
               Mr(h2,h) = Mt(h2).*mr(h);
           end
        end
        [zt,toln] = SolveCoefAuto(Ebin,Mr,N1,nI,k,tol,BC);
        Mb = AnalMom(Ebin,zt,ks,nI);
        for i = 1:nI-1
            P(i,:) = zt(1,i) + zt(2,i)*(Dp(i,:)-Ebin(i)) +
             zt(3,i)*(Dp(i,:)-Ebin(i)).^2;
        end
        b = any(Mb(1,:) < 0);
    end
    Ms = Mb;
    Dpn = Dp;
    Ebinn = Ebin;
else
    Ms = Mb;
    Dpn = Dp;
    Ebinn = Ebin;
end

figure(2)
plot(Dpn(1,:),P(1,:),Dpn(2,:),P(2,:),Dpn(3,:),P(3,:),Dpn(4,:),P(4,:),...
    Dpn(5,:),P(5,:),Dpn(6,:),P(6,:));
xlim([Dp1,Dpend]);

return
%-----------------------------------------------------------------------
function Ma = AnalMom(Ebin,zt,ks,nI)

Ma = zeros(length(ks),nI-1);
for i = 1:nI-1
    for j = 1:length(ks)
        It1 = Ebin.^(ks(j)+1);
        It2 = Ebin.^(ks(j)+2);
        It3 = Ebin.^(ks(j)+3);
        I1 = diff(It1)/(ks(j)+1);
        I2 = diff(It2)/(ks(j)+2);
        I3 = diff(It3)/(ks(j)+3);
        Ma(j,i) = zt(1,i)*I1(i) + zt(2,i)*(I2(i)-Ebin(i)*I1(i)) +...
            zt(3,i)*(I3(i) - 2*Ebin(i)*I2(i) + Ebin(i)^2*I1(i));
    end
end
```

```
return
%-------------------------------------------------------------------------
```

# REFERENCES


[1] van der Hoef, M. A.; Ye, M.; van Sint Annaland, M.; Andrews, A. T.; Sundaresan, S.; Kuipers, J. A. M. Multiscale Modeling of Gas-Fluidized Beds. In *Computational Fluid Dynamics*; Marin, G. B., Ed.; Advances in Chemical Engineering; Academic Press: Ghent, Belgium, 2006; Vol. 31; pp 65–149.

[2] Beetstra, R.; van der Hoef, M. A.; Kuipers, J. A. M. Drag force of intermediate Reynolds number flow past mono- and bidisperse arrays of spheres. *AIChE J.* **2007**, *53*, 489–501.

[3] Burton, T. M.; Eaton, J. K. Fully resolved simulations of particle-turbulence interaction. *J. Fluid Mech.* **2005**, *545*, 67–111.

[4] Fede, P.; Simonin, O. Numerical study of the subgrid fluid turbulence effects on the statistics of heavy colliding particles. *Phys. Fluids* **2006**, *18*, 45103–45117.

[5] Fox, R. O. Large-eddy simulation tools for multiphase flows. *Annu. Rev. Fluid Mech.* **2012**, *44*, 47–76.

[6] Fox, R. O.; Marchisio, D. L. Multiphase reacting flows: Modeling and simulation. Int. Cent. Mech. Sci. Courses Lect. New York, USA, 2007; p 269.

[7] Lucci, F.; Ferrante, A.; Elghobashi, S. Modulation of isotropic turbulence by particles of Taylor length-scale size. *J. Fluid Mech.* **2010**, *650*, 5–55.

[8] Marchisio, D. L.; Fox, R. O. *Computational Models for Polydisperse Particulate and Multiphase Systems*; Cambridge Series in Chemical Engineering; Cambridge University Press: Cambridge, UK, 2013; p 508.

[9] Minier, J.-P.; Peirano, E. The pdf approach to turbulent polydispersed two-phase flows. *Phys. Rep.* **2001**, *352*, 1–214.

[10] Monahan, S. M.; Fox, R. O. Effect of model formulation on flow-regime predictions for bubble columns. *AIChE J.* **2007**, *53*, 9–18.

[11] Pai, M. G.; Subramaniam, S. A comprehensive probability density function formalism for multiphase flows. *J. Fluid Mech.* **2009**, *628*, 181–228.

[12] Riboux, G.; Risso, F.; Legendre, D. Experimental characterization of the agitation generated by bubbles rising at high Reynolds number. *J. Fluid Mech.* **2010**, *643*, 509–539.

[13] Tenneti, S.; Subramaniam, S. Particle-resolved direct numerical simulation for gas-solid flow model development. *Annu. Rev. Fluid Mech.* **2014**, *46*, 199–230.

[14] Andrews IV, A. T.; Loezos, P. N.; Sundaresan, S. Coarse-grid simulation of gas-particle flows in vertical risers. *Ind. Eng. Chem. Res.* **2005**, *44*, 6022–6037.

[15] Cloete, S.; Johansen, S. T.; Amini, S. An assessment of the ability of computational fluid dynamic models to predict reactive gas-solid flows in a fluidized bed. *Powder Technol.* **2012**, *215-216*, 15–25.

[16] Goldschmidt, M. J. V.; Kuipers, J. A. M.; Van Swaaij, W. P. M. Hydrodynamic modelling of dense gas-fluidised beds using the kinetic theory of granular flow: Effect of coefficient of restitution on bed dynamics. *Chem. Eng. Sci.* **2001**, *56*, 571–578.

[17] Jenkins, J. T.; Savage, S. B. A theory for the rapid flow of identical, smooth, nearly elastic, spherical particles. *J. Fluid Mech.* **1983**, *130*, 187–202.

[18] Kuipers, J. A. M.; Duin, K. J. V.; Beckum, F. P. H. V.; Swaaij, W. P. M. V. A numerical model of gas-fluidized beds. *Chem. Eng. Sci.* **1992**, *47*, 1913–1924.

[19] Kuwagi, K.; Horio, M. A numerical study on agglomerate formation in a fluidized bed of fine cohesive particles. *Chem. Eng. Sci.* **2002**, *57*, 4737–4744.

[20] Lathouwers, D.; Bellan, J. Modeling of dense gas–solid reactive mixtures applied to biomass pyrolysis in a fluidized bed. *Int. J. Multiph. Flow* **2001**, *27*, 2155–2187.

[21] Lim, K. S.; Zhu, J. X.; Grace, J. R. Hydrodynamics of gas-solid fluidization. *Int. J. Multiph. Flow* **1995**, *21, Supple*, 141–193.

[22] Mahalatkar, K.; Kuhlman, J.; Huckaby, E. D.; O'Brien, T. Computational fluid dynamic simulations of chemical looping fuel reactors utilizing gaseous fuels. *Chem. Eng. Sci.* **2011**, *66*, 469–479.

[23] Mahalatkar, K.; Kuhlman, J.; Huckaby, E. D.; O'Brien, T. CFD simulation of a chemical-looping fuel reactor utilizing solid fuel. *Chem. Eng. Sci.* **2011**, *66*, 3617–3627.

[24] Makkawi, Y. T.; Wright, P. C.; Ocone, R. The effect of friction and inter-particle cohesive forces on the hydrodynamics of gassolid flow: A comparative analysis of theoretical predictions and experiments. *Powder Technol.* **2006**, *163*, 69–79.

[25] Seo, M. W.; Nguyen, T. D. B.; Lim, Y. I.; Kim, S. D.; Park, S.; Song, B. H.; Kim, Y. J. Solid circulation and loop-seal characteristics of a dual circulating fluidized bed: Experiments and CFD simulation. *Chem. Eng. J.* **2011**, *168*, 803–811.

[26] Sun, B.; Gidaspow, D. Computation of circulating fluidized-bed riser flow for the fluidization VIII benchmark test. *Ind. Eng. Chem. Res.* **1999**, *38*, 787–792.

[27] Oberkampf, W. L.; Roy, C. J. *Verification and validation in scientific computing*; Cambridge University Press: New York, USA, 2010; pp 1–17.

[28] Strohmaier, E.; Dongarra, J.; Simon, H.; Meuer, M. Performace Development of High Performance Computing. `http://www.top500.org/statistics/perfdevel`, (Accessed Jan 8, 2016).

[29] Desjardins, O.; Fox, R. O.; Villedieu, P. A quadrature-based moment method for dilute fluid-particle flows. *J. Comput. Phys.* **2008**, *227*, 2514–2539.

[30] Fox, R. O. A quadrature-based third-order moment method for dilute gas-particle flows. *J. Comput. Phys.* **2008**, *227*, 6313–6350.

[31] Luo, L.-S. Some recent results on discrete velocity model and ramifications for Lattice Boltzmann equations. *Comput. Phys. Commun.* **2000**, *129*, 63–74.

[32] Morris, A. B.; Varghese, P. L.; Goldstein, D. B. Improvement of a discrete velocity Boltzmann equation solver with arbitrary post-collision velocities. *AIP Conf. Proc.* **2008**, *1084*, 458–463.

[33] Morris, A. B.; Varghese, P. L.; Goldstein, D. B. Monte Carlo solution of the Boltzmann equation via a discrete velocity model. *J. Comput. Phys.* **2011**, *230*, 1265–1280.

[34] Platkowski, T.; Illner, R. Discrete velocity models of the Boltzmann equation: A survey on the mathematical aspects of the theory. *SIAM Rev.* **1988**, *30*, pp. 213–255.

[35] Dufour, G.; Villedieu, P. A second-order multi-fluid model for evaporating sprays. *ESAIM Math. Model. Numer. Anal.* **2005**, *39*, 931–963.

[36] Gelbard, F.; Seinfeld, J. H. Numerical solution of the dynamic equation for particulate systems. *J. Comput. Phys.* **1978**, *28*, 357–375.

[37] Kumar, S.; Ramkrishna, D. On the solution of population balance equations by discretization - I. A fixed pivot technique. *Chem. Eng. Sci.* **1996**, *51*, 1311–1332.

[38] Ramkrishna, D.; Borwanker, J. D. A puristic analysis of population balance - I. *Chem. Eng. Sci.* **1973**, *28*, 1423–1435.

[39] Capecelatro, J.; Desjardins, O. An Euler-Lagrange strategy for simulating particle-laden flows. *J. Comput. Phys.* **2013**, *238*, 1–31.

[40] Gui, N.; Fan, J. R. Numerical simulation of pulsed fluidized bed with immersed tubes using DEM-LES coupling method. *Chem. Eng. Sci.* **2009**, *64*, 2590–2598.

[41] Grad, H. On the kinetic theory of rarefied gases. *Commun. Pure Appl. Math.* **1949**, *2*, 331–407.

[42] Hulburt, H. M.; Katz, S. Some problems in particle technology: A statistical mechanical formulation. *Chem. Eng. Sci.* **1964**, *19*, 555–574.

[43] Marchisio, D. L.; Fox, R. O. Solution of population balance equations using the direct quadrature method of moments. *J. Aerosol Sci.* **2005**, *36*, 43–73.

[44] McGraw, R. Description of aerosol dynamics by the quadrature method of moments. *Aerosol Sci. Technol.* **1997**, *27*, 255–265.

[45] Frenklach, M. Method of moments with interpolative closure. *Chem. Eng. Sci.* **2002**, *57*, 2229–2239.

[46] Fox, R. Higher-order quadrature-based moment methods for kinetic equations. *J. Comput. Phys.* **2009**, *228*, 7771–7791.

[47] Desjardins, O.; Fox, R. A quadrature-based moment closure for the Williams spray equation. *Proc. of the Summer Program 2006 - Center for Turbulence Research*. 2006; pp 223–234.

[48] Fan, R.; Marchisio, D. L.; Fox, R. O. Application of the direct quadrature method of moments to polydisperse gassolid fluidized beds. *Powder Technol.* **2004**, *139*, 7–20.

[49] Fan, R.; Fox, R. O. Segregation in polydisperse fluidized beds: Validation of a multi-fluid model. *Chem. Eng. Sci.* **2008**, *63*, 272–285.

[50] Fox, R. Bivariate direct quadrature method of moments for coagulation and sintering of particle populations. *J. Aerosol Sci.* **2006**, *37*, 1562–1580.

[51] Fox, R.; Laurent, F.; Massot, M. Numerical simulation of spray coalescence in an Eulerian framework: Direct quadrature method of moments and multi-fluid method. *J. Comput. Phys.* **2008**, *227*, 3058–3088.

[52] Gavi, E.; Rivautella, L.; Marchisio, D.; Vanni, M.; Barresi, A.; Baldi, G. CFD modelling of nano-particle precipitation in confined impinging jet reactors. *Chem. Eng. Res. Des.* **2007**, *85*, 735–744.

[53] Gavi, E.; Marchisio, D. L.; Barresi, A. A. CFD modelling and scale-up of confined impinging jet reactors. *Chem. Eng. Sci.* **2007**, *62*, 2228–2241.

[54] Selma, B.; Bannari, R.; Proulx, P. Simulation of bubbly flows: Comparison between direct quadrature method of moments (DQMOM) and method of classes (CM). *Chem. Eng. Sci.* **2010**, *65*, 1925–1941.

[55] Silva, L.; Rodrigues, R.; Mitre, J.; Lage, P. Comparison of the accuracy and performance of quadrature-based methods for population balance problems with simultaneous breakage and aggregation. *Comput. Chem. Eng.* **2010**, *34*, 286–297.

[56] Wang, L.; Fox, R. O. Comparison of micromixing models for CFD simulation of nanoparticle formation. *AIChE J.* **2004**, *50*, 2217–2232.

[57] Buffo, A.; Vanni, M.; Marchisio, D. L. Multidimensional population balance model for the simulation of turbulent gas-liquid systems in stirred tank reactors. *Chem. Eng. Sci.* **2012**, *70*, 31–44.

[58] Buffo, A.; Vanni, M.; Marchisio, D. L.; Fox, R. O. Multivariate quadrature-based moments methods for turbulent polydisperse gas-liquid systems. *Int. J. Multiph. Flow* **2013**, *50*, 41–57.

[59] Mazzei, L.; Marchisio, D. L.; Lettieri, P. Direct quadrature method of moments for the mixing of inert polydisperse fluidized powders and the role of numerical diffusion. *Ind. Eng. Chem. Res.* **2010**, *49*, 5141–5152.

[60] Dette, H.; Studden, W. J. *The Theory of Canonical Moments with Applications in Statistics, Probability, and Analysis*; Jon Wiley and Sons: New York, USA, 1997; p 327.

[61] Yuan, C.; Fox, R. Conditional quadrature method of moments for kinetic equations. *J. Comput. Phys.* **2011**, *230*, 8216–8246.

[62] Fox, R. Optimal moment sets for multivariate direct quadrature method of moments. *Ind. Eng. Chem. Res.* **2009**, *48*, 9686–9696.

[63] Laurent, F.; Massot, M. Multi-fluid modeling of laminar poly-dispersed spray flames: Origin, assumptions and comparison of the sectional and sampling methods. *Combust. Theory Model.* **2001**, *5*, 537–572.

[64] de Chaisemartin, S.; Fréret, L.; Kah, D.; Laurent, F.; Fox, R. O.; Reveillon, J.; Massot, M. Eulerian models for turbulent spray combustion with polydispersity and droplet crossing. *Comptes Rendus Mécanique* **2009**, *337*, 438–448.

[65] Doisneau, F.; Thomine, O.; Laurent, F.; Vié, A. Eulerian modeling and simulation of small scale trajectory crossing and coalescence for moderate-Stokes-number spray flows. *Proc. of the Summer Program 2012 - Center for Turbulence Research*. 2012; pp 365–374.

[66] Doisneau, F.; Dupays, J.; Murrone, A.; Laurent, F.; Massot, M. Eulerian versus Lagrangian simulation of unsteady two-way coupled coalescing two-phase flows in solid propellant combustion. *Comptes Rendus Mec.* **2013**, *341*, 44–54.

[67] Kah, D.; Laurent, F.; Fréret, L.; Chaisemartin, S.; Fox, R. O.; Reveillon, J.; Massot, M. Eulerian quadrature-based moment models for dilute polydisperse evaporating sprays. *Flow, Turbul. Combust.* **2010**, *85*, 649–676.

[68] Kah, D.; Laurent, F.; Massot, M.; Jay, S. A high order moment method simulating evaporation and advection of a polydisperse liquid spray. *J. Comput. Phys.* **2012**, *231*, 394–422.

[69] Schneider, L.; Lostec, N. L.; Villedieu, P.; Sadiki, A. A moment method for polydisperse sprays. *Comptes Rendus Math.* **2009**, *347*, 691–696.

[70] Schneider, L.; Le Lostec, N.; Villedieu, P.; Sadiki, A. A moment method for splashing and evaporation processes of polydisperse sprays. *Int. J. Multiph. Flow* **2010**, *36*, 261–272.

[71] Chalons, C.; Fox, R. O.; Massot, M. A multi-Gaussian quadrature method of moments for gas-particle flows in a LES framework. *Proc. of the Summer Program 2010 - Center for Turbulence Research*. 2010; pp 347 – 358.

[72] Laurent, F.; Vié, A.; Chalons, C.; Fox, R. O.; Massot, M. A hierarchy of Eulerian models for trajectory crossing in particle-laden turbulent flows over a wide range of Stokes numbers. *Proc. of the Summer Program 2012 - Center for Turbulence Research*. 2012; pp 193–204.

[73] Masi, E.; Simonin, O.; Riber, E.; Sierra, P.; Gicquel, L. Y. M. Development of an algebraic-closure-based moment method for unsteady Eulerian simulations of particle-laden turbulent flows in very dilute regime. *Int. J. Multiph. Flow* **2014**, *58*, 257–278.

[74] Vié, A.; Chalons, C.; Fox, R. O.; Laurent, F.; Massot, M. A multi-Gaussian quadrature method of moments for simulating high Stokes number turbulent two-phase flows. *Annu. Res. Briefs 2011 - Cent. Turbul. Res.* **2011**, 309–320.

[75] Vié, A.; Masi, E.; Simonin, O.; Massot, M. On the direct numerical simulation of moderate-stokes number turbulent particulate flows using algebraic closure-based

and kinetic-based moment methods. *Proc. of the Summer Program 2012 - Center for Turbulence Research*. 2012; pp 355–364.

[76] Vié, A.; Laurent, F.; Massot, M. Size-velocity correlations in high order moment methods for polydisperse evaporating sprays: Modeling and numerical issues. *J. Comput. Phys.* **2013**, *237*, 177–210.

[77] Yuan, C.; Laurent, F.; Fox, R. O. An extended quadrature method of moments for population balance equations. *J. Aerosol Sci.* **2012**, *51*, 1–23.

[78] Massot, M.; Laurent, F.; Kah, D.; De Chaisemartin, S. A robust moment method for evaluation of the disappearance rate of evaporating sprays. *SIAM J. Appl. Math.* **2010**, *70*, 3203–3234.

[79] Balachandar, S.; Eaton, J. K. Turbulent dispersed multiphase flow. *Annu. Rev. Fluid Mech.* **2010**, *42*, 111–133.

[80] Pedel, J.; Thornock, J. N.; Smith, S. T.; Smith, P. J. Large eddy simulation of polydisperse particles in turbulent coaxial jets using the direct quadrature method of moments. *Int. J. Multiph. Flow* **2014**, *63*, 23–38.

[81] Ladd, A. J. C. Dynamical simulations of sedimenting spheres. *Phys. Fluids A* **1993**, *5*, 299–310.

[82] Schneiderbauer, S.; Aigner, A.; Pirker, S. A comprehensive frictional-kinetic model for gasparticle flows: Analysis of fluidized and moving bed regimes. *Chem. Eng. Sci.* **2012**, *80*, 279–292.

[83] Balachandar, S.; Prosperatti, A. IUTAM Symposium on Computational Approaches to Multiphase Flow. In *IUTAM Symposium at Argonne National Laboratory*; Moreau, R., Ed.; Fluid Mechanics and Its Applications; Springer Science & Business Media: Illinois, USA, 2006; Vol. 81; p 445.

[84] Loth, E. Numerical approaches for motion of dispersed particles, droplets and bubbles. *Prog. Energy Combust. Sci.* **2000**, *26*, 161–223.

[85] van der Hoef, M. A.; van Sint Annaland, M.; Deen, N. G.; Kuipers, J. A. M. Numerical simulation of dense gas-solid fluidized beds: A multiscale modeling strategy. *Annu. Rev. Fluid Mech.* **2008**, *40*, 47–70.

[86] Subramaniam, S. Statistical modeling of sprays using the droplet distribution function. *Phys. Fluids* **2001**, *13*.

[87] Cercignani, C. *The Boltzmann Equation and its Applications*, 1st ed.; Applied Mathematical Sciences Series; Springer–Verlag: New York, USA, 1988; p 455.

[88] Chapman, S.; Cowling, T. G. *The Mathematical Theory of Non-uniform Gases: An Account of the Kinetic Theory of Viscosity, Thermal Conduction and Diffusion in Gases*, 3rd ed.; Cambridge Mathematical Library; Cambridge University Press: Cambridge, UK, 1970.

[89] Gombosi, T. I. *Gaskinetic Theory*, 1st ed.; Cambridge Atmospheric and Space Science Series; Cambridge University Press: Cambridge, UK, 1994; p 295.

[90] Fox, R. O.; Vedula, P. Quadrature-based moment model for moderately dense polydisperse gas-particle flows. *Ind. Eng. Chem. Res.* **2010**, *49*, 5174–5187.

[91] van Sint Annaland, M.; Bokkers, G. A.; Goldschmidt, M. J. V.; Olaofe, O. O.; Hoef, M. a. V. D.; Kuipers, J. A. M. Development of a multi-fluid model for poly-disperse dense gas-solid fluidised beds, part I: Model derivation and numerical implementation. *Chem. Eng. Sci.* **2009**, *64*, 4222–4236.

[92] Mouhot, C.; Pareschi, L.; Rey, T. Convolutive decomposition and fast summation methods for discrete-velocity approximations of the Boltzmann equation. *ESAIM Math. Model. Numer. Anal.* **2013**, *47*, 1515–1531.

[93] Yeoh, G. H.; Tu, J. *Computational Techniques for Multiphase Flows*, 1st ed.; Elsevier Science: Oxford, UK, 2009; p 664.

[94] Ramkrishna, D. *Population Balances: Theory and Applications to Particulate Systems in Engineering*; Academic Press: San Diego, USA, 2000; p 355.

[95] LeVeque, R. J. *Finite Volume Methods for Hyperbolic Problems*; Cambridge Texts in Applied Mathematics; Cambridge University Press: Cambridge, UK, 2002; p 553.

[96] LaViolette, R.; Berry, R.; McGraw, R. Homogeneous nucleation of metals in a plasma-quench reactor. *Plasma Chem. Plasma Process.* **1996**, *16*, 249–264.

[97] Lanczos, C. *Applied Analysis*; Dover Books on Mathematics; Dover Publications: New York, USA, 1988; p 539.

[98] Press, W. H.; Teukolsky, S. A.; Vetterling, W. T.; Flannery, B. P. *Numerical Recipes 3rd Edition: The Art of Scientific Computing*, 3rd ed.; Cambridge University Press: New York, USA, 2007; p 1235.

[99] Barthelmes, G.; Pratsinis, S. E.; Buggisch, H. Particle size distributions and viscosity of suspensions undergoing shear-induced coagulation and fragmentation. *Chem. Eng. Sci.* **2003**, *58*, 2893–2902.

[100] L. Marchisio, D.; Dennis Vigil, R.; O. Fox, R. Implementation of the quadrature method of moments in CFD codes for aggregationbreakage problems. *Chem. Eng. Sci.* **2003**, *58*, 3337–3351.

[101] Mukhopadhyay, A.; Jasor, G.; Polifke, W. Simulation of pure sedimentation of raindrops using quadrature method of moments. *Atmos. Res.* **2012**, *106*, 61–70.

[102] Wan, B.; Ring, T. A. Verification of SMOM and QMOM population balance modeling in CFD code using analytical solutions for batch particulate processes. *China Particuology* **2006**, *4*, 243–249.

[103] Qamar, S.; Noor, S.; ul Ain, Q.; Seidel-Morgenstern, A. Bivariate extension of the quadrature method of moments for batch crystallization models. *Ind. Eng. Chem. Res.* **2010**, *49*, 11633–11644.

[104] Yoon, C.; McGraw, R. Representation of generally mixed multivariate aerosols by the quadrature method of moments: I. Aerosol dynamics. *J. Aerosol Sci.* **2004**, *35*, 561–576.

[105] Fox, R. O. *Computational Models for Turbulent Reacting Flows*, 1st ed.; Cambridge Series in Chemical Engineering; Cambridge University Press: Cambridge, UK, 2003; p 419.

[106] Mazzei, L. Limitations of quadrature-based moment methods for modeling inhomogeneous polydisperse fluidized powders. *Chem. Eng. Sci.* **2011**, *66*, 3628–3640.

[107] Mazzei, L.; Marchisio, D. L.; Lettieri, P. New quadrature-based moment method for the mixing of inert polydisperse fluidized powders in commercial CFD codes. *AIChE J.* **2012**, *58*, 3054–3069.

[108] Raman, V.; Pitsch, H. Quadrature moments method for the simulation of turbulent reactive flows. *Annu. Res. Briefs-2003* **2003**, 261–275.

[109] Van Capelleveen, M. Dynamic modeling of the continous melamine crystallization process using the DQMOM method. M.Sc. Thesis, TU Delft, Delft University of Technology, March 2011.

[110] Reynolds, A. M.; Lo Iacono, G. On the simulation of particle trajectories in turbulent flows. *Phys. Fluids* **2004**, *16*, 4353–4358.

[111] Vikas, V.; Wang, Z. J.; Fox, R. O. Realizable high-order finite-volume schemes for quadrature-based moment methods applied to diffusion population balance equations. *J. Comput. Phys.* **2013**, *249*, 162–179.

[112] Cheng, J. C.; Vigil, R.; Fox, R. A competitive aggregation model for flash nanoprecipitation. *J. Colloid Interface Sci.* **2010**, *351*, 330–342.

[113] Cheng, J. C.; Fox, R. O. Kinetic modeling of nanoprecipitation using CFD coupled with a population balance. *Ind. Eng. Chem. Res.* **2010**, *49*, 10651–10662.

[114] Tambour, Y. A Lagrangian sectional approach for simulating droplet size distribution of vaporizing fuel sprays in a turbulent jet. *Combust. Flame* **1985**, *60*, 15–28.

[115] Laurent, F.; Massot, M.; Villedieu, P. Eulerian multi-fluid modeling for the numerical simulation of coalescence in polydisperse dense liquid sprays. *J. Comput. Phys.* **2004**, *194*, 505–543.

[116] de Chaisemartin, S.; Fréret, L.; Kah, D.; Laurent, F.; Fox, R. O.; Réveillon, J.; Massot, M. Turbulent combustion of polydisperse evaporating sprays with droplets crossing: Eulerian modeling and validation in the infinite Knudsen limit. *Proc. of the Summer Program 2008 - Center for Turbulence Research*. 2008; pp 265–276.

[117] Chalons, C.; Kah, D.; Massot, M. Beyond pressureless gas dynamics: Quadrature-based velocity moment models. *Commun. Math. Sci.* **2012**, *10*, 1241–1272.

[118] Larat, A.; Massot, M.; Vié, A. A stable, robust and high order accurate numerical method for Eulerian simulation of spray and particle transport on unstructured meshes. *Annual Research Briefs 2012 - Center for Turbulence Research*. 2012; pp 205–216.

[119] Sabat, M.; Larat, A.; Vié, A.; Massot, M. Comparison of Realizable Schemes for the Eulerian Simulation of Disperse Phase Flow. In *Finite Volumes for Complex Applications VII - Elliptic, Parabolic and Hyperbolic Problems*, 1st ed.; Fuhrmann, J., Ohlberger, M., Rohde, C., Eds.; Springer International Publishing: Berlin, 2014; Vol. 78; p 518.

[120] Vié, A.; Laurent, F.; Massot, M. A high order moment method for the simulation of polydisperse two-phase flows. *Comptes Rendus Mec.* **2013**, *341*, 55 – 64.

[121] Kah, D.; Vie, A.; Chalons, C.; Massot, M. Second-order scheme for quadrature-based velocity high order moment methods for disperse two-phase flows. *Annual Research Briefs 2011 - Center for Turbulence Research*. 2011; pp 321 – 334.

[122] Doisneau, F.; Laurent, F.; Murrone, A.; Dupays, J.; Massot, M. Eulerian multi-fluid models for the simulation of dynamics and coalescence of particles in solid propellant combustion. *J. Comput. Phys.* **2013**, *234*, 230–262.

[123] Pedel, J.; Thornock, J. N.; Smith, P. J. Large eddy simulation of pulverized coal jet flame ignition using the direct quadrature method of moments. *Energy & Fuels* **2012**, *26*, 6686–6694.

[124] Pedel, J.; Thornock, J. N.; Smith, P. J. Ignition of co-axial turbulent diffusion oxy-coal jet flames: Experiments and simulations collaboration. *Combust. Flame* **2013**, *160*, 1112–1128.

[125] Reid, C. M. An Instrumentalist Approach to Validation: A Quantitative Assessment of a Novel Coal Gasification Model. Ph.D. Dissertation, University of Utah, May 2012.

[126] Estivalezes, J.-L.; Villedieu, P. A new second order positivity preserving kinetic schemes for the compressible Euler equations. *Fourteenth International Conference on Numerical Methods in Fluid Dynamics*. 1995; pp 96–100.

[127] Deshpande, S. M.; Kulkarni, P. S.; Ghosh, A. K. New developments in kinetic schemes. *Comput. Math. with Appl.* **1998**, *35*, 75–93.

[128] Perthame, B. Boltzmann-type schemes for gas dynamics and the entropy property. *SIAM J. Numer. Anal.* **1990**, *27*, 1405–1421.

[129] Perthame, B. Second order Boltzmann schemes for compressible Euler equations in one and two space dimensions. *Siam J. Numer. Anal.* **1992**, *29*, 1–19.

[130] Bouchut, F.; Jin, S.; Li, X. Numerical approximations of pressureless and isothermal gas dynamic. *SIAM J. Numer. Anal.* **2004**, *41*, 135–158.

[131] Estivalezes, J. L.; Villedieu, P. High-order positivity-preserving kinetic schemes for the compressible Euler equations. *SIAM J. Numer. Anal.* **1996**, *33*, 2050–2067.

[132] Vikas, V.; Wang, Z. J.; Passalacqua, A.; Fox, R. O. Realizable high-order finite-volume schemes for quadrature-based moment methods. *J. Comput. Phys.* **2011**, *230*, 5328–5352.

[133] John, V.; Thein, F. On the efficiency and robustness of the core routine of the quadrature method of moments (QMOM). *Chem. Eng. Sci.* **2012**, *75*, 327–333.

[134] McGraw, R.; Wright, D. L. Chemically resolved aerosol dynamics for internal mixtures by the quadrature method of moments. *J. Aerosol Sci.* **2003**, *34*, 189–209.

[135] Sack, R.; Donovan, A. F. An algorithm for Gaussian quadrature given modified moments. *Numer. Math.* **1971**, *18*, 465–478.

[136] Smoot, L. D.; Pratt, D. T. In *Pulverized-Coal Combustion and Gasification: Theory and Applications for Continuous Flow Processes*, 1st ed.; Smoot, L. D., Pratt, D. T., Eds.; Plenum Press: New York, USA, 1979; p 333.

[137] John, V.; Angelov, I.; Oncul, A. A.; Thevenin, D. Techniques for the reconstruction of a distribution from a finite number of its moments. *Chem. Eng. Sci.* **2007**, *62*, 2890–2904.

[138] Knott, G. D. *Interpolating Cubic Splines*, 1st ed.; Birkhäuser Basel: New York, USA, 2000; pp XII, 244.

[139] de Souza, L. M.; Janiga, G.; John, V.; Thevenin, D. Reconstruction of a distribution from a finite number of moments with an adaptive spline-based algorithm. *Chem. Eng. Sci.* **2010**, *65*, 2741–2750.

[140] Hyland, K. E.; McKee, S.; Reeks, M. W. Derivation of a PDF kinetic equation for the transport of particles in turbulent flows. *J. Phys. A. Math. Gen.* **1999**, *32*, 6169.

[141] Riber, E.; Moureau, V.; García, M.; Poinsot, T.; Simonin, O. Evaluation of numerical strategies for large eddy simulation of particulate two-phase recirculating flows. *J. Comput. Phys.* **2009**, *228*, 539–564.

[142] Athanassoulis, G. A.; Gavriliadis, P. N. The truncated Hausdorff moment problem solved by using kernel density functions. *Probabilistic Eng. Mech.* **2002**, *17*, 273–291.

[143] Kociszewski, A. The existence conditions for maximum entropy distributions, having prescribed the first three moments. *J. Phys. A. Math. Gen.* **1986**, *823*, 823–827.

[144] Murphy, J. J.; Shaddix, C. R. Combustion kinetics of coal chars in oxygen-enriched environments. *Combust. Flame* **2006**, *144*, 710–729.

[145] Tognotti, L.; Longwell, J. P.; Sarofim, A. F. The products of the high temperature oxidation of a single char particle in an electrodynamic balance. *Symp. Combust.* **1991**, *23*, 1207–1213.

[146] François, B.; François, J. Duality solutions for pressureless gases, monotone scalar conservation laws, and uniqueness. *Commun. Partial Differ. Equations* **1999**, *24*, 2173–2189.

[147] Jaynes, E. T. Information theory and statistical mechanics. *Phys. Rev.* **1957**, *106*, 620–630.

[148] Tagliani, A. Hausdorff moment problem and maximum entropy: A unified approach. *Appl. Math. Comput.* **1999**, *105*, 291–305.

[149] Levermore, C. D. Moment closure hierarchies for kinetic theories. *J. Stat. Phys.* **1996**, *83*, 1021–1065.

[150] Perlman, M. D. Jensen's inequality for a convex vector-valued function on an infinite-dimensional space. *J. Multivar. Anal.* **1974**, *4*, 52–65.

[151] Abramowitz, M.; Stegun, I. A. *Handbook of Mathematical Functions: With Formulas, Graphs, and Mathematical Tables*; Dover Publications: Washington D.C., 1964; Vol. 55; p 1046.

[152] Ormoneit, D.; White, H. An efficient algorithm to compute maximum entropy densities. *Econom. Rev.* **1999**, *18*, 127–140.